Ministry of Education and Science of the Republic of Kazakhstan
Acad. E.A. Buketov Karaganda University
RSE "Institute of Applied Mathematics" CS MES RK

Tanasheva N. K.

MATHEMATICAL MODELING OF WIND POWER PLANTS BASED ON THE MAGNUS EFFECT

Monograph

Karaganda, 2021

UDC 510
LBC 22.1
M 39

Recommended for publication by the Academic Council
KarU named after E.A.Buketov

Recommended for publication by the Academic Council RSOE « Institute of Applied Mathematics» MDDIAI RK

REVIEWERS:

T. A. Koketai, doctor of physical and mathematical sciences, professor of E. A. Buketov Karaganda University

Sh. N. Kuttykozhaeva, doctor of physical and mathematical sciences, professor of Sh. Ualikhanov Kokshetau University

Tanasheva N. K.

M 39 Mathematical modeling of wind power plants based on the Magnus effect: Monograph. - Nur-Sultan: publishing house "Altyn kitap", 2021. – 108 pages.

ISBN 978-9965-869-99-0

The monograph is the first to obtain data on numerical modeling of wind power plants based on the Magnus effect with a different number of blades. The features of modeling turbulent flows around a cylindrical working element - a blade - are considered. Universal aerodynamic numerical dependencies of wind power plants were obtained by means of mathematical modeling, which were compared with experimental data obtained on prototypes.

Designed for university students, teachers, undergraduates, PhD students in technical specialties and researchers.

UDC 510
LBC 22.1

ISBN 978-9965-869-99-0

CONTENTS

DEFINITIONS, DESIGNATIONS AND ABBREVIATIONS…….. 5

INTRODUCTION……. 6

1 FUNDAMENTALS OF WIND POWER PLANT MODELING…….. 10
1.1 Overview of existing modeling methods for wind turbines of various types…. 10
1.2 The current state of the problem…… 16

2 THE METHOD OF NUMERICAL MODELING OF AERODYNAMIC CHARACTERISTICS……... 18
2.1 Equations of thermal convection…… 18
2.2 Equations of motion…… 21
2.3 Elements of the vorticity theory……. 23
2.4 The ANSYS program. Boundary conditions…….. 25
2.5 Stages of modeling in ANSYS…… 30

3 MATHEMATICAL MODELING OF AERODYNAMIC CHARACTERISTICS OF WIND POWER PLANTS BASED ON THE MAGNUS EFFECT…….. 36
3.1 Aerodynamics of the rotating cylinder system based on the Magnus effect….. 36
3.2 The process of modeling a two-bladed wind power plant…….. 36
3.3 Flow pattern and pressure field explaining the physical picture of the appearance of aerodynamic forces around the object of study……... 39
3.4 Results simulation of a two-bladed wind turbine…… 41

4 MATHEMATICAL MODELING OF A THREE-BLADED WIND POWER PLANT BASED ON THE MAGNUS EFFECT……. 44
4.1 Results of mathematical modeling of aerodynamic characteristics of a wind power plant based on the Magnus effect……. 48
4.2 Calculation of the aerodynamic coefficients of the rotating cylinder of a wind power plant based on the Magnus effect……. 50
4.3 The flow field in the vicinity of the wind wheel…… 54

5 CALCULATION OF THE ELECTROPHYSICAL PARAMETERS OF A MAGNETOELECTRIC ELECTRIC GENERATOR ON PERMANENT MAGNETS ……. 62
5.1 Electric generator of a wind power plant based on semiconductor electronics.. 62
5.2 Results of electrophysical parameters of a magnetoelectric electric generator... 69

6 DEVELOPMENT OF AN EXPERIMENTAL WIND POWER PLANT WITH BLADES IN THE FORM OF ROTATING CYLINDERS OF CONSTANT CROSS-SECTION WITH A SMOOTH SURFACE…….. 74
6.1 Assembly of an experimental wind power plant based on the Magnus effect… 74
6.2 Accounting for the influence of gyroscopic forces on the working part of the wind turbine……. 80

7 ANALYSIS OF THEORY AND EXPERIMENT…….... 87
7.1 Analysis of the results of the study of the wind utilization coefficient from the speed of a wind power plant with blades in the form of rotating cylinders…... 87
7.2 Analysis of theoretical results on the pressure distribution in the vicinity of a wind power plant……. 90
7.3 Comparative analysis of the theory and experiment of aerodynamic characteristics of a wind power plant…….. 96

CONCLUSION……. 98

LIST OF USED SOURCES…….. 100

DEFINITIONS, DESIGNATIONS AND ABBREVIATIONS

In this monograph, the following terms are used with appropriate definitions:

A wind wheel is a working organ of a wind turbine, used to convert the kinetic energy of the incoming air flow into mechanical energy for the rotation of the wind turbine shaft.

A wind turbine is a device that converts wind energy into rotational motion energy. The main working body of the wind turbine is a rotating unit-a wheel driven by the wind and rigidly connected to the shaft, the rotation of which drives the equipment that performs useful work.

The following designations and abbreviations are used in this monograph:

RES - renewable energy sources;
WW-wind wheel;
RD-rectifier device;
WPS - wind power station;
WPP - wind power plant;
WEUC (ξ) - wind energy utilization coefficient;
WT-wind turbine.

INTRODUCTION

Finding environmentally friendly energy sources, searching for new energy saving technologies, rational and efficient use of energy resources-all these issues are a feature of the formation of the modern world. Due to the growing number of the world's population and the increasing energy needs, the search for the right and energy-efficient alternative energy sources is an urgent issue.

Based on this, not only in Kazakhstan, but also around the world, the search for new types of energy and the study of its sources are an urgent issue at the present time. Such issues as the risks of global warming, the reduction of natural resources of energy sources, its environmentally unsafe impact on the environment, the rapid growth in the number of consumers in energy sources are the main topics for discussion and decision at the highest levels of international and state representatives.

Before the discovery of electricity, the use of wind energy was on a par with work using human hands and water energy. However, with the development of technologies such as electricity and steam, this type of energy began to be forgotten over time. When choosing an output and an energy source, environmental factors play a primary role.

In the case of nuclear power plants, it is possible to observe an increase in the labor intensity of electric energy production due to increased requirements and criteria in relation to the environment. It is also necessary to reduce the production of fossil fuels, since this family of fuels worsen the environmental situation, there are mechanical problems and difficulties in mining, as well as due to the large number of non-explosive cases in mines that have claimed people's lives. Nowadays, due to the development of highly efficient technologies, new methods of fossil fuel extraction have come: gas and oil extraction by fountain, as well as coal by open methods. But nevertheless, these mining methods do not solve the global problems that were mentioned above. In the future, an insufficient amount of fuel will lead to a fuel crisis, which will affect all spheres of human activity, from household amenities to industry.

It has been proved that the wind energy resources of our republic are 10 times greater than the energy value of fossil fuels, and 100 times the total electric energy. But nevertheless, the transformation of all wind energy resources in Kazakhstan is not an easy task. The economic benefit in obtaining electric energy from wind potentials consists in the accumulation of energy, for the supply of energy in calm weather conditions, as well as in the case of an excess, its transfer to the electric grid.

It is safe to say that the environmental indicators of the environment, which have been worsened due to the emissions of harmful substances from traditional sources of electricity generation, will only increase due to the use of wind power plants. It has been established that 2,100 tons / year of carbon dioxide can be prevented due to 1 MW of energy obtained with the help of wind flows, thereby having a negative impact on the global situation with global warming[1].

Most likely, in the future, alternative energy will not be able to completely displace fossil energy sources from the energy market, but nevertheless, for far-located areas from the power grid, RES will be the only way out [2]

Such alternative energy sources include wind power, for which information about the wind characteristics of the territory where the wind power plant is expected to be located in the future plays a particularly important role [1-5].

Renewable energy resources occupy a special position in the development of the energy sector of the Republic of Kazakhstan [1]. In the Message of the President of the Republic of Kazakhstan – Leader of the Nation N. A. Nazarbayev to the people of Kazakhstan dated December 14, 2012, the Strategy "Kazakhstan-2050": a new political course of the established state indicates the need to develop the production of alternative types of energy, and the active introduction of technologies using solar and wind energy [5]. In Kazakhstan, the energy potential of renewable energy sources (wind energy, hydropower, solar energy) has good indicators. But nevertheless, about 0.4 % of the total figure is the amount of energy generated using RES [4].

On the territory of Kazakhastan, powerful wind currents prevail, which are directed from the South-West and North-East of the country, the reason for this is that the country is located in the northern hemisphere. Also, the primary role for the development of wind energy in Kazakhstan is played by the fact that the speed of the incoming air flow is on average 6 m/s and even higher in some areas. This phenomenon is an attractive feature of the country. According to experts in the field of wind energy, it is set at 1,900 billion rubles.kWh can be obtained of electric energy per year. It should also be noted separately Central Kazakhstan, which has the highest wind resources.

To improve the situation with greenhouse gas emissions in the country, it is necessary to develop, optimize and improve the use of renewable energy sources. The issue of the global use of alternative energy sources remains relevant, based on the plans of the Government of Kazakhstan to increase the capacity and generation of electric energy.

According to the latest research data conducted within the framework of the wind energy development program organized by the United Nations, such territorial zones as the Western regions (Atyrau and Mangystau), Southern regions (Turkestan and Almaty regions), Central regions (Karaganda region) and Northern regions (Akmala region) have high wind energy indicators for the development of wind energy. Due to the unique steppe type of territorial occupancy of the country, there is a potential to bring the power of the wind power plant to 1000 MW. Further detailed studies to determine the wind potential of Kazakhstan are necessary for the construction and development of a number of wind farms. According to research conducted using computer mathematical modeling, a forecast was formed where it is indicated that 300 MW will be produced in 2015, and by 2024 the figure will reach 2000 MW. In the territories of the Southern and Western regions of Kazakhstan, by 2025, a significant shortage in electric energy can be observed, which will grow every year, due to the growth of market prices for natural gas and for imported electric energy from nearby Asian countries. To solve this situation for

the better, it is necessary to introduce alternative energy sources into the country's energy market, which also solve the problem with greenhouse gas emissions [3].

Features of the use of alternative energy sources:

1. It is possible to reduce the number of carbon dioxide emissions, thanks to the large energy potential, and developed technologies and installations for generating electric energy. But nevertheless, for the effective development of this area, a huge support is needed in the face of the state and the government of the country.

2. According to the cost of the produced electric energy, some types of RES have high indicators that are not available for economic reasons for the rural population. It is necessary to carefully study the technologies and find more cost-effective solutions for each case.

3. In some cases, in order to cover all the finances for the production, development and implementation of aggregates, it is necessary to state in detail more detailed facts in plans and strategies. Based on what, there is a problem in the directional planning of the financial side of projects and plans

4. Due to insufficient information and data, many technologies and projects do not have their rapid development. Information collection, analysis and research play an important role in the implementation of projects and technologies.

5. At the certification stage, evaluations, which are evaluation indicators for the development of projects, there are a lot of deviations. In this situation, the problem is the results of an incomplete study on monitoring and evaluating technologies.

6. In the event that the project or technologies are ready for implementation, it is necessary to create special structures and divisions for correcting defects, accidents, as well as for servicing installations and repairs [4]

The question of the use and research of alternative energy sources is a question that has a global mastshab.International organizations, in order to increase the speed of development and introduction of alternative energy sources and technologies, hold international forums, where the heads of countries take part.

Relying on the above facts, we can say that the development and study of wind power plants operating at low speeds of the incoming air flow is an urgent and popular task [3-4]. Existing wind turbines of various designs at low wind speeds do not always have sufficient efficiency. The efficiency of some wind turbine designs is currently little studied. One of the little-studied promising wind turbines is a wind turbine with blades in the form of rotating cylinders of constant cross-section [1-4].

Wind power plants operating on the basis of the Magnus effect have the following advantages [4-6]:

- generation of electric energy at low air flows , but the most repetitive, starting from 2-4 m/s;

- the possibility of power supply of energy consumption objects remote from the central electric highways and networks (farms and peasant farms, border posts, communication points and posts, remote people's homes, remote construction sites, subsidiary farms, mountain camps, etc.);

- there is no need to create a stand-alone electrical network, you can install the installation.

To create an effective wind power plant, it is necessary to carefully conduct research on the study of aerodynamic characteristics, as well as the flow field around the power elements [5,6].

To this purpose, mathematical modeling using the latest computer technologies and turbulence models will be applied for a better and effective study of the operation of wind power plants based on the laws of aerodynamics [4-6]. Modeling of complex energy objects makes it possible to avoid too large costs necessary for their direct study [4,5].

This monograph was made with the financial of the "Best University Teacher-2020"

1. FUNDAMENTALS OF WIND POWER PLANT MODELING

1.1 Overview of existing methods for modeling wind power plants of various types

When developing and constructing wind turbines, the interaction of physical processes (the shape of the blades, the flow of air, etc.) is taken into account.Test studies are mainly operated with limited data volumes. Since, in some cases, experiments are not always possible during full-scale tests, both for economic and technical reasons [4-7]. At the moment, theoretical studies are carried out using mathematical modeling in a turbulent flow obtained during the operation of a wind turbine [8]. Currently, there are many works on mathematical modeling of wind turbines [4]. In order to increase the energy supply and energy efficiency of autonomous systems, wind turbines of small and medium power are increasingly used as alternative sources [7].

In connection with the above, there is a great need to conduct various scientific research related to the optimization and management and regulation of the operating modes of generating equipment. Basically, it is convenient to use and investigate mathematical modeling methods as a tool for such energy systems, as a result of which there is a big task of creating a mathematical model of a wind turbine [5-12].

The authors of [12] obtained the results of numerical modeling for solving an aerodynamic problem with respect to a wind turbine with a vertical axis of rotation. This work is developed on the basis of the Navier-Stokes equations. The solution of the algorithm of non-stationary Navier-Stokes equations based on an implicit scheme in mobile curved coordinates is implemented. The results of a numerical study of the dynamics and aerodynamics of a wind power plant on the example of a Darrier, Savonius rotor and their elements are presented.

The paper [13] presents the results of mathematical calculation of the dynamics of rotation and rotation of a wind power plant. The results of the distribution of the angle of attack of the blade along the azimuth of rotation at the angle of oblique blowing by 300 are shown (Figure 1.1). It is established that the flow in the presence of wind misaligned with the axis of rotation leads to a significant unevenness of the angles of attack and, accordingly, the distribution of forces on the blades during rotation [13].

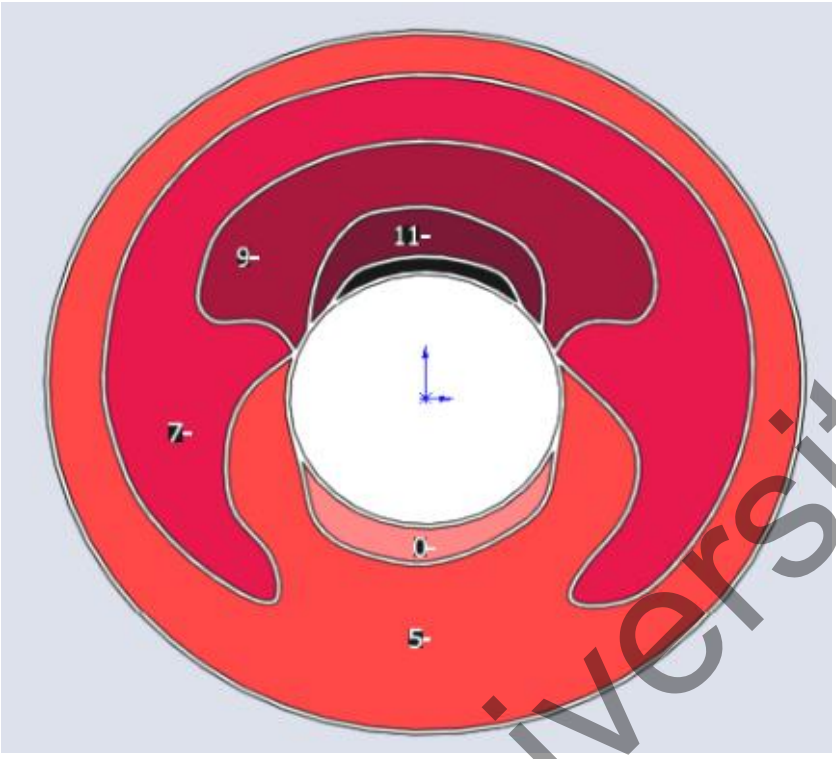

Fig.1.1. Distribution of aerodynamic angles of attack of a wind turbine

The authors of the scientific work [14] carried out mathematical modeling of a wind generator, used the construction of a functional model of a wind turbine using the Model-Based Calibration Toolbox (MBCT) with subsequent export to the Simulink environment (MATLAB). The process of creating a mathematical picture [14] consists in plotting a function of three variables. The functions of three variables demonstrate the dependence of the moment of the wind generator on the air flow velocity and the angular velocity of rotation of the main shaft.

Figure 1.2 shows the operating characteristics of the simulated wind generator in three-dimensional form, obtained in MBCT [14].

In [15], a nonlinear computational model was developed in the MATLAB programming environment, where the optimization of the main geometric characteristics of wind turbine blades is shown. The optimization of the blade was carried out in a quasi-static mode. The purpose of the work is to use an individual approach to solving specific technical problems. To debug and demonstrate the operation of the program, the design parameters of a previously developed wind turbine with a capacity of 5 kW are used in the model [15]. The model can be used both for analyzing the operation of horizontal-axial wind turbines with specified parameters, and for their synthesis according to specified operating characteristics. During the tests of the numerical model, optimized values of the geometric parameters of the blades of a three-bladed wind wheel were obtained, which provide an increase in the theoretically achievable power factor of the wind wheel in the calculated operating mode [15].

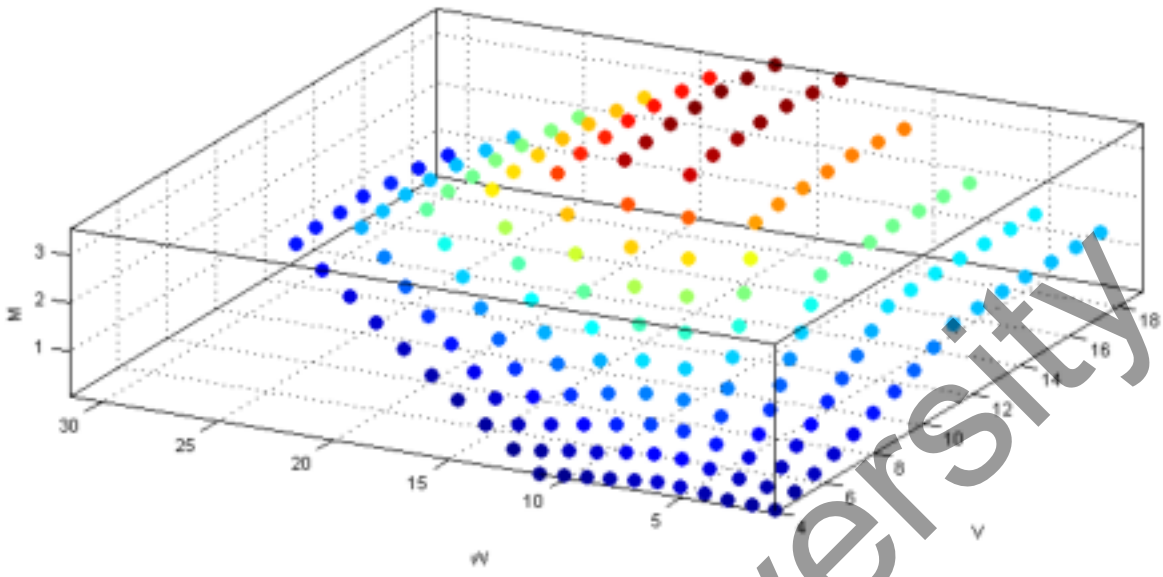

Fig.1.2. Mechanical and operational characteristics of a wind turbine

Finding the Cp power factor for calculating a profile with unknown aerodynamic parameters, which in turn depends on complicated and nonlinear aerodynamic processes formed when the wind interacts with the working surface of the wind wheel blade, is a difficult task [16]. For this purpose, you can use a special computer program WT_PERF, which is based on updating algorithms, with which you can calculate the relationship of the power factor from the wind speed Cp(V) [16].

The work [17] is devoted to the improvement of the 2D CFD model of the Darya wind wheel. The model was implemented using the ANSYS Fluent program designed for preliminary calculation of wind turbine performance and geometry optimization. The results of tests for a 2D model of a wind turbine are presented[17]. The numerical and experimental data agree well. The work is the basis for the development of accurate 3D CFD non-stationary models and can be used to test the simplest 1D models[17].

The authors of the work [18] reviewed the methods and approaches of micromechanics materials that can be used to model composites of wind turbine blades. The use of various methods for modeling the strength, stiffness and service life of composite materials makes it possible to analyze the suitability of various groups of materials for the manufacture of wind turbine blades [18].

The development of a 3D CFD model of the horizontal type of the wind turbine rotation axis using the Ansys Fluent program is shown in [19]. The model is designed to predict the performance of a wind turbine and evaluate the capabilities of the 1D model, previously developed by the authors [19]. These two models were compared in terms of accuracy, predictability and calculation time. The strategy of forming a high-quality grid and optimizing turbulence models is presented. The results of these tests were applied to

the turbulence model by changing the local correlation parameters. The same parameters were used for a 3D model of a wind turbine[19]. A model of a movable support system is used to simulate rotation and estimate the 3D flow along the rotor blades. The application of a 3D model on a new micro-wind turbine is shown.

The article [20] presents a model of a wind turbine simulator with a fixed angular pitch. The task of the work is to develop and create a wind turbine simulator. An analytical model representing a wind turbine simulator was obtained to describe the simulation results using the MATLAB / Simulink program [20]. The wind turbine simulator can display mechanical power and torque characteristics.

Figure 1.3 shows the simulated power characteristics of a wind turbine.

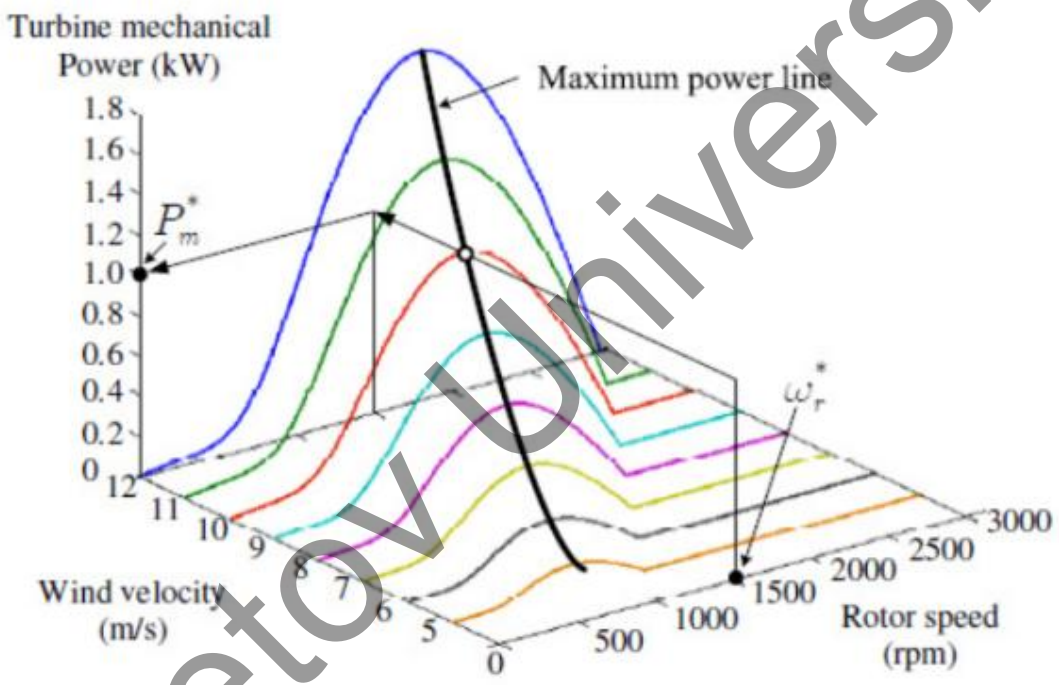

Fig.1.3. Power characteristics of a wind turbine

The article [21] presents a model of the load of wind turbine gears for simulating real and changing operating conditions in order to simulate wind turbine vibrations. The indicators of the incoming air flow, which generates chaotic various loads on the transmission components of the generating load on the teeth and gear bearings during the transmission of torque, are given. Based on the results, it can be seen that the proposed approach agrees very well with the experimental data [21].

The authors of the article [22] considered a mathematical model of a wind turbine for an environment with weak and migrating winds. The method of forming a description of energy professions, as well as their block diagram using a mathematical

language, is shown. The possibilities and prospects of using the device for analyzing energy flows are revealed.

The article [23] presents a method for calculating the wind energy potential. The parameters of the autonomous power supply system are determined, the structure and algorithm of operation are developed, a mathematical model of the installation and a control scheme are created. The automated system is checked for stability and the results of numerical and experimental research are presented.

The article [24] considers the issues of mathematical modeling of wind power installations. The results of a computer study of the modes of wind turbines with asynchronous machines and their comparison with the results of experimental studies of the modes of operation of an asynchronous generator in various modes of its operation are presented.

The paper [25] shows the need to use combined autonomous power supply systems based on renewable energy sources. The possibilities of effective research of such systems using their computer modeling based on the package of visual block simulation Simulink of the MATLAB matrix system are presented.

In [26], the issues of logical modeling of a complex technical system that is capable of converting wind and solar energy into electrical energy with subsequent accumulation for further use are considered. Such a technique can be used in the logical analysis and design of new complex technical systems.

In [27], studies were conducted on various types of mathematical models of the incoming air flow velocity and the development of a method for optimizing the operation of wind turbines based on fuzzy logic using a fuzzy wind speed model. Modeling the wind speed is a rather difficult task, since this energy source is constantly changing in time and space. As a result of the research, 4 dominant wind speed models were identified: deterministic, probabilistic, spectral and fuzzy. Each of them finds its own field of application[27]. So, from an energy point of view, at the level of technical and economic developments, the probabilistic model or the Weibull distribution is most applicable. The deterministic model allows us to find the power of wind turbines at a given average wind speed. In those studies where gusts and strong wind changes are taken into account, it is necessary to refer to the spectral model. The fuzzy wind model is convenient and most relevant when modeling wind turbine control processes, since it allows you to form a fairly flexible control system.

In the process of building automatic power supply systems based on wind turbines, they face such problems as choosing the right ratio of battery capacities, properly configuring automation systems, improving the performance of control systems, etc. [28]. These problems, as well as others, can be solved based on the method of modeling the operating modes of wind turbines, which requires a dynamic wind model. From the standpoint of wind energy, the longitudinal component of wind speed is of the greatest interest, which is modeled in the article [28]. The Kaimal spectral model was used to model the dynamic component of wind speed [28]. The degree of modeling accuracy can be adjusted using the developed model. In addition, it has a simple structure, is

easily implemented by means of simple application programs and can find practical application in scientific research on small wind power.

Questions concerning the influence of the angle of inclination of the blade surface on the performance of wind turbines are considered in [29]. For various wind parameters, the results of numerical research and calculations of the angles of inclination of the blade surface are obtained.The analysis of the dependencies of the speed and power indicators of rotation on the angle of inclination is carried out. Vector pictures of the main forces influencing a flat surface when moving around a fixed axis are shown.

The effects of changes in grid voltage and frequency on the performance of the grid connected to a wind-electric generating system for different wind speeds are studied in [30]. The simulation of the induction of the generator, wind turbine and other network components was carried out using the MATLAB / Simulink program. A simple modeling procedure has been developed for preliminary determination of the system efficiency, and the simulation results are presented.

The article [31] is dedicated to the study of a wind turbine simulator. The simulator is designed to generate wind energy on its shaft and provide static and dynamic characteristics of the proposed turbine. The general structure of the simulator consists of two subsystems: a "virtual simulator" that implements real-time simulation of a wind turbine based on a mathematical model [31] and an electromechanical tracking system that receives a signal from a virtual simulator and provides a measurable output variable transmitted as a response variable to the virtual simulator.

Figure 1.4 shows the graphical interface of the developed wind turbine simulator in real mode.

The work [32] is devoted to the creation of a computer simulation model of a hybrid wind turbine with an asynchronous generator with permanent magnets in the MatLab Simulink system for the study of static and dynamic processes. The adequacy of the developed model was tested in the operating conditions of the wind turbine on a pilot basis. The dependences of the volume of electricity generated by a hybrid wind turbine on the selected voltage of an intermediate DC energy storage device for various wind conditions are established.

Fig.1.4. Graphical interface of the wind turbine simulator in real mode

1.2 The current state of the problem

The need for the development and construction of wind turbines operating at low wind speeds on the territory of Kazakhstan, where there is no centralized power supply, is determined by some important points: because the value of the area of the Republic of Kazakhstan is large (2.7 million km2) centralized power supply is inefficient; huge losses of electricity during transportation from a low population density of the Republic of Kazakhstan (6.93 people/km2). To solve the current problems with the country's electronic supply, it is necessary to apply and implement low-power wind turbines as local autonomous sources of electric energy, which in turn will cover the needs for electric energy of the population living in remote and sparsely populated areas[32-34].

In the passport data of many wind turbines, 2 m/s are indicated as the initial wind speed for energy generation, unfortunately, in practice, at a wind speed of 2.5-4 m/s, none of them generates electric energy[33]. Even the content of the multiplier does not improve this situation [34].

The developments of wind turbines of Kazakhstani scientists and engineers, who took into account the climate of the country, are mainly wind turbines with a vertical axis of rotation and, in this regard, certain limitations: low limit for self-starting of a wind power plant; the height of the wind turbine mast is low, and as a result, the limited

winds at high altitudes; due to existing fatigue loads, rapid failure of the blades occurs; the inability to turn the angle of installation of the blades; low coefficient of wind energy use (< 30%), as well as low efficiency of operation at low wind speeds [35].

Currently, the well-known wind power plants of the horizontal rotation type of well-known companies are designed for generating electric energy from 5 to 25 m/s, which must be installed focusing on the wind flow, and it is also inefficient to use in the wind atlas of the Republic of Kazakhstan, since self-disconnection occurs at the strongest air flows (more than 20 m/s), and are ineffective at low speeds up to 6 m/s [35].

The above points contribute to the search for new methods and ways to optimize the designs of wind power plants with a horizontal axis of rotation, since there are no wind turbines for areas with low wind speeds[35].

At the same time, it is possible to optimize the designs of wind turbines designed for small values of air flows (less than 6 m/s), using a lot of theoretical and practical experience[36-40].

2. THE METHOD OF NUMERICAL MODELING OF AERODYNAMIC CHARACTERISTICS

2.1. Equations of thermal convection

In the case when macroscopic motion is excluded in the liquid, the liquid is able to exist in mechanical equilibrium.

For a liquid in a state of equilibrium located in a homogeneous gravity field $grad(p) = \rho\bar{g}$, at an oscillating temperature in the liquid, the Euler equation can be satisfied.

Based on the above, the question of the stability of the equilibrium is formed [41]. In order for the equilibrium to be stable, certain conditions must be met. In the opposite case, if the conditions are not met, the nature of the equilibrium is unstable, which is characterized by disorder in the liquid, which in turn is called *thermal convection* [42]. The stability condition of the mechanical equilibrium is directly proportional to the condition of the absence of convection. Convection can be observed if the following conditions (2.1)are not met:

$$-\frac{dT}{dz} < \frac{g\beta T}{c_p}, \tag{2.1}$$

where, c_p – specific heat capacity at constant pressure, $\beta = \frac{1}{V}(\frac{\partial V}{\partial T})_p$ – temperature coefficient of expansion; that is, if the temperature falls in the direction from the bottom up, and its gradient exceeds the absolute value specified in the condition.

We derive an equation describing convection [42]. In this case, the liquid is characterized as an incompressible medium. Based on this, the change in density can be neglected, since it is assumed that the pressure is almost constant, which facilitates the solution of systems of equations.

But nevertheless, due to the uneven heating of the liquid, it is impossible to ignore the instability of density, which leads to the emergence of forces that contribute to convective motion.

To describe the convection of a liquid as an incompressible medium, the Boussinesq model is used. The corresponding approximate equations are usually called the convection equations in the Boussinesq approximation [43].

In this situation, the variable temperature has the form $T = T_0 + T'$, where T_0 is a constant average value, from which the temperature unevenness is calculated [43]. We will assume T' that it is small compared to . Let's write the density of the liquid in the form with a constant . Due to the insignificance of the temperature change T', the density change ρ' caused by it is also small, and we can write (2.2):

$$\rho' = \left(\frac{\partial \rho_0}{\partial T} \right)_p T' = -\rho_0 \beta T', \tag{2.2}$$

where, $\beta = \rho^{-1}(\partial\rho / \partial T)$ – temperature coefficient of expansion.

The value p_0 will not be const when $p = p_0 + p'$. This pressure at (equal T_0 to and p_0) temperature and density corresponds to mechanical equilibrium, and changes in accordance with the hydrostatic equation, with increasing height

$$p_0 = -\rho_0 gz + const, \tag{2.3}$$

where, z- coordinate is counted vertically upwards.

Based on this, we obtain a system of equations describing the thermogravitational convection of an incompressible fluid in the Boussinesq approximation[43]:

Navier-Stokes equation (2.4):

$$\frac{\partial \bar{\upsilon}}{\partial t} + (\bar{\upsilon}\nabla)\bar{\upsilon} = -\nabla \frac{p'}{\rho_0} + \nu \Delta \bar{\upsilon} - \beta \bar{g} T' \tag{2.4}$$

The equation of thermal conductivity (2.5):

$$\frac{\partial T'}{\partial t} + \bar{\upsilon}\nabla T' = \chi \Delta T'. \tag{2.5}$$

The continuity equation (2.6):

$$div(\bar{\upsilon}) = 0, \tag{2.6}$$

where, $\bar{\upsilon}$ – velocity vector, p' – pressure change, T' – temperature change, ν – coefficient of kinematic viscosity, ρ_0 – hydrostatic density value, $\chi = \frac{k}{c_p \rho}$ – coefficient of thermal diffusivity, k – coefficient of thermal conductivity, c_p – specific heat capacity at constant pressure [39-41].

Based on the assumptions based on equations (2.2) – (2.4), we can say that the main regularity is the leakage of (not strong) convection: in addition to the equation of motion (2.2), where the deviation is taken into account from the lifting force, the deviations of the plane from the average value are considered small, which are caused by the heterogeneity of the temperature regime. Some inconsistency of the Boussenes

approximation means taking into account the inhomogeneity of the density in the equation of motion. It is established that the equations efficiently determine the important parameters of thermal convection in the laboratory conditions[39-41].

Under certain conditions, the setting of temperature and heat flow can be seen on the limits of the cavity that the liquid fills.

Under certain conditions, it is possible to see the establishment of temperature and heat flow only within the limits of the cavity that the liquid fills. Then, the equations and boundary conditions will have the following characteristics: the characteristic length of the cavity L, the characteristic temperature difference Θ, the time τ, which characterizes the unsteadiness of the external conditions, and the liquid parameters ν, χ, gß. 2 independent dimensionless combinations can be constructed from these values (2.7):

$$\mathrm{R} = \frac{g\beta\Theta L^3}{\nu\chi},\ \mathrm{P} = \frac{\nu}{\chi} \tag{2.7}$$

where, R,P ,– the so-called Rayleigh numbers (R), Prandtl (P). The Prandtl number depends only on the properties of the substance of the liquid itself; the Rayleigh number is the main characteristic of convection.

If the numbers R and P of the flow are equal, then the two flows are similar. The Nusselt number characterizes the heat transfer during convection in a gravitational field (2.8):

$$\mathrm{N} = \alpha l / \kappa, \tag{2.8}$$

where, $\alpha = \frac{q}{T_1 - T_0}$ – heat transfer coefficient between solids and liquids, κ – coefficient of thermal conductivity of the medium, *l* – characteristic size.

The nature of the convection movement can be both turbulent and laminar. The beginning of turbulence is characterized by the Rayleigh number, based on this, the nature of the movement is turbulent, for large numbers R .

A flow where a liquid or gas moves without mixing and pulsations (that is , random and rapid changes in velocity and pressure) by layers is called laminar.

In a flow where multi-layered nonlinear fractal waves and ordinary linear waves of various sizes are spontaneously formed, without the presence of external, random, disturbing forces and/or in their presence when the velocity of the liquid or gas increases, it is called turbulent[41-43].

2.2 Equations of motion

Consider the motions of an incompressible viscous fluid with unchanged physical properties. The equations describing the motion of an incompressible viscous fluid express the conservation of mass and the amount of motion (2.9), (2.10):

$$\nabla \cdot \bar{\upsilon} = 0 \tag{2.9}$$

$$\frac{\partial}{\partial t}\bar{\upsilon} + \frac{1}{2}\nabla(\bar{\upsilon}\cdot\bar{\upsilon}) + (\nabla\times\bar{\upsilon})\times\bar{\upsilon} + 2\bar{\Omega}\times\bar{\upsilon} + \bar{\Omega}\times(\bar{\Omega}\times\bar{r}) = \\ = -\frac{1}{\rho}\nabla P + \bar{F} - \nu\nabla\times(\nabla\times\bar{\upsilon}), \tag{2.10}$$

where, $\bar{\upsilon}$ – the velocity of a particle measured in a coordinate system rotating with a constant angular velocity $\bar{\Omega}$; $\bar{r}$, t, P, ν, $\bar{F}$ represent, respectively, the radius-vector of the particle, time, pressure, density, kinematic viscosity and mass force related to the unit of mass. The mass force is assumed to be conservative $\bar{F} = \nabla A$, so that it, together with the centrifugal force and P, can be written in the form of reduced pressure (2.11).

$$p = P + \rho A - \frac{1}{2}\rho(\bar{\Omega}\times\bar{r})\cdot(\bar{\Omega}\times\bar{r}) \tag{2.11}$$

This makes the equation easier (2.12)

$$\frac{\partial}{\partial t}\bar{\upsilon} + \bar{\upsilon}\cdot\nabla\bar{\upsilon} + 2\bar{\Omega}\times\bar{\upsilon} = -\frac{1}{\rho}\nabla p - \nu\nabla\times(\nabla\times\bar{\upsilon}) \tag{2.12}$$

The invariant vector representation is used less often than the full form of convective acceleration $\bar{\upsilon}\cdot\nabla\bar{\upsilon}$.

If we enter $\bar{\Omega} = 0$, then from the previous equations we get the equations of motion in the inertial coordinate system.

In an inertial and rotating velocity system, particles are joined by wedges $\bar{\upsilon}_{inert} = \bar{\Omega}\times\bar{r} + \bar{\upsilon}_{rot}$.

Since sliding along solid impermeable surfaces or crossing them is impossible, it is necessary that the viscous liquid should move along with these surfaces. The establishment of the normal component of the velocity under the condition of the absence of sliding or a relative tangential one [42-45] is possible if the surface is permeable.

Parts that rotate uniformly at an angular velocity $\overline{\Omega}_W$, focused on the boundary surface. Boundary condition on such a surface (2.13)

$$\overline{\upsilon} = (\overline{\Omega}_W - \overline{\Omega}) \times \bar{r} \tag{2.13}$$

The description of the initial velocity field ends with the formulation of problems(2.14)

$$\overline{\upsilon}(\bar{r}, 0) = \overline{\upsilon}_*(\bar{r}) \tag{2.14}$$

Based on this, we can conclude that in a fixed domain with boundary conditions (2.15) and (2.16), it is necessary to solve equations (2.13) and (2.14).

Let L, Ω^{-1}, U they characterize the typical length, time, and relative velocity of the particle. By writing down the normalized values $L\bar{r}$, $\Omega^{-1}t$, $U\overline{\upsilon}$, $\Omega\bar{k}$, $p\Omega ULp$ of variables $\bar{r}$, t, $\overline{\upsilon}$, $\overline{\Omega}$, p, it is possible to obtain the equation in a dimensionless form [46]:

$$\nabla \cdot \overline{\upsilon} = 0 \tag{2.15}$$

$$\frac{\partial}{\partial t}\overline{\upsilon} + \varepsilon \overline{\upsilon} \cdot \nabla \overline{\upsilon} + 2\hat{\bar{k}} \times \overline{\upsilon} = -\nabla p - E \nabla \times (\nabla \times \overline{\upsilon}) \tag{2.16}$$

with appropriate boundary conditions. (The icon marks the unit vector.) Based on this, two parameters are detected: the Ekman number (2.17).

$$E = \frac{\nu}{\Omega L^2} \tag{2.17}$$

and the Rossby number by the formula (2.18)

$$\varepsilon = \frac{U}{\Omega L} \tag{2.18}$$

The Ekman number is an approximate measure of the ratio of the characteristic viscosity force to the Coriolis force and is essentially the inverse of the Reynolds number. In parallel, the Rossby number is the ratio of the convective acceleration to the Coriolis acceleration, as well as a general estimate of the relative value of the nonlinear terms. When applying rotational effects, the value of the Ekman number is very small. In practice, the value 10^{-5} is common to it and in the future the assumption E << 1 is applied without further reservations. The Rossby number is on the order of one or less; in the linear model, it is assumed that its value is infinitely small [46-48].

The dimensionless vortex equation in a rotating system is solved by the formula (2.19)

$$\frac{\partial}{\partial t}\overline{\omega} + \cdot\nabla\{(\varepsilon\,\overline{\omega} + 2\hat{\bar{k}})\times\overline{\upsilon}\} = -E\,\nabla\times\nabla\times\overline{\omega}\,, \tag{2.19}$$

where, $\overline{\omega} = \nabla\times\overline{\upsilon}$ - in a rotating system, the nontrivial state of solid rotation is responsible for the trivial solution of these equations, $\overline{\upsilon}$ = 0. The dimensional velocity is $\overline{\upsilon}_{inert} = \hat{\bar{k}}\times\bar{r}$, in an inertial system. Over time, in a closed uniformly rotating vessel, the viscous liquid tends to this natural state of rigid rotation

2.3 Elements of the vorticity theory

First of all, it is necessary to introduce the differences between the relative $\overline{\omega}$ and absolute $\overline{\omega}_a$ vortices measured in a uniformly rotating and inertial system, respectively.

$$\overline{\omega}_a = \nabla\times\overline{\upsilon}_{inert} = 2\overline{\Omega} + \nabla\times\overline{\upsilon}_{rot} = 2\overline{\Omega} + \overline{\upsilon} \tag{2.20}$$

The same difference is established for closed-loop circulation, which solves equation (2.21)

$$\Gamma_a = \oint_L \overline{\upsilon}_{inert}\cdot d\bar{s} = \oint_L \overline{\upsilon}_{rot}\cdot d\bar{s} + \oint_L \overline{\Omega}\times\bar{r}\cdot d\bar{s} = \Gamma + \oint_L \overline{\Omega}\times\bar{r}\cdot d\bar{s}\,, \tag{2.21}$$

Some transformation of the last integral leads to the form (2.22)

$$\Gamma_a = \Gamma + \oint_L \hat{\bar{n}}\times\hat{\bar{k}}\cdot d\Sigma = \Gamma + 2\Omega\Sigma_p\,, \tag{2.22}$$

where, Σ_p — surface projection Σ, bounded by a contour L, on a plane perpendicular to the vector $\overline{\Omega} = \Omega\hat{\bar{k}}$; $\hat{\bar{n}}$ — the unit vector normal to Σ.

The application of Stokes ' theorem gives an equivalent definition of circulation (2.23)

$$\Gamma_a = \int \bar{\tau}_a\cdot\hat{\bar{n}}d\Sigma\,, \tag{2.23}$$

The vorticity at a certain point is proportional to the instantaneous angular momentum of a spherical fluid element (rigid) at this point, where the instantaneous angular velocity of the particle is equal to $1/2\,\overline{\omega}_a$. The line in the tangent fluid $\overline{\omega}_a$ is called a vortex line. Vortex lines passing through each point of a small closed curve form a vortex tube.

The phenomenon when the cross-sectional area of the tube is small, and the value of the indicator $\bar{\tau}_a \cdot \hat{\bar{n}} d\Sigma$ is constant everywhere along the tube is called intensity [42-45]. This follows from the divergence theorem (2.24)

$$\nabla \cdot \overline{\omega}_a = 0, \tag{2.24}$$

enclosed between the sections $\Delta\Sigma_1$ and $\Delta\Sigma_2$ applied to the volume of the vortex tube. Based on this, it is established that the circulation covering the side surface of the tube is unchanged along a certain contour. Vortex lines cannot arise or end in a liquid, in the case when they are closed, or end at solid boundaries.

With the help of vortex tubes of the same intensity penetrating into the medium, it is possible to imagine the structure of the vorticity field. The central vortex line determines the location of each tube. As the pipes approach, the density of the pipes increases and it is also proportional to the vorticity. Compensating for the reduction in the cross-sectional area, the vorticity increases when the vortex tube is stretched with a constant intensity [46-48].

In inertial space, an exact approximation of the vorticity equation it may look like this (2.25)

$$\frac{d}{dt}\overline{\omega}_a = \frac{\partial}{\partial t}\overline{\omega}_a + \overline{\upsilon}_a \cdot \nabla \overline{\omega}_a = \overline{\omega}_a \cdot \nabla \overline{\upsilon}_a - \nabla \frac{1}{\rho} \times \nabla P + \nu \nabla^2 \overline{\omega}_a \tag{2.25}$$

gives the ratio between the three processes causing this change (right part) and between the convective rate of change of absolute vorticity (left part) . These processes are given in the following order: stretching and rotation of vortex lines, the appearance of vorticity due to changes in density, and the diffusion transfer of vorticity from neighboring elements.

The following are the traditional theorems about the vorticity of inviscid liquids

Lagrange's theorem states that the vorticity field $\overline{\omega}_a = 0$ is 0 if it is zero at the initial moment in an inviscid medium with constant density.

Based on the formula, the closed-loop circulation transformation, the *Kelvin Theorem* (2.26)is drawn out:

$$\frac{d}{dt}\Gamma = -\oint \frac{1}{\rho}\nabla P \cdot d\bar{s}\,, \tag{2.26}$$

Based on this, we can conclude that the circulation along the contour remains unchanged all the time when the liquid is homogeneous or barotropic P = P (P) and there is no dissipation.

The phenomenon when the intensity of a vortex tube remains constant all the time under conditions when it passes together with a liquid explains the Helmholtz Theorem.

The change in the relative vorticity and circulation under the action of the main rotation is shown by the data of the theorem, which were written for a rotating coordinate system[41-48].

2.4 The ANSYS program. Boundary conditions

Calculation methods of wind turbines of various types of devices have been actively developing for a long time with amazing results.

The interrelated problem of wind turbine dynamics and aerodynamics can be solved using numerical modeling. The principle of this method is the solutions of non-stationary Navier-Stokes equations in mobile curved coordinates implemented on the basis of an implicit scheme. In [14-18], wind turbine models were developed and the prediction of wind turbine performance and evaluation of the model's capabilities, as well as its aerodynamic characteristics, were obtained.

The simulation is carried out using the Ansys Fluent software package. Such complex problems as modeling the flow of gases and liquids for industrial tasks, taking into account the phenomenon of turbulence, heat transfer and chemical reactions, can be solved using the Ansys Fluent software package.

Gorenje in furnaces, wing flow, external flow of oil and gas industry installations, convective cooling of the semitrodnik, even the flow of blood in the circulatory system, all this is an example of the application of the Ansys Fluent program [49,50].

The basis of the mathematical solution of the problem is the finite volume method and the solution of the Navier-Stokes equation.With the second order of accuracy, partial derivatives are approximated, time derivatives are approximated according to the implicit second-order Euler scheme. The software package ANSYS [51,53] was used for calculation and modeling. The model belongs to the family of 2 parametric turbulence models, contains transport equations for the kinetic energy of turbulence and its dissipation [51,53].

ANSYS FLUENT is an easy, fault-tolerant tool that allows even unskilled specialists in the field of modeling to achieve high labor productivity.

The calculation technology of the ANSYS program is considered the leader in the number of complicated technical models offered for calculations on unstructured grids. The program contains complexes of elements of different configurations: quadrilaterals

and triangles for two-dimensional calculations, hexahedra, tetrahedra, polyhedra, prisms, pyramids for three-dimensional calculations[50,51].

Grids can be built using the tools of the ANSYS program or using the tools of other programs.

Creating a grid is an integral part of the computer modeling process. The grid affects the accuracy, convergence, and speed of the solution. In addition, the time required to create a model grid is often a significant part of the time required to obtain results from numerical modeling. Therefore, the better and more automated the tools for creating grids, the better the solution.

ANSYS offers the perfect solution-from simple automatic grid creation to a carefully designed grid. Powerful automation capabilities make it easier to initially create a new geometry grid by disabling the physical settings and using smart default settings so that the grid can be obtained on the first attempt.

ANSYS provides the flexibility to create meshes of varying complexity from pure hexadecimal to highly detailed hybrid; the user can place the correct grid in the right place and there is a guarantee that the simulation will accurately confirm the physical model.

ANSYS has a number of tools for creating grids that are suitable for almost all physical tasks. While gearing technologies have been developed to meet the needs of a specific field — solid, liquid, electromagnetic, shell, 2-D or beam models — access to these technologies is available in all areas of physics.

The ANSYS Meshing grid preprocessor is well known to users engaged in strength calculations. The main advantage of the presented tool is versatility, convenience and a high degree of automation, and, of course, a friendly interface. You can also parameterize almost every element of the grid settings, since this product is used by default in the Ansys Workbench environment component. Workbench Meshing allows you to build unstructured (Hexa/Tet) meshes and create prismatic layers (Inflation) [49,51].

However, the full potential of grid generators used to build unstructured meshes for hydrodynamic problems is revealed in Ansys Fluent Meshing. This product is based on its predecessors TGrid and Gambit. This tool is integrated with the Ansys Fluent package, which completely eliminates (or minimizes) any errors in transferring the source grid to the solver. Now Ansys Fluent Meshing is actively developing, supplemented with improvements and useful innovations, raising the bar of quality and the level of user convenience. [50,51].

The ideology of grid construction in Ansys Fluent Meshing is somewhat different from other grid generators of Ansys products. The surfaces of the geometric model are immediately divided by a grid at the import stage, so all further operations are performed based on this feature of the tool. The main power of the package is the built-in scripts for working with" clean "and" dirty " geometry, which allow you to build a high-quality grid in almost three clicks, even for complex multicomponent assemblies. It is also worth noting a wide range of tools for editing, diagnosing and "treating" problem

grids. In addition to all of the above, Ansys Fluent Meshing can generate meshes with a dimension of up to a billion finite volumes. All this, together with the unique technology of filling the three-dimensional grid TGrid, guarantees high quality of its elements even without smoothing procedures. [50,51].

The nonstationary turbulent (low-Reynolds) flow around a two-dimensional body of arbitrary shape, oscillating near the plane interface of media or in an unlimited liquid, is considered. It is assumed that the mass forces exerting effects in the liquid are known and unchanged over time [53]. At the initial moment of time, all the flow characteristics are also known: pressure, components of the velocity vector, density and kinematic viscosity of the liquid [54]. The values of hydrodynamic characteristics at the boundaries of the computational domain, as well as the law of displacement of a streamlined body are known for the entire time interval [55].

It is necessary to find the state of the velocity and pressure fields at subsequent time points, as well as the integral hydrodynamic characteristics of the flow [53-55].

Mass conservation equation (2.27):

$$\nabla \cdot (\rho \vec{V}) = 0, \tag{2.27}$$

where, ρ – density;

$\vec{V}$ – gas velocity vector.

The equation of conservation of momentum (2.28):

$$\nabla \cdot (\rho \vec{V}\vec{V}) + \nabla p = \nabla \cdot \tau_{eff} \quad , \tag{2.28}$$

$$\tau_{eff} = \tau + \tau_{turb}$$

where, τ_{eff} - the equation of conservation of momentum; τ_{turb} - turbulent stress tensor; τ - viscous stress tensor.

$$\tau = \mu\left[(\nabla \vec{V} + \nabla \vec{V}^T) - (\frac{2}{3} \nabla \cdot \vec{V})U \right], \tag{2.29}$$

where, U – the unit tensor; μ – the dynamic viscosity of the gas.

Turbulence model

The velocity gradient is related to the turbulent stress tensor by the following dependence, as stated by the Boussinesq hypothesis (2.30) [55]:

$$\tau_{turb} = \mu_{turb}(\nabla \vec{V} + \nabla \vec{V}^T) - \frac{2}{3}(\rho\kappa + \mu_{turb}\nabla \vec{V})U \ , \tag{2.30}$$

To find the turbulent viscosity μ_{turb} The k-ε Launder-Spaulding model (2.31) is used [53,54]:

$$\mu_{turb} = \rho C_{\mu} \frac{k^2}{\varepsilon} \ , \tag{2.31}$$

where, k - kinetic energy of turbulent pulsations; ε – the rate of dissipation of turbulent kinetic energy.

$$\nabla \cdot (\rho k \vec{V}) = \nabla \left[(\mu + \frac{\mu_{turb}}{\sigma_k}) \nabla k \right] + G_k - \rho$$

$$\nabla \cdot (\rho k \vec{V}) = \nabla \left[(\mu + \frac{\mu_{turb}}{\sigma_k}) \nabla \varepsilon \right] + C_{1\varepsilon} \frac{\varepsilon}{k} G_k - C_{2\varepsilon} \rho \frac{\varepsilon^2}{k}, \tag{2.32}$$

where, G_k – production of turbulent kinetic energy due to shear flow (effect of velocity gradients) [54];

$G_k = 2\mu_{turb} S \div S$ Here S – strain tensor, $S = \frac{1}{2}(\nabla \vec{V} + \nabla \vec{V}^T)$.

Basic mathematical operators.
C – scalar; $\vec{v}$ – vector; T – tensor;

$$\vec{A} = A_x \vec{x}_0 + A_y \vec{y}_0 , \tag{2.33}$$

where, $\vec{x}_0$, $\vec{y}_0$ – orts of the cartesian coordinate system;

$$T = \begin{pmatrix} T_{xx} & T_{xy} \\ T_{yx} & T_{yy} \end{pmatrix}, \tag{2.34}$$

Gradient from a scalar:

$$\nabla C = \frac{\partial C}{\partial x} + \frac{\partial C}{\partial y} \vec{y}_0 , \tag{2.35}$$

Divergence from the vector:

$$\nabla \cdot \vec{A} = \frac{\partial A_x}{\partial x} + \frac{\partial A_y}{\partial y} \ , \tag{2.36}$$

A dyad of two vectors :

$$\nabla\vec{A} = \begin{matrix} \frac{\partial A_x}{\partial x} & \frac{\partial A_y}{\partial x} \\ \frac{\partial A_x}{\partial y} & \frac{\partial A_y}{\partial y} \end{matrix} \qquad \vec{A}\vec{B} = \begin{matrix} A_x B_x & A_x B_y \\ A_y B_x & A_y B_y \end{matrix} , \tag{2.37}$$

The product of a vector by a tensor:

$$\Delta T = \left(\frac{\partial T_{xx}}{\partial x} + \frac{\partial T_{yx}}{\partial y} \right) \vec{x}_0 + \left(\frac{\partial T_{xy}}{\partial x} + \frac{\partial T_{yy}}{\partial y} \right) \vec{y}_0 \tag{2.38}$$

The product of a tensor on a vector:

$$T \cdot \vec{V} = \left(T_{xx} V_x + T_{xy} V_y \right) \vec{x}_0 + \left(T_{yx} V_x + T_{yy} V_y \right) \vec{y}_0 \tag{2.39}$$

Double product of tensors:

$$T : D = T_{11} D_{11} + T_{12} D_{21} + T_{21} D_{12} + T_{22} D_{22} , \tag{2.40}$$

Boundary conditions. Boundary conditions on the *wall.*

The condition of sticking and not leaking: $\vec{V} = 0$;

$$\frac{\partial k}{\partial n} = 0 , \quad \varepsilon_p = \frac{C_\mu^{3/4} \cdot k_p^{3/2}}{\kappa \cdot y_p} , \tag{2.41}$$

where, k = 0,4187 – Karman's constant; index P – refers to the center of the wall cell of the difference grid.

Boundary conditions at the <u>input.</u>

$$U = U_{in} ; V = 0. \tag{2.42}$$

The turbulent flow parameters are determined by setting the intensity of turbulent pulsations I and setting the hydraulic diameter D_{hyd} [54].

$$k = \frac{3}{2}\left(I \cdot V_{\text{in let}}\right)^2;\ \ \varepsilon = C_{\mu}^{3/4} \cdot \frac{k^{3/2}}{\ell};\ \ \ell = 0.07 \cdot D_{hyd}. \qquad (2.43)$$

Boundary conditions at the *output* boundary $\frac{\partial \varphi}{\partial x} = 0$.

The next stage is the numerical implementation of the described mathematical model of the flow of a viscous incompressible fluid [53,54].

2.5 Stages of modeling in ANSYS

The process of studying the modeling of the airflow flow around the blade using the Fluent software package includes the following solution steps, which are shown in the block diagram (Figure 2.1) [56].

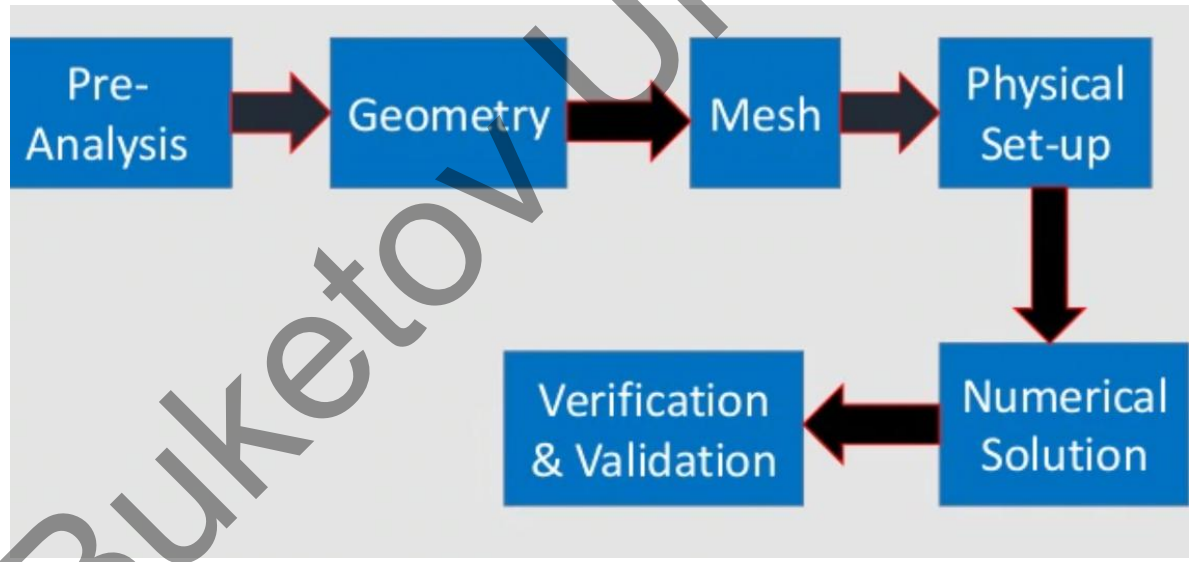

Fig. 2.1. Stages of solving the problem in the Fluent software package

Based on the given block diagram, the following stages of mathematical modeling can be distinguished [50-56]:

1) Pre analysis. Before conducting mathematical modeling of the working elements of a wind power plant, it is necessary to determine which parameters need to be found and under what boundary conditions a numerical study will be carried out.

2) Geometry. At this stage, the geometry is created using the COMPASS 3D and Design Modeler programs. Ansys DesignModeler (Figure 2.2) provides unique modeling functions that include creating parametric geometry, creating a conceptual model, modifying CAD geometry, automatic cleaning and adjustment, as well as several custom tools designed for fluid flow analysis, structural and other types of analysis.

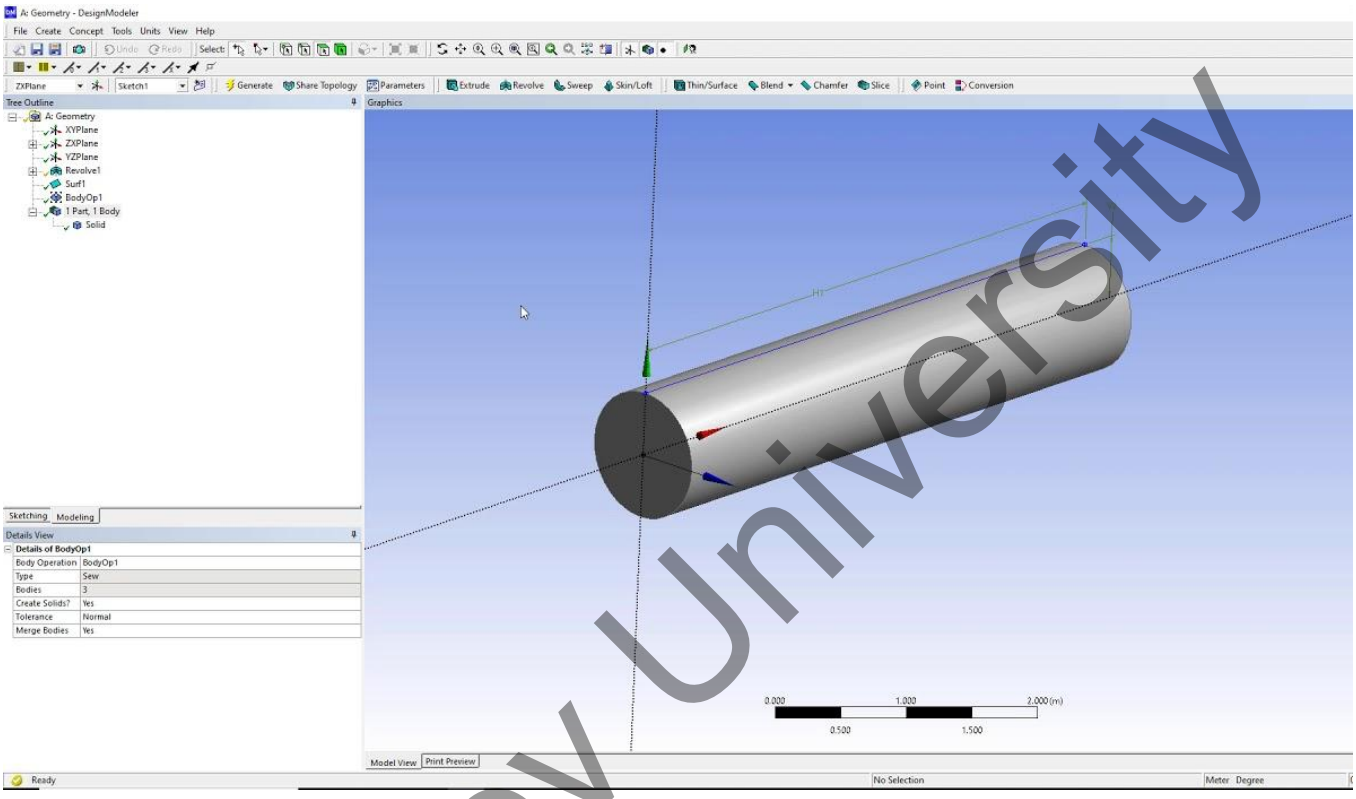

Fig.2.2 Design Modeler Working window

First of all, in order to obtain an accurate solution to the issue under study, it is necessary to build a computational model. To obtain numerical results that coincide as much as possible with the experimental ones with increased quality, without the probability of the formation of non-physical images of the flow, it is necessary to correctly create a computational model, which must be competently divided into finite elements[48-51]. Facilitating the process of obtaining the simulation result, high convergence and stability values can be obtained using a high-quality computational model and grid.

3) Mesh. ANSYS Meshing allows you to generate grid models for different types of analysis (almost all areas of physics). Each of the grid methods satisfies the specific requirements of a particular field (mechanics of deformable solids, fluid dynamics, electromagnetism, etc.) and allows using a simplified formulation of the problem (shell, two-dimensional and beam models) [52].

Below are the boundary conditions that are set at this stage the construction of the calculated grid:

At the entrance:

- Pressure inlet-pressure
- Velocity inlet-speed
- Mass flow - mass flow
- Wall-wall

At the exit:

- Pressure outlet-pressure
- Outflow-the output stream

The resulting calculated grid is exported to the mesh format for further modeling in the ANSYS FLUENT program [46-48].

4) Setup. The working window of ANSYS FLUENT is shown in Figure 2.3. In the left part of the working window of FLUENT there are three main elements: Problem Setup, Solution and Results. With the help of these elements, a turbulence model is configured, a solution method is selected, and the results of solving a mathematical modeling are processed [52].

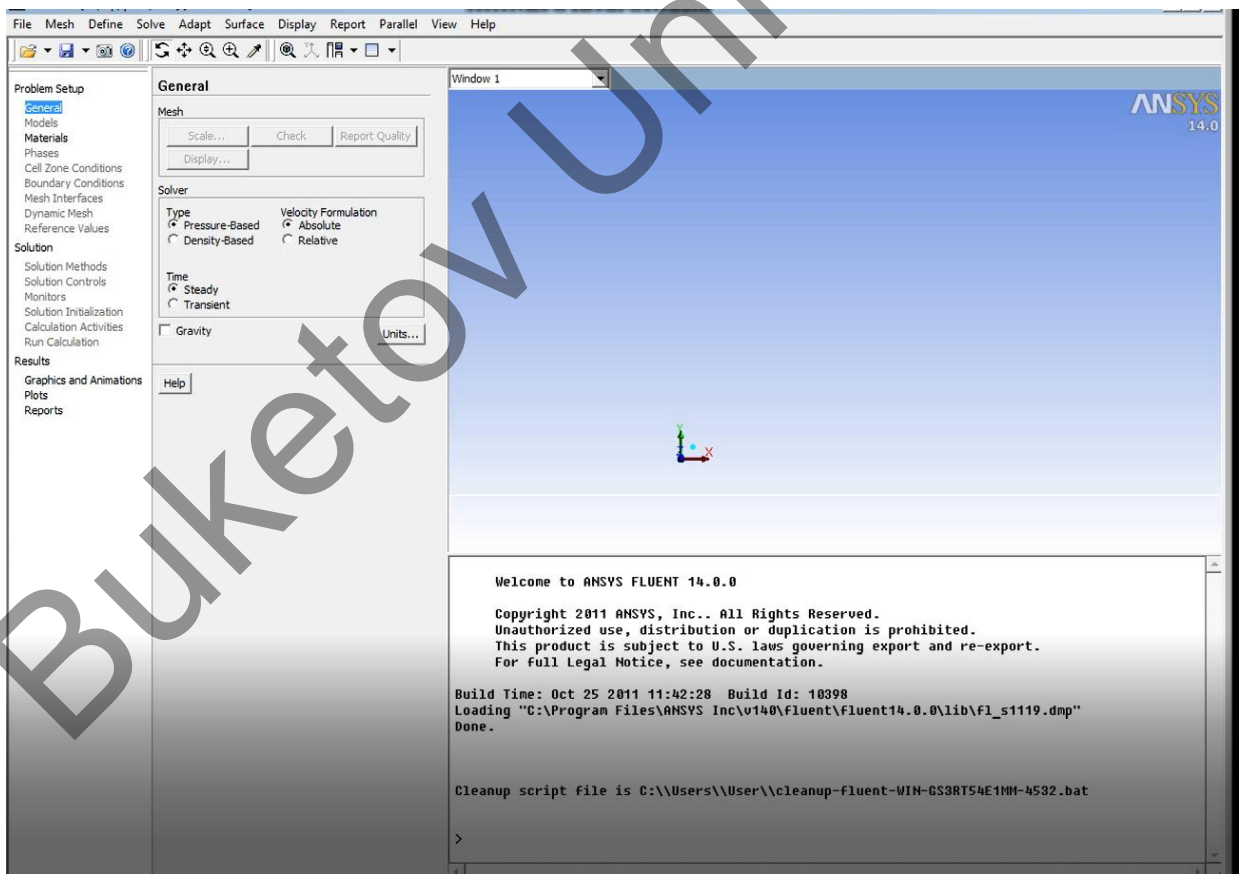

Fig.2.3 The ANSYS FLUENT working window

The main link in setting up the solver is the choice of the turbulence model (Figure 2.4).

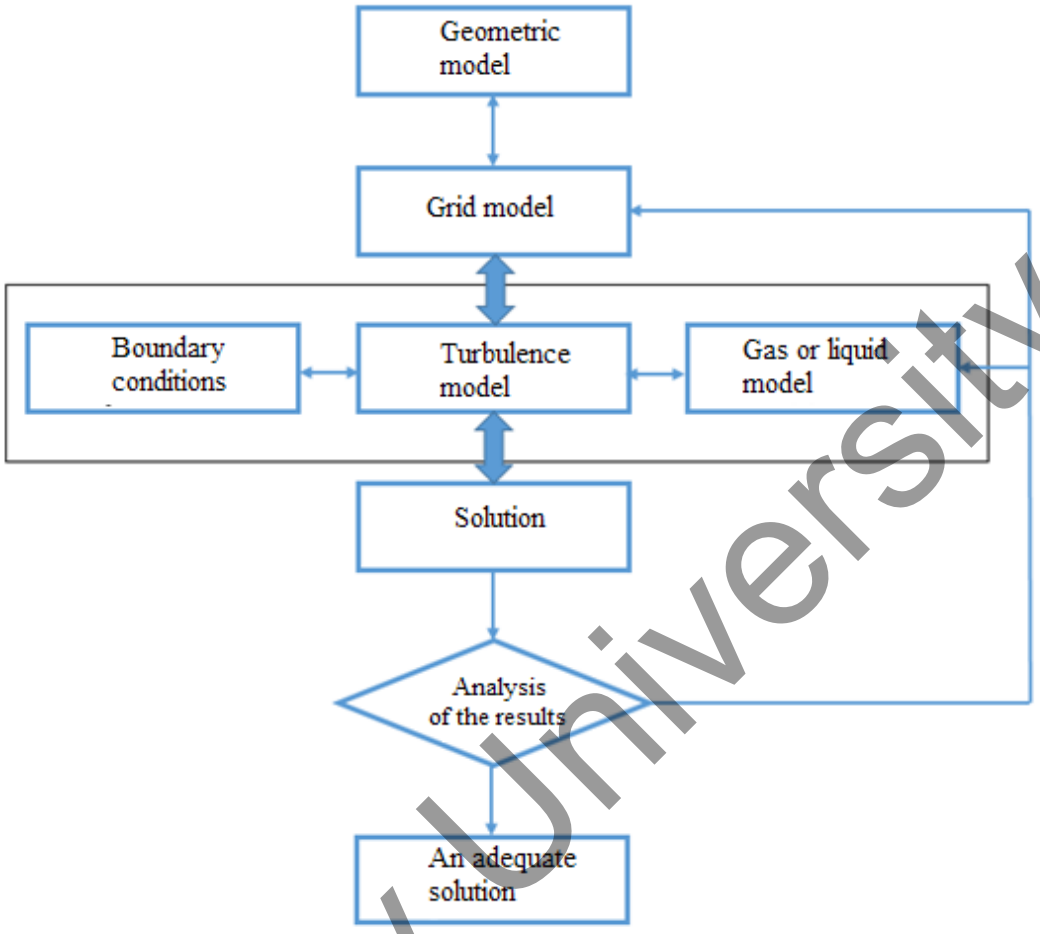

Fig.2.4 Choosing a turbulence model

The k-ε model was chosen as the turbulence model (Figure 2.5). A widely used model in the field of computational fluid dynamics (CFD) is the K-epsilon turbulence model (k-ε), which is used to model the average flow characteristics for turbulent flow conditions. This is a model with two equations that gives a general description of turbulence using two transport equations[52].

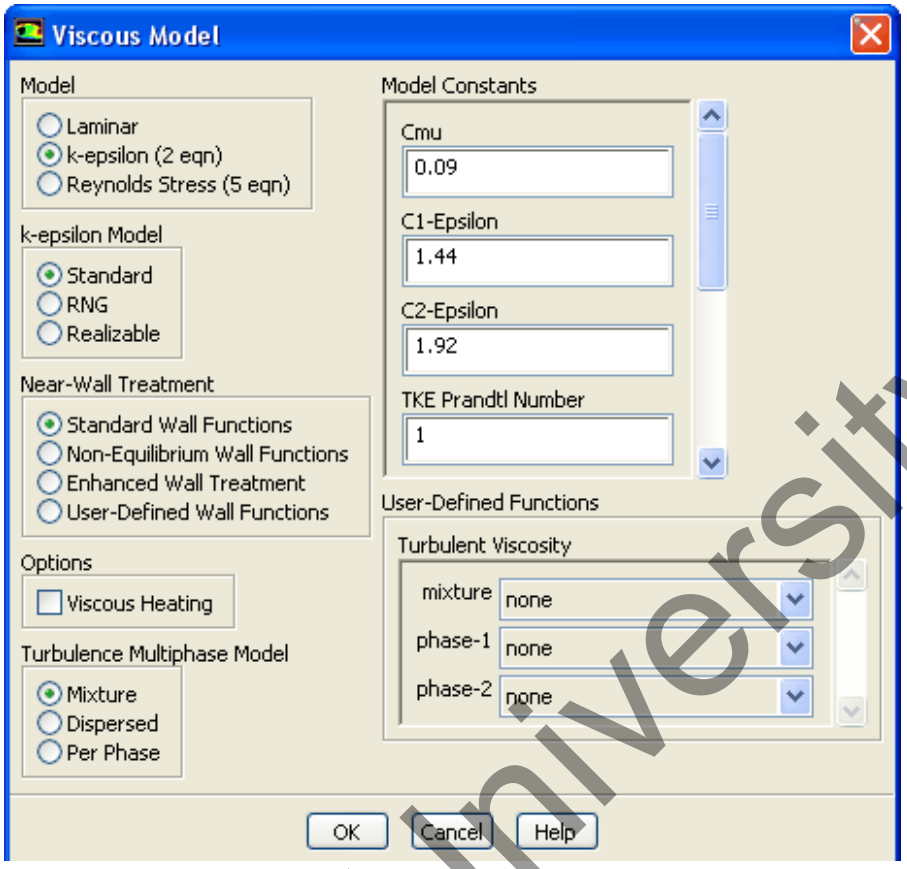

Fig.2.5 k-ε turbulence model

5) Numerical solution. To solve the problem under consideration, an algorithm was used to calculate the flow field SIMPLE (Semi-Implicit Method for Pressure-Linked Equations) (Figure 2.6), which means a semi-implicit method for pressure-linking equations. Discretization (obtaining a finite-difference analog of the original system of differential equations) is performed by the control volume method.

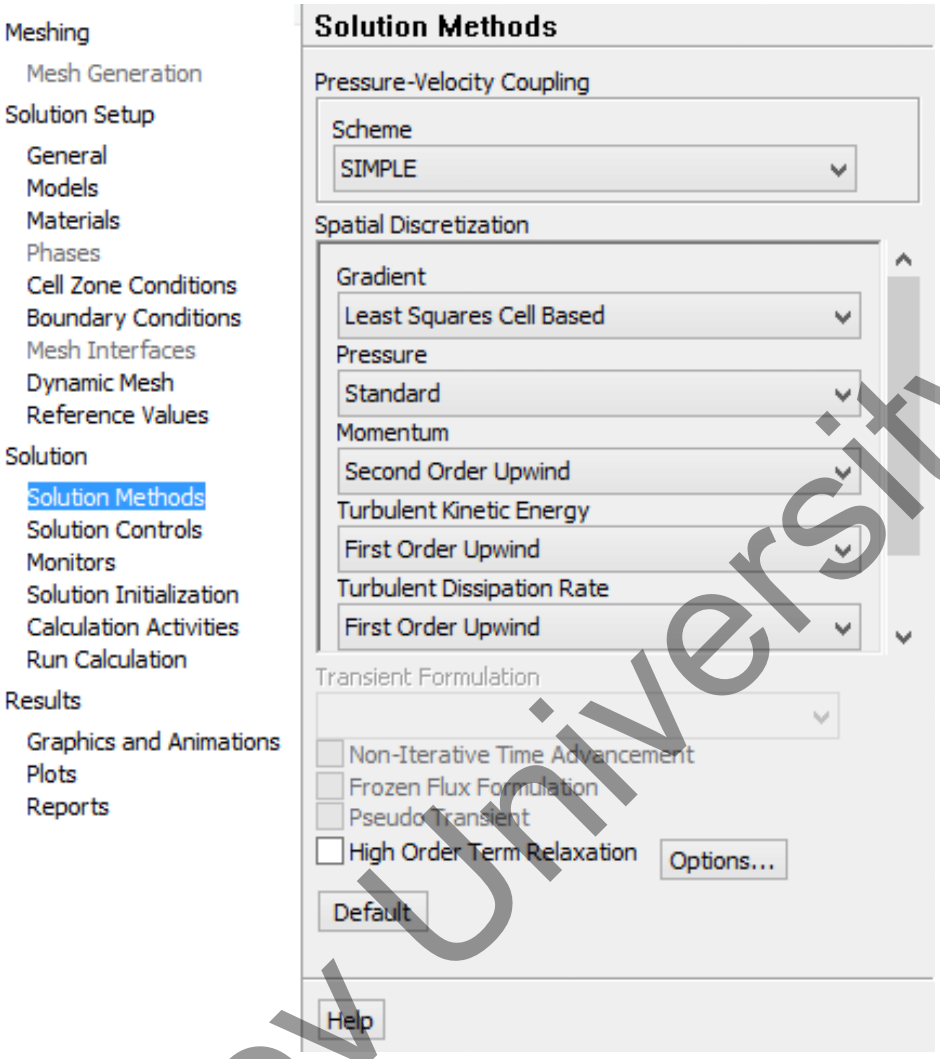

Fig.2.6 Computational solution

6) Verification and validation. The next stage of solving the problem is the processing of the calculation results. Proper use of the postprocessor allows you to assess the adequacy of the calculations made, see the structure of the flow and collect comprehensive information about it. The ability to correctly and fully present the results obtained can significantly facilitate the analysis of the flow pattern and the search for ways to improve it [49-57].

3 MATHEMATICAL MODELING OF AERODYNAMIC CHARACTERISTICS OF WIND POWER PLANTS BASED ON THE MAGNUS EFFECT

3.1 Aerodynamics of the rotating cylinder system based on the Magnus effect

The establishment of dependencies for short cylinders with different end geometries, taking into account changes in the relative length, is necessary for many engineering calculations, studied in detail in the works of S. I. Isataev and O. Zhangunov [58].

Indeed, near the ends of the cylinder of finite length, there is a significant deviation from the picture of a flat flow – the spatial flow prevails. This, in turn, affects the entire aerodynamics of the streamlined body. A significant effect on the aerodynamic drag coefficients of a cylinder of limited length is shown in [59], in which cylinders with flat ends are studied. With a relative length of $L/D = 40$, the value of this coefficient differs by 18% from the data for an infinite cylinder.

A significant reduction in drag and lift entails a reduction in the conditional length of the cylinder [60]. It is established that at L/D = 1.0, the drag force of a short cylinder is 1.3 times higher than that of a ball with such parameters. Based on this, it can be seen that the influence of the shape of the ends on the aerodynamics of short cylinders is significant.

However, some theoretical idea of the influence of the finite length of a transversely streamlined cylinder can be obtained by considering the transverse flow of an ideal incompressible fluid around the ellipsoids of rotation, depending on their elongation, *a/b*, where *a* and *b* are the lengths of the major and minor semi – axes of the ellipsoid. Therefore, we first consider the calculation of the transverse flow around the ellipsoid of rotation by an incompressible ideal fluid.

To calculate the aerodynamic characteristics and mathematical modeling in this paper, we consider a wind-energy installation with blades in the form of rotating cylinders with a smooth surface, created on the basis of the Magnus effect [60-66].

3.2 The process of modeling a two-bladed wind power plant

The process of studying the simulation of air flow around rotating cylinders using the Fluent software package includes the following solution stages: construction of a computational model, construction of a finite-difference grid, launch of the Ansys Fluent solver, processing of the results obtained [60].

To obtain accurate results of the problem being solved, it is necessary to correctly build a calculated model. A computational model correctly divided into finite elements contributes to obtaining an accurate solution of the problem, reduces the probability of non-physical flow patterns and contributes to achieving results close to those obtained experimentally [66-79].

The construction of the model geometry can be carried out in two ways:

1. Creating a geometry by internal means of the program;
2. Creating a model in CAD programs and further importing them.

The internal program Ansys – Gambit was used to build a two-dimensional model of the wind turbine blade.

To build a three-dimensional model of the wind turbine blade, the Kompas-3D_V15 software package was used (Figures 3.1) [50].

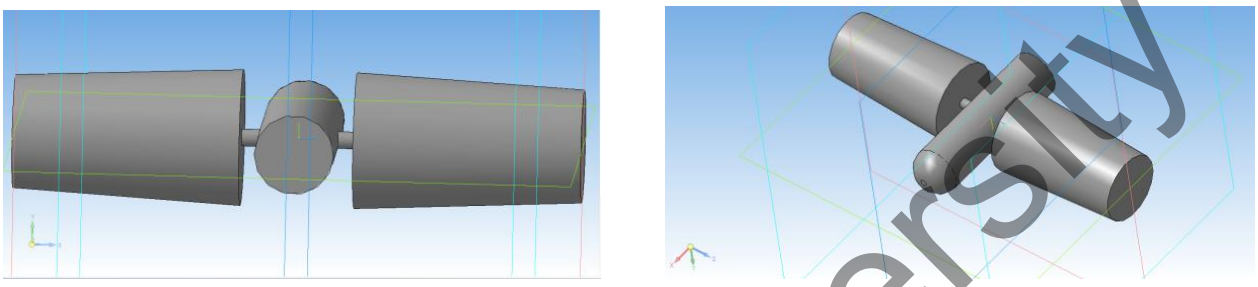

a) front view b) side view

Fig. 3.1. Three-dimensional model of a wind turbine with rotating cylinders

The blades of rotating cylinders are cylindrical elements with the following geometric dimensions: D=12 cm, d=10 cm, l=20 cm.

The parameters of the T-1-M wind tunnel [52,53] are suitable for the streamlined area of the wind turbine.

To proceed to the next stage, the obtained geometric model was exported to the Gambit program and a finite-difference grid was built on the basis of this model [50]. The quality of the grid was checked and the boundaries of the calculated area were set, on which the boundary conditions will be set in the future. Next, the finite-difference grid was exported to the Fluent program.

To determine the effect of the size of the difference grid (number of cells) of the two-dimensional blade model on the drag force, calculations were performed for three difference grids using the model used [49,50]. Table 3.1 shows numerical comparisons of the results of drag forces obtained for different difference grids. The value F_1-corresponds to the drag force obtained from the model used on a grid of 20,000 knots, F_2-40,000 knots, and F_3 – 160,000 knots.

Table 3.1 shows that the differences in the of the drag forces for the grids of 40,000 and 160,000 nodes are almost minimal, and the difference grid of 20,000 nodes has a significant difference [58,59].

Therefore, for a two-dimensional model of a wind turbine in the future, it will be more relevant to use a grid of 40,000 nodes.

Table 3.1

Comparison of drag forces for different difference grids

Velocity, m/s	Drag force		
	F_1, H	F_2, H	F_3, H
4	1,48873618	1,55746091	1,56246019
5	1,76396827	2,39871623	2,4198883
6	3,1004501	3,2549665	3,2643102

To study the effect of the size of the difference grid of a three-dimensional model of the blade on the drag force, a calculation was made for two variants of difference grids: 1-1,000,000 nodes, 2-1,400,000 nodes. Table 3.2 shows the results of calculations of the drag force for various finite-difference grids. The value F1 corresponds to the drag force obtained by the model used on a grid of 1,000,000 nodes, F2 – 1,400,000 nodes, and F3-data obtained experimentally [58,59].

Table 3.2

Comparison of drag forces for different difference grids

Velocity, m/s	Drag force		
	F_1	F_2	F_3
4	1.487361	1.565914	1.551317
6	3.463968	3.264948	3.285612
8	5.100450	5.760617	5.781125

Table 3.2 shows that the values of the resistance force obtained experimentally and by numerical modeling on a finite-difference grid of 1400,000 cells have a slight difference [58,59]. In this regard, for further calculations, we will use a grid of 1,400,000 cells (Figure 3.2).

Modeling in Ansys Fluent is based on the solution of the Navier-Stokes equations, energy and continuity. The system of equations describing the gas flow in vector form is presented in the form [49]:

Boundary conditions at the output boundary:

$$\frac{\partial \varphi}{\partial x} = 0. \qquad (3.1)$$

A standard characteristic package of empirical constants was used for the k–ε turbulence model [50]:

$$C_\mu = 0.09, C_{\varepsilon 1} = 1.44, C_{\varepsilon 2} = 1.92, \sigma_k = 1.0, \sigma_\varepsilon = 1.3. \quad (3.2)$$

The dimensions of the calculated area were taken in accordance with the dimensions of the wind tunnel.

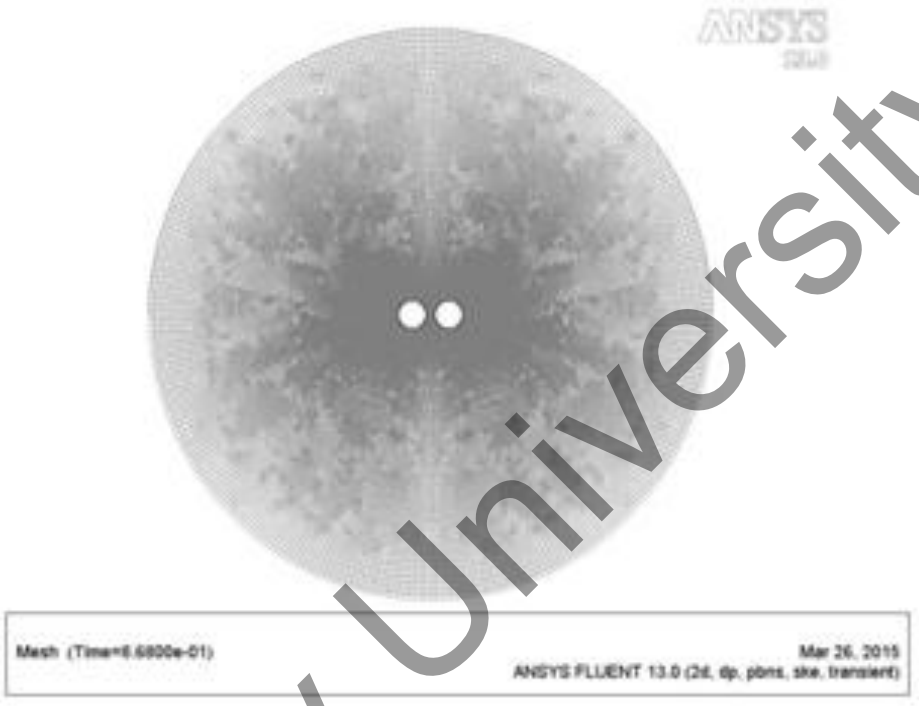

Fig.3.2. Finite-difference grid of rotating cylinders

Numerical modeling was carried out on the basis of solving two – dimensional equations described in the second chapter, boundary conditions (3.1) - (3.2) using the Patankar method, an implicit second-order scheme of accuracy in space for convective terms of the equations, a two-parameter turbulence model k-ε [50].

3.3 Flow pattern and pressure field explaining the physical picture of the appearance of aerodynamic forces around the object of study

At the next stage: the properties of the working fluid and the region are selected; the area is scaled; the type of solver is set; a non-stationary solution model is selected; a turbulent flow model is selected; the turbulence model options are set; the nature of the wall function is set; the air flow velocity at the input boundary is set; the turbulence intensity and hydraulic diameter are set; the main model parameters (Reference Values) are set, relative to which the values of the resistance coefficient are calculated; a method for solving a system of equations is set; a method for calculating pressure and velocity

gradients is selected; a method for calculating moments and the energy equation is specified; information about the coefficient of resistance and lifting force is output; the initial approximation is initialized; the number of iterations is set; the step of change in time is specified; the program for solving the model is launched [50]. After starting the solver, graphs of the dependence of the drag coefficient and lifting force on the time step are displayed in a separate window. There are 20 iterations per time step [49].

The next stage of the solution is the processing of the calculation results.

During the simulation, the patterns of the distribution of the total pressure in the area of numerical integration (Figure 3.3) and current lines (Figure 3.4) were obtained.

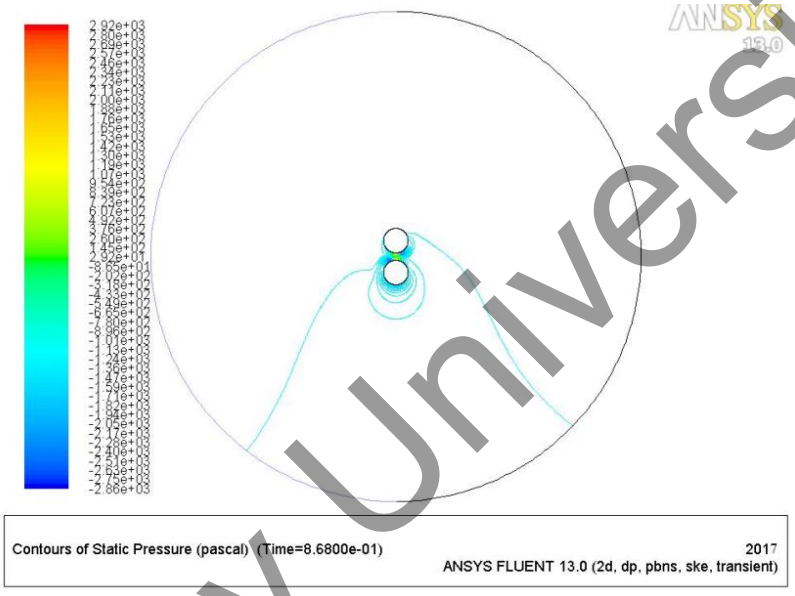

Fig.3.3. Total pressure distribution field

Figure 3.3 shows that a region of increased pressure is observed between the cylinders at the point of contact of the pressure fields of each cylinder, and a rarefaction region is formed behind the cylinders [56].

Figure 3.4 shows the field of distribution of current lines, from which it can be seen that two circulation zones are formed.

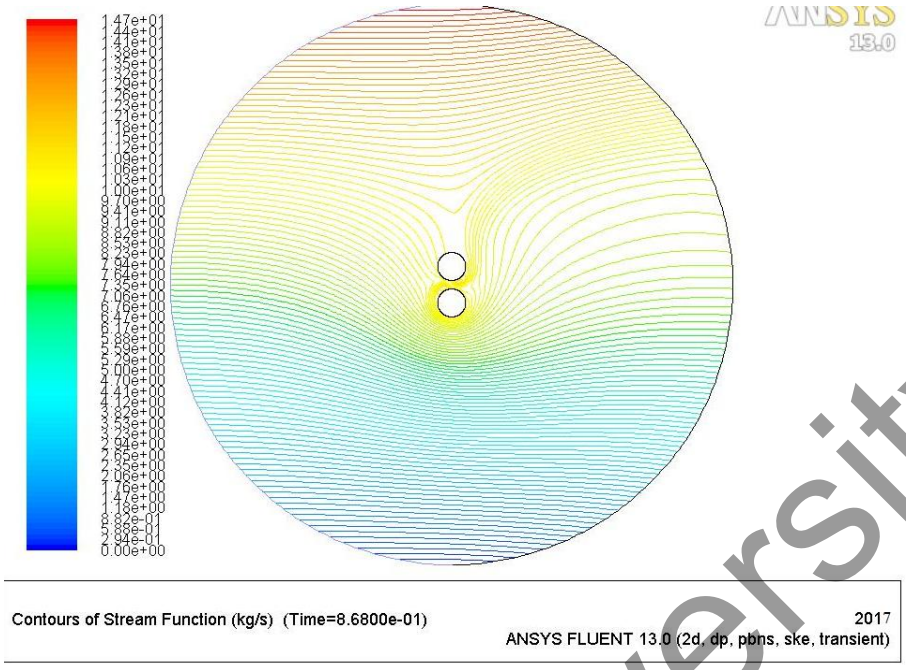

Fig.3.4. Current line distribution field

One circulation zone is located in the lower part of the cylinder, since it moves clockwise, and the second is in the upper part of the second cylinder, since it moves counterclockwise [58]. It follows from this that the cylinders contain a symmetrical character with respect to the axis of symmetry located in their centers.

And it can also be assumed that a vortex-free zone will arise between the two circulation zones.

3.4 Results simulation of a two-bladed wind turbine

A 3D axisymmetric geometric grid model was built in the GAMBIT package [49].

Figure 3.5 shows the flow pattern of a two-blade wind turbine obtained in the Ansys Fluent program.

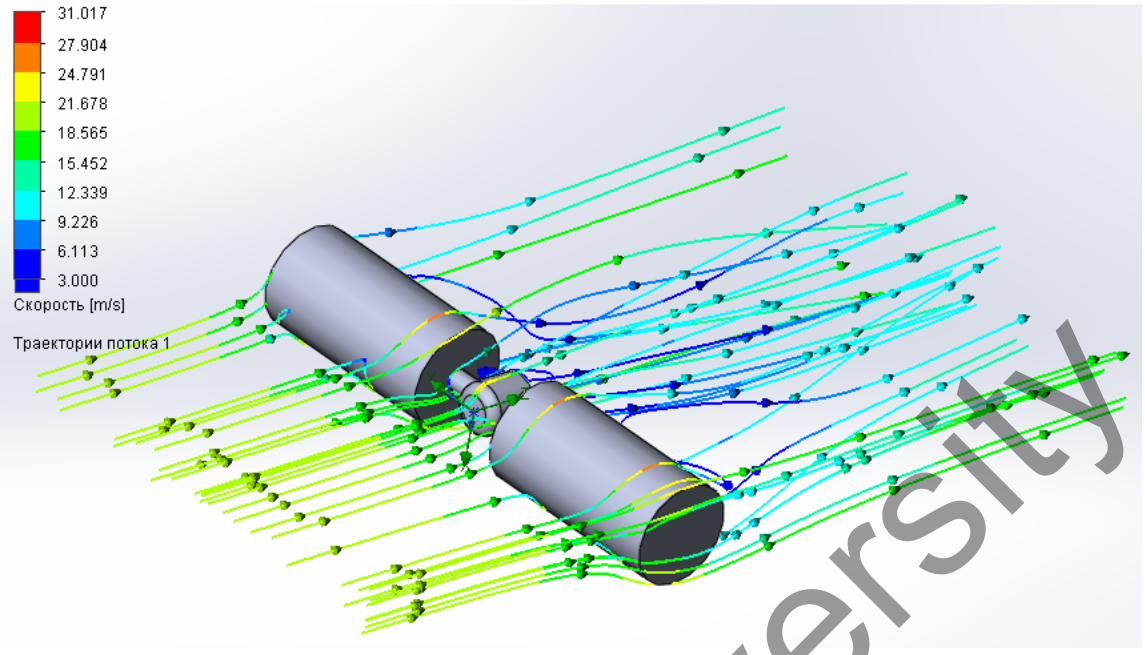

Fig.3.6. The flow pattern of the air flow velocity

Figures 3.7 and 3.8 show the dependences of the drag force and lifting force on the speed of the incoming flow at a turbulence intensity equal to 10% and a constant angular velocity equal to 1000 rpm [59].

The data of the numerical experiment (Figure 3.8) are approximated by the power dependence:. As the speed of the incoming flow increases, the drag force increases.

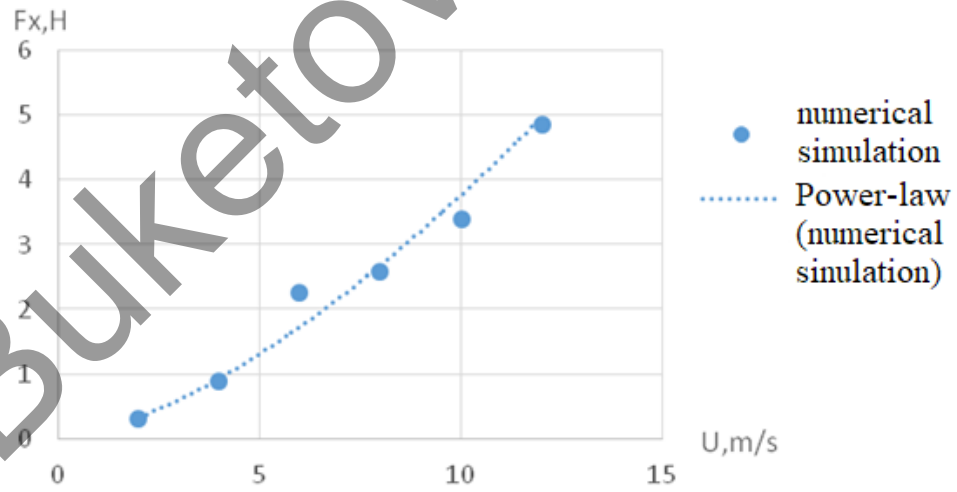

Fig.3.8. The dependence of the drag force on the speed of the incoming flow at an angular velocity equal to 1000 rpm

The data of the numerical study can be approximated by a polynomial dependence $F_y = -0.2257V^2 + 4.9479V - 3.7068$ (Figure 3.9). It follows that with increasing wind speed, the lifting force increases while reaching its maximum at 10 m/s, it falls.

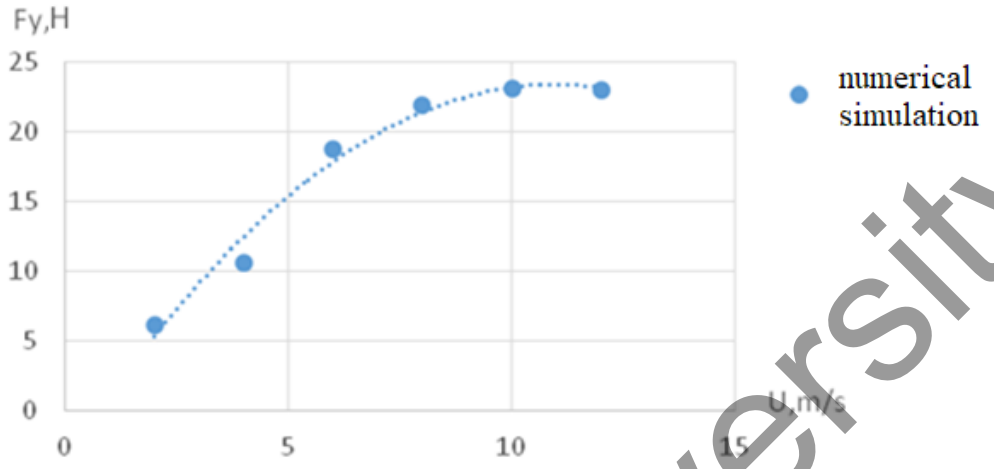

Fig.3.9. The dependence of the lifting force on the velocity of the incoming flow at an angular velocity equal to 1000 rpm.

The obtained results are of an applied nature and can be used with them in the design of a multi-blade wind turbine with rotating cylinders of variable and constant cross-section for field tests. The results of experimental studies show that the use of rotating cylinders of variable cross-section makes it possible to use the additional driving force arising during the flow due to the Magnus effect and convert the energy of the air flow starting from a speed of 3m/s.

4. MATHEMATICAL MODELING OF A THREE-BLADED WIND POWER PLANT BASED ON THE MAGNUS EFFECT

For the theoretical study of the aerodynamics of a three-bladed wind power plant based on the Magnus effect, a mathematical model was created [60.61].

Theoretical calculations and mathematical modeling were carried out jointly with Russian scientists from Tomsk State University in the AnsysFluent software package [61].

Figure 4.1 shows a wind wheel with three cylinders.

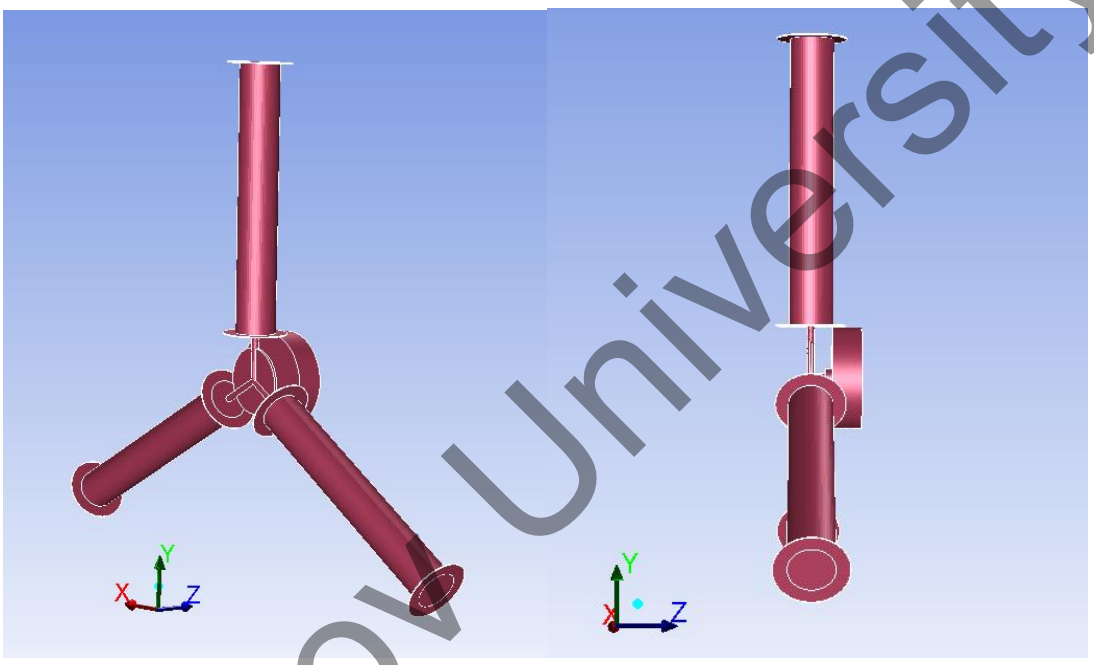

Fig.4.1. A wind wheel with three cylinders

In this case, we consider the flow of air around a wind wheel consisting of three working cylinders located in the xy plane at an angle of 120 ° to each other relative to the z axis of rotation of the wind wheel, Figure 4.1. In the XY plane, the axes of rotation of the cylinders are located, which coincides with the Z axis. The axis of rotation of the wind wheel coincides with the Z axis. Each working cylinder rotates at a speed n relative to its longitudinal axis. The directions of the axes of rotation of the working cylinders are set by the following triples of coordinates: (0, 1, 0), (cos(π/6), –sin(π/6), 0), (–cos(π/6), –sin(π/6), 0). The wind wheel rotates around the *z* axis at a speed of n_1.

Earlier, the author conducted theoretical studies of aerodynamic characteristics on an experimental model of a wind turbine with blades in the form of rotating cylinders, the results of which were published in [63,64].

The main assumptions made when describing the flow of air flowing around a wind power plant [61]

1. Due to the low values of the Mach numbers (the ratio of the gas velocity to the local speed of sound, M<<0.1) the air flow is described by the equations valid for the incompressible medium.

2. Due to the large Reynolds numbers (the ratio of inertial forces to viscosity forces, $Re>10^4$), the flow is turbulent.

3. Due to the low values of Mach numbers and insignificant temperature differences in the vicinity of the wind wheel, the flow is isothermal [60].

A system of equations describing the flow of air flowing around a wind wheel

$$\frac{\partial u_j}{\partial x_j} = 0 \tag{4.1}$$

$$\frac{\partial \rho u_i}{\partial t} + \frac{\partial \rho u_i u_j}{\partial x_j} + \frac{\partial p}{\partial x_i} = \frac{\partial \tau_{ij}}{\partial x_j} \tag{4.2}$$

where $\tau_{ij} = \left(\mu + \mu_t\right)\left[\frac{\partial u_j}{\partial x_i} + \frac{\partial u_i}{\partial x_j}\right]$ – stress tensor;

The Realizable k-ε Turbulence Model

The equation of turbulent energy (4.3):

$$\frac{\partial \rho k}{\partial t} + \frac{\partial \rho k u_j}{\partial x_j} = \frac{\partial}{\partial x_j}\left[\left(\mu + \frac{\mu_t}{\sigma_k}\right)\frac{\partial k}{\partial x_j}\right] + G_k - \rho\varepsilon \tag{4.3}$$

Equation of the specific velocity of turbulent energy dissipation (4.4):

$$\frac{\partial \rho \varepsilon}{\partial t} + \frac{\partial \rho \varepsilon u_j}{\partial x_j} = \frac{\partial}{\partial x_j}\left[\left(\mu + \frac{\mu_t}{\sigma_\varepsilon}\right)\frac{\partial \varepsilon}{\partial x_j}\right] + \rho\varepsilon\left(C_1 S - C_2 \frac{\varepsilon}{k + \sqrt{\nu\varepsilon}}\right) \tag{4.4}$$

Production of turbulent kinetic energy $G_k = \mu_t S^2$, where $S = \sqrt{2S_{ij}S_{ij}}$ – modulus of the strain rate tensor (4.5):

$$C_1 = \max\left(0.43, \frac{\eta}{\eta + 5}\right),\ \eta = S\frac{k}{\varepsilon},\ C_2 = 1.9. \tag{4.5}$$

Coefficient of turbulent viscosity $\mu_t = \rho C_\mu \frac{k^2}{\varepsilon}$,

where $C_\mu = \frac{1}{A_0 + A_s \frac{kU^*}{\varepsilon}}$, $U^* = \sqrt{S_{ij}S_{ij} + \Omega_{ij}\Omega_{ij}}$, $\Omega_{ij} = \overline{\Omega_{ij}} - \varepsilon_{ijk}\omega_k$.

$\overline{\Omega_{ij}}$ – the vorticity tensor in a coordinate system moving with angular velocity ω_k.

$$A_0 = 4.04,\ A_s = 6\cos(\phi),\ \phi = \frac{1}{3}\cos^{-1}\left(\sqrt{6}W\right),\ W = \frac{S_{ij}S_{jk}S_{ki}}{\tilde{S}^3},\ \tilde{S} = \sqrt{S_{ij}S_{ij}},$$

$$S_{ij} = \frac{1}{2}\left(\frac{\partial u_i}{\partial x_j} + \frac{\partial u_j}{\partial x_i}\right),\ \Omega_{ij} = \frac{1}{2}\left(\frac{\partial u_i}{\partial x_j} - \frac{\partial u_j}{\partial x_i}\right)$$

ε_{ijk} – components of the Levi-Civitt tensor.

Turbulent Prandtl numbers $\sigma_k = 1,\ \sigma_\varepsilon = 1.2$.

Boundary conditions

For the turbulent kinetic energy on the wall of the studied region, the boundary conditions are written in the following form (4.6):

$$\frac{\partial k}{\partial n} = 0 \tag{4.6}$$

and the rate of dissipation of turbulent kinetic energy ε in the wall region is calculated from the condition of equality of the production of kinetic energy of turbulent pulsations and its dissipation and the assumption of the logarithmic distribution of the average gas velocity (4.7) [60,61]:

$$\varepsilon_p = \frac{C_\mu^{0.75} k_p^{1.5}}{\kappa y_p} \tag{4.7}$$

where κ=0.42. Value y_p this is the distance from the center of the wall cell to the wall, if $y_p > \frac{\mu}{\rho C_\mu^{0.25} k_p^{0.5}} y^*$, otherwise $y_p = \frac{\mu}{\rho C_\mu^{0.25} k_p^{0.5}} y^*$. Here $y^* = 11.225$

Boundary conditions at the entrance to the region (4.8), (4.9):

$$u_x = 0, u_y = 0, u_z = V \tag{4.8}$$

$$\varepsilon = C_{\mu}^{0.75} \frac{k^{1.5}}{0.07 D_h}, \; k = \frac{3}{2}(V \cdot I)^2 \tag{4.9}$$

where D_h – the hydraulic size of the input area of the region was assumed to be equal to 1 m.

I – the intensity of turbulent pulsations was assumed to be equal to 0.1.

Boundary conditions at the exit from the region: $p = p_{ex}$.

Boundary conditions on the walls of the wind turbine: $u_i = U(t,x,y,z)$,

where $U(t,x,y,z)$ is the speed of movement of the walls, which is influenced by the speed of rotation of the cylinders around the axis of the wind turbine and the speed of rotation of the working cylinders around their own longitudinal axis[61-65].

Methods for solving the system of equations (4.1-4.9)

The system of equations (4.1-4.9) is solved in the Ansys-Fluent package using the finite volume method and the approach of multiple (nested) coordinate systems [49,50].

The entire region was divided into three types of nested subdomains (Figure 4.2): subdomains of the 1st type (cylinders) built around the working cylinders of the wind wheel and the working cylinders rotating at a speed (1); subdomain of the 2nd type (cylinder) built around the wind wheel minus the cylindrical subdomains of the 1st type (2); subdomain of the 3rd type (sphere) surrounding the subdomain of the 2nd type minus (3) [60-62].

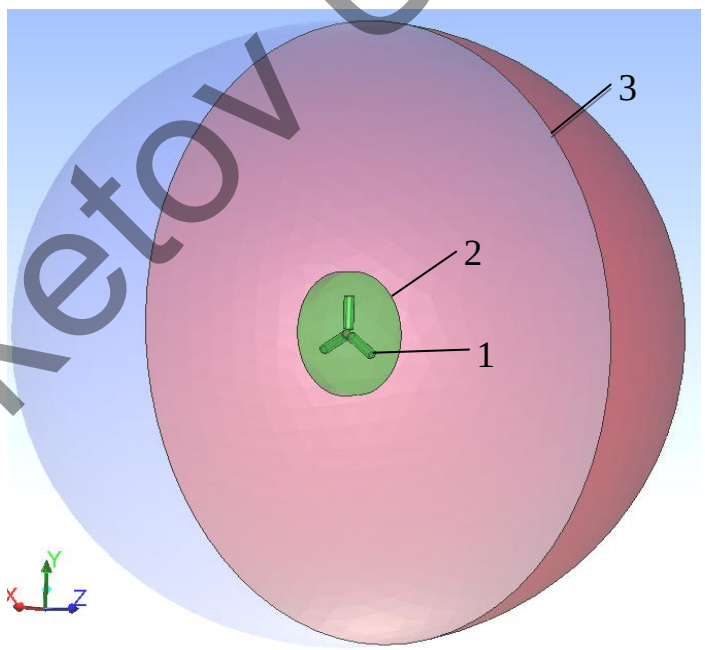

Fig. 4.2. Calculation area

The radius of the outer spherical subdomain (3) is assumed to be 10 m, the cylindrical subdomain (2) has a radius of 2 m and a height of 0.5 m, the cylindrical subdomains (1) have a radius of 0.15 m and a height of 1.06 m [60.61].

A finite-volume grid constructed in subdomains of the 1st type consists of hexagonal cells, and in subdomains of the 2nd and 3rd type-of tetragonal cells. The grid view in the *z*= 0 plane is shown in Figure 4.3. The grid is shown in the XY plane, the cross section of the Z=0 area. The total number of cells is 742858 [60.61].

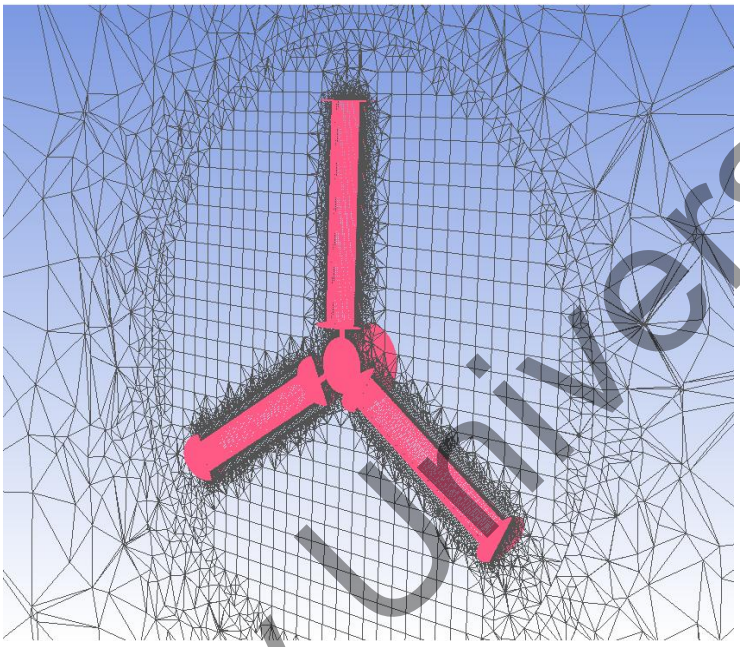

Fig. 4.3. Finite-volume grid

A counter-flow difference scheme of the second order of accuracy in space was used to approximate the convective terms of the system of equations (4.1-4.2). The central difference scheme was used to approximate second-order derivatives. To coordinate the pressure field and the velocity field, the SIMPLE scheme was used [61-64]. The time derivatives were resolved with the second order of accuracy.

4.1 Results of mathematical modeling of aerodynamic characteristics of a wind power plant based on the Magnus effect

This section presents the time-averaged values of the drag force of all cylinders, the lifting force acting on one cylinder, the moment of force acting on the wind wheel, as well as the drag coefficient and the lifting force coefficient of one cylinder obtained for a mobile wind wheel[60-65].

The time averaging was performed according to the formula: $\langle f \rangle = \frac{1}{T}\int_0^T f(t)dt$.

The value of the averaging time interval T was chosen to be from 3 s to 5 s, which is much longer than the period of rotation of the cylinders around its own axis of 0.02 s at the lowest rotation speed of 300 rpm [60].

Figures 4.4-4.6 show mathematical calculations of the aerodynamic characteristics of a wind power plant with blades in the form of rotating cylinders based on the Magnus effect acting on a movable wind wheel. The number of cylinder revolutions is 300 rpm, 500 rpm, 700 rpm [61].

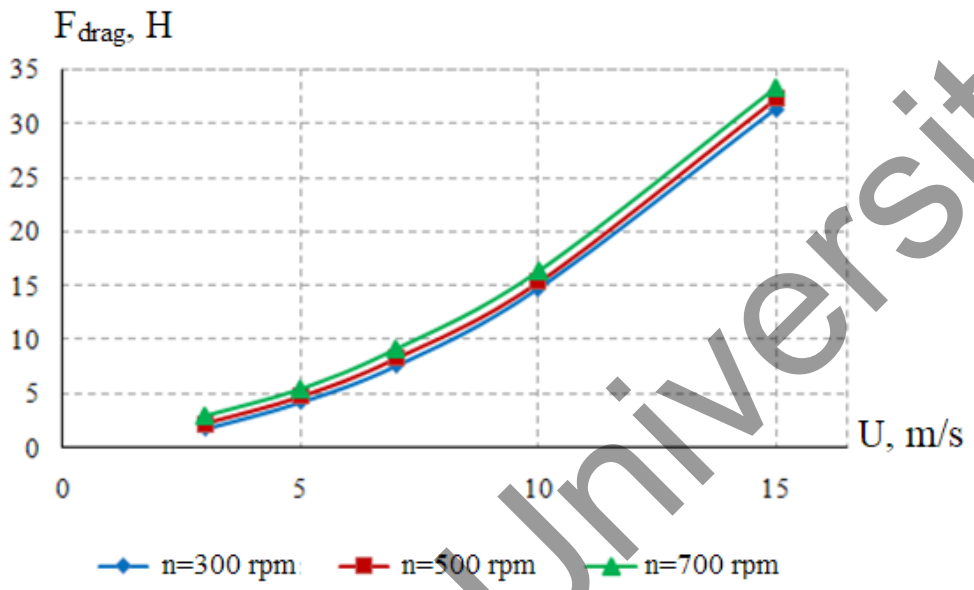

Fig.4.4.The dependence of the drag force of the wind wheel on the speed of the incoming flow

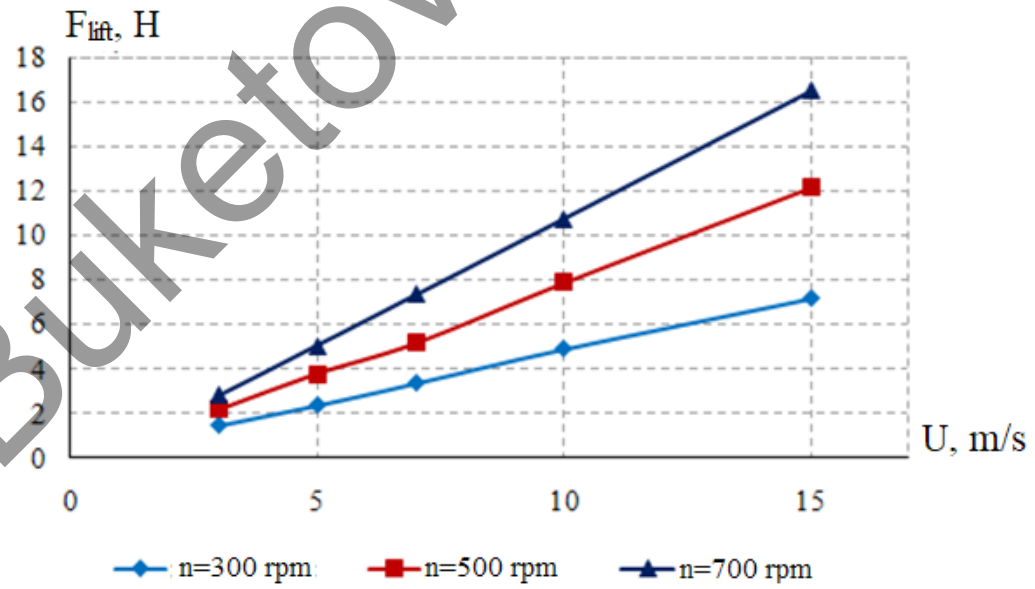

Fig.4.5.The dependence of the lifting force of the cylinder on the speed of the incoming flow

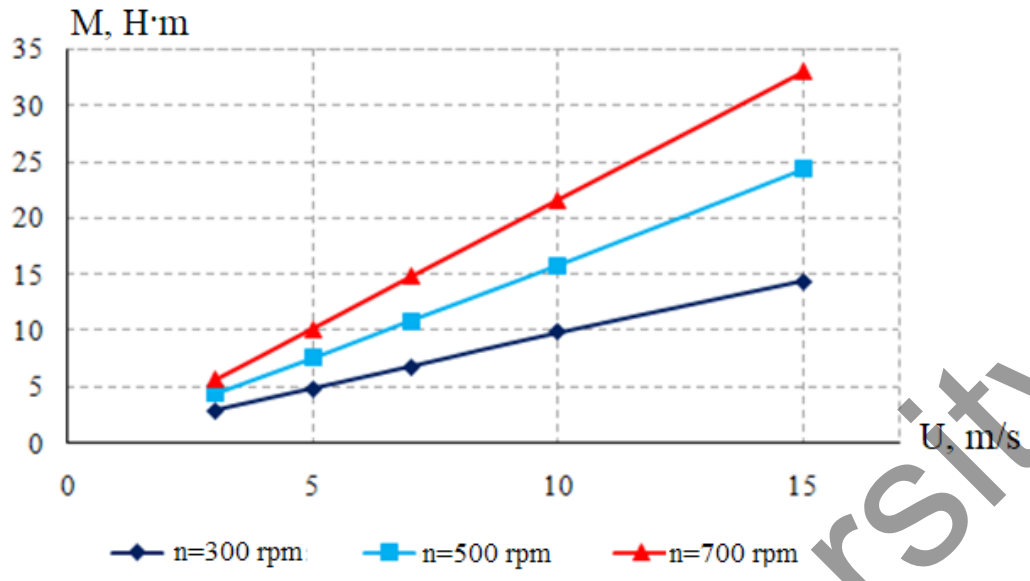

Fig.4.6. Dependence of the moment of forces acting on a moving wind wheel on the speed of the incoming flow

The analysis of the data shown in figures 4.4-4.6 shows that the moment of forces acting on a moving wind wheel rises linearly both with an rise in the speed of the incoming flow and with an grow in the speed of rotation of the cylinders around its own axis in the range from 300 rpm to 700 rpm [61].

The speed of rotation of the cylinders entails an increase in the drag force of the wind wheel to the wind according to a law close to linear. With an increase in the flow velocity, the resistance force increases according to the quadratic law [60-65].

4.2 Calculation of the aerodynamic coefficients of the rotating cylinder of a wind power plant based on the Magnus effect

The drag coefficient is calculated according to the formula (4.10):

$$C_x = \frac{F_{drag}}{\frac{1}{2}\rho V^2 S} \tag{4.10}$$

The value of the lift coefficient can be found using the following formula (4.11):

$$C_y = \frac{F_{lift}}{\frac{1}{2}\rho V^2 S} \tag{4.11}$$

The area of the mid-section of each cylinder S (taking into account the end protrusions) is equal to 0.15144 m^2.

Tables 4.1 and 4.2 show the force coefficients obtained as a result of numerical modeling [65].

Table 4.1

Coefficient of drag of the rotating cylinder

n(rpm)	V=3 m/s	V=5 m/s	V=7 m/s	V=10 m/s	V=15 m/s
300	0.6825	0.5934	0.5549	0.5265	0.4998
500	0.8720	0.6733	0.6005	0.5503	0.5146
700	1.1257	0.7793	0.6643	0.5846	0.5310

Table 4.2

Lifting force coefficient of one cylinder

n(rpm)	V=3 m/s	V=5 m/s	V=7 m/s	V=10 m/s	V=15 m/s
300	1.6841	1.0115	0.7319	0.5254	0.3421
500	2.5650	1.6143	1.1700	0.8454	0.5818
700	3.3480	2.1566	1.6113	1.1574	0.7894

The dependences of the drag coefficient of the cylinder on the Reynolds number are shown in Figure 4.7.

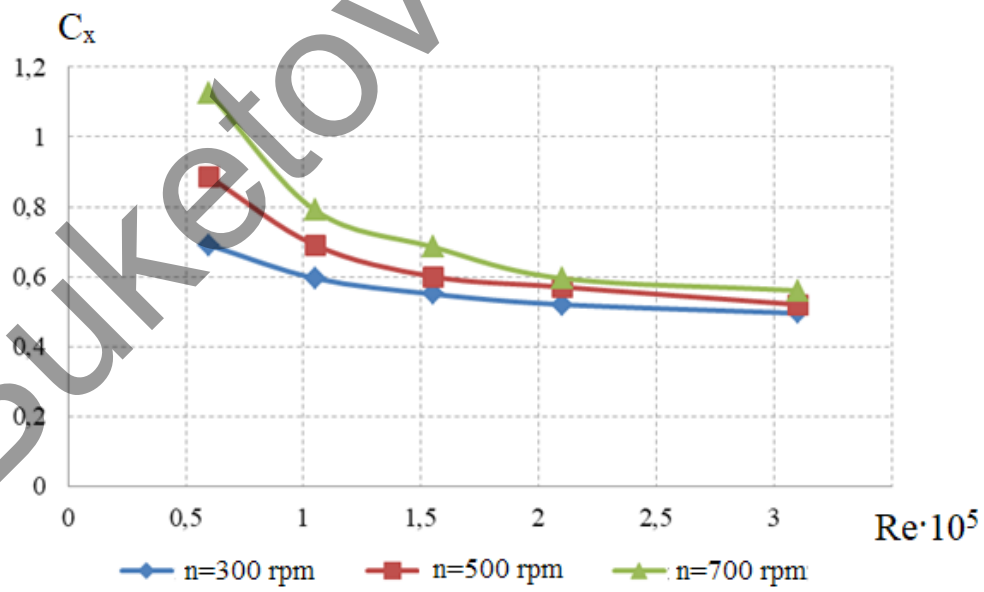

Fig.4.7.Dependence of the drag coefficient of the cylinder on the Reynolds number

The data obtained as a result of numerical calculation can be approximated by the following analytical dependencies (4.12) [62,63]:

$$C_x(\mathrm{Re},n) = A(n)\left(\mathrm{Re}\cdot 10^5\right)^{B(n)} \qquad (4.12)$$

where, $A(n) = 0.1005 + 2.6376\cdot 10^{-4} n$, $B(n) = -1.7946\cdot 10^{-2} n^{0.55944}$, n – the number of revolutions of the cylinder per minute.

Figure 4.7 shows the rotation of the cylinders in the case of a movable wind wheel. The air viscosity is assumed to be equal to $1.795\cdot 10^{-5}$ Pa·s, and the density is 1.225 kg/m^3. The drag coefficient of the cylinder increases with an increase in its rotation speed and with a decrease in the number of Re [60].

As you can see, the formula (12) for contains one dimensionless and one dimensional parameter, which is not quite convenient. We introduce a dimensionless speed of rotation of the cylinder: $\alpha = 2\pi nr/V$. Here r is the radius of the cylinder [63].

Figure 4.8 shows the dependency $C_x(\alpha,n)$. As you can see, the resistance coefficient weakly depends on n and all points are well described by the function $C_x(\alpha) = 0.4592\exp(0.4867\alpha)$.

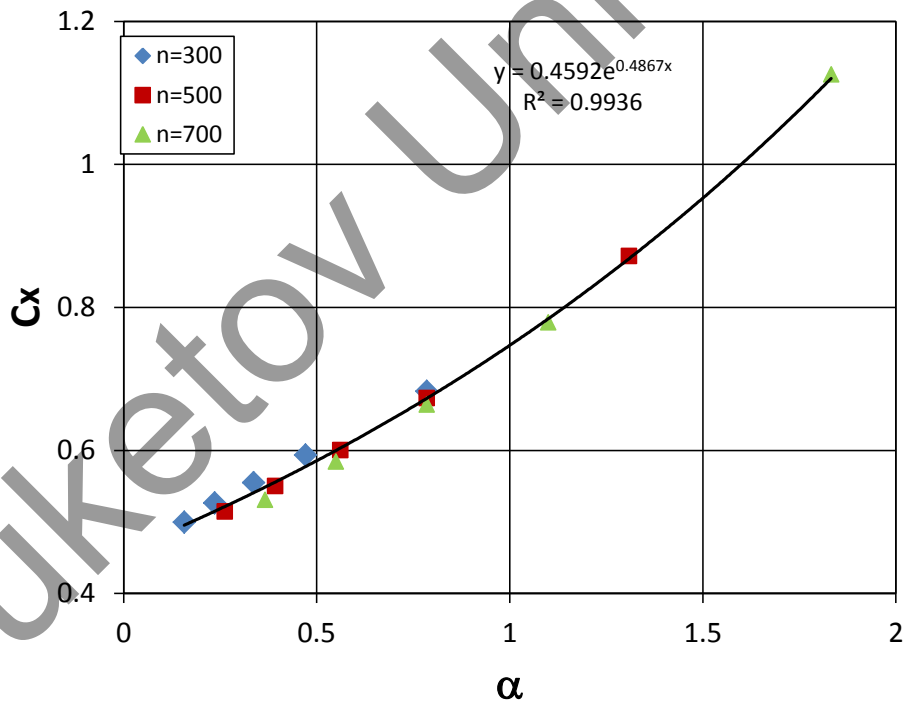

Fig. 4.8. Dependence of the drag coefficient on the dimensionless speed of rotation of the cylinder

The tendency of the drag coefficient in the absence of rotation (α=0) to a constant value is due to the fact that in the considered range of wind speeds, the flow around the cylinder occurs in a developed turbulent mode, where the drag coefficient has a constant value [65].

Figure 4.9 shows the dependence of the cylinder lift coefficient on the Reynolds number, constructed from the cylinder diameter and the incoming flow velocity, for different cylinder rotation speeds in the case of a movable wind wheel [65].

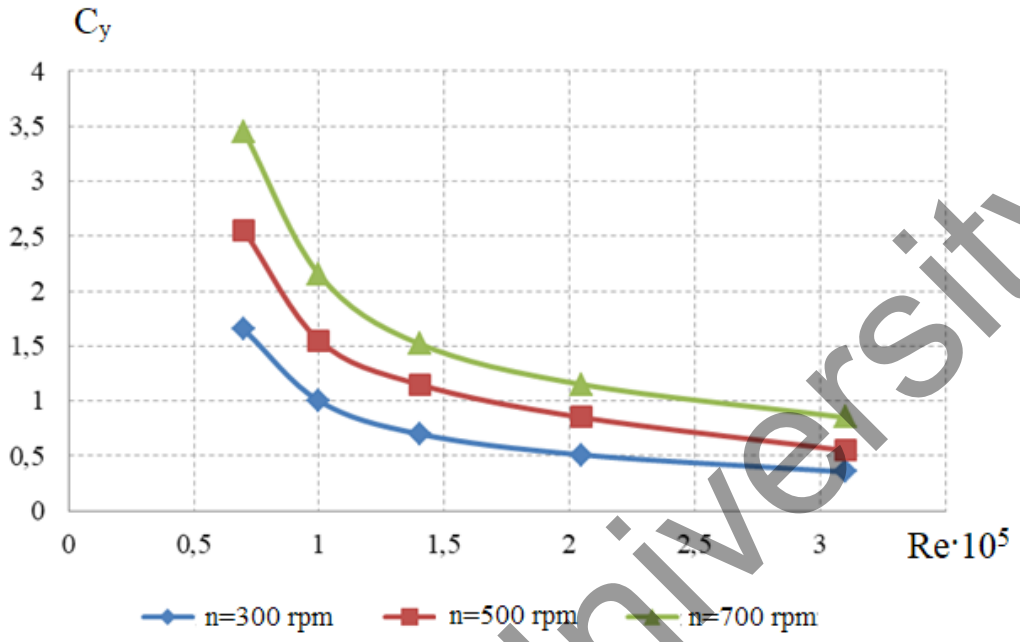

Fig. 4.9.Dependence of the cylinder lift coefficient on the Reynolds number

Here, as with the drag coefficient (Figure 4.8), the value of the lift coefficient (Figure 4.9) increases with an increase in the speed of its rotation and with a decrease in the number of Re. The obtained data are approximated by the formulas [61]:

$$C_y(\mathrm{Re},n) = A(n)\left(\mathrm{Re}\cdot 10^5\right)^{B(n)}, \text{ где } A(n) = 7.0702\cdot 10^{-3} n^{0.87626},$$
$$B(n) = 1.8290 n^{-0.10920}$$

The dependence of the lifting force coefficient of the cylinder can be constructed depending on the relative speed of rotation of the cylinders α (Figure 4.10). As you can see, all the calculated data fall on one curve [61]: $C_y(\alpha) = 2.002\alpha^{0.9281}$.

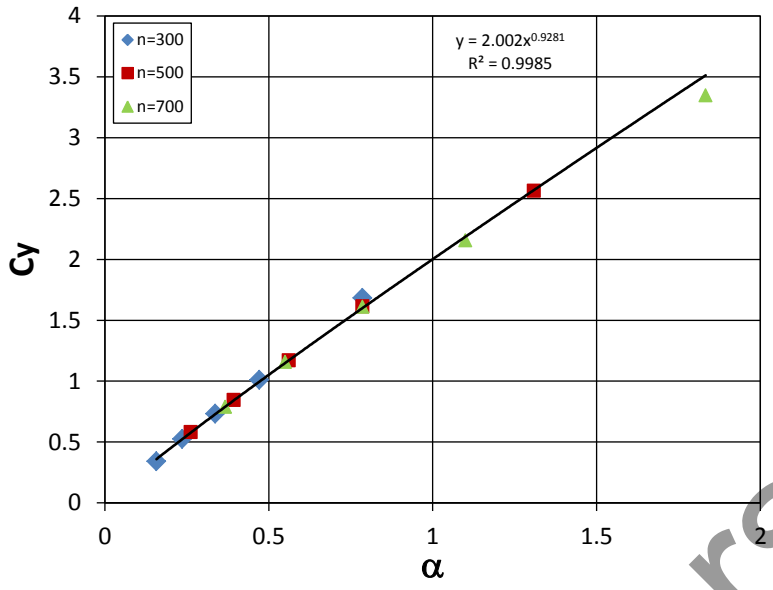

Fig. 4.10.Dependence of the lifting force coefficient on the dimensionless rotation speed

4.3 The flow field in the vicinity of the wind wheel

Figure 4.11 shows the distributions of the longitudinal velocity in the vicinity of a movable wind wheel (plane $z = 0$) for different speeds of rotation of the cylinders at the speed of the blowing flow V=10 m/s. At low speeds of rotation of the cylinders (Figure 4.11 a), the flow field is close to symmetrical with respect to the three planes of symmetry passing along the axes of the cylinders, while higher speeds of rotation of the cylinders lead to deformation of the longitudinal velocity field (Figure 4.11 b), but the longitudinal velocity field retains symmetry when rotated by 120° relative to the z axis [61].

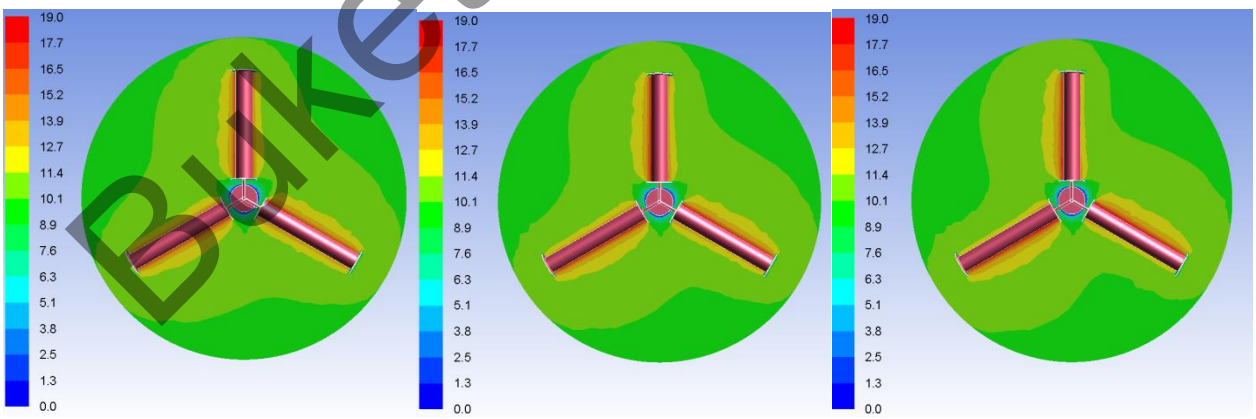

a) b) c)

a – n=300 rpm; *b*-500 rpm; *c*-700 rpm

Fig. 4.11. Distribution of the longitudinal velocity u_z in the vicinity of a movable wind wheel

The deformation of the flow field occurs due to an increase in the air flow velocity on one side of the cylinder (left, Figure 4) and a decrease in the flow velocity on the other side (right, Figure 4) caused by the rotation of the cylinders around their axes in a positive direction (counterclockwise) [61-63].

Figure 4.12 shows the projections of the velocity vectors on the plane $x = 0$ in the vicinity of the central disk. It can be seen that vortex zones are formed behind the central disk, in which the flow turns towards the main flow. The flow pattern in this region is qualitatively the same for the cylinder rotation speed in the range from 300 rpm to 700 rpm [60].

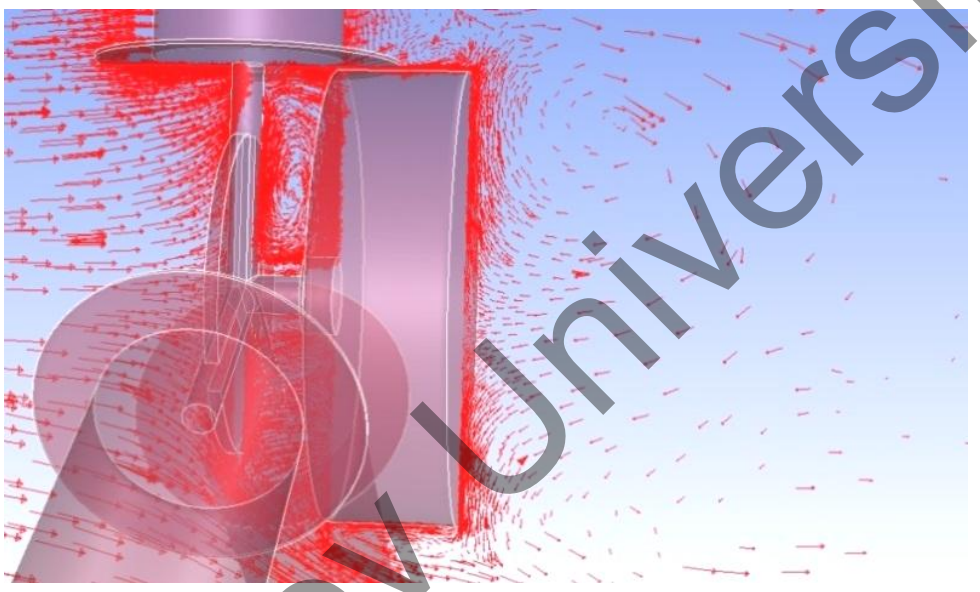

Fig. 4.12. Velocity field in the plane x=0 (plane YZ, section x=0)

Figure 4.13 shows the projections of the normalized velocity vectors $\vec{u}/|u|$ on the plane z=0.15 m for a movable wind wheel with cylinders rotating around their axes at a speed of 500 rpm [60].

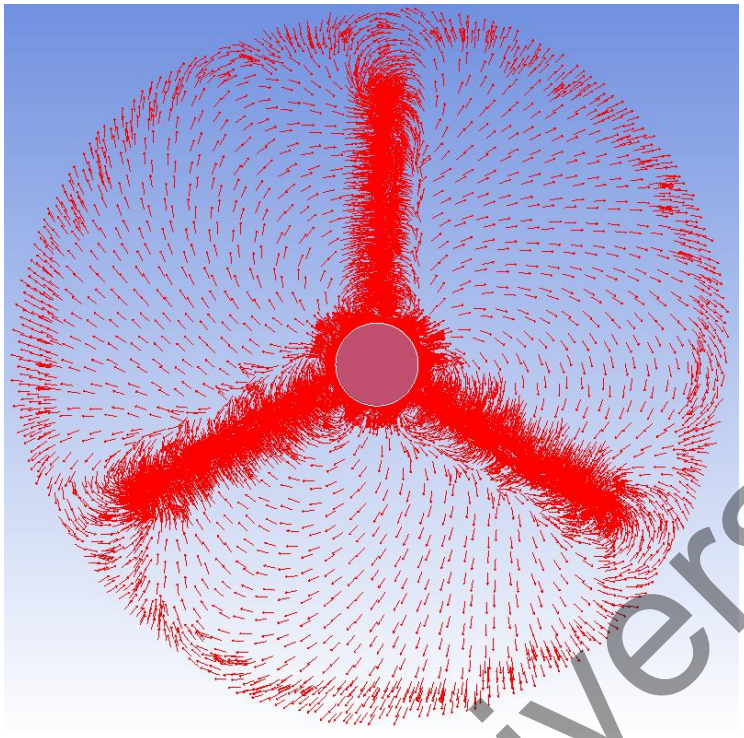

Fig. 4.13. Flow pattern in the plane z=0.15 m

It can be assumed that the nature of the movement of the air flow is complex: in the vicinity of the center of the wind wheel, the current is twisted clockwise, and at the periphery, the air moves in a direction close to the radial, while in the vicinity of the ends of the cylinders, the air flows counterclockwise [60].

Figure 4.14 shows the influence of the rotation speed of the wind wheel n_1 on its resistance force to the incoming flow for different flow velocities [61].

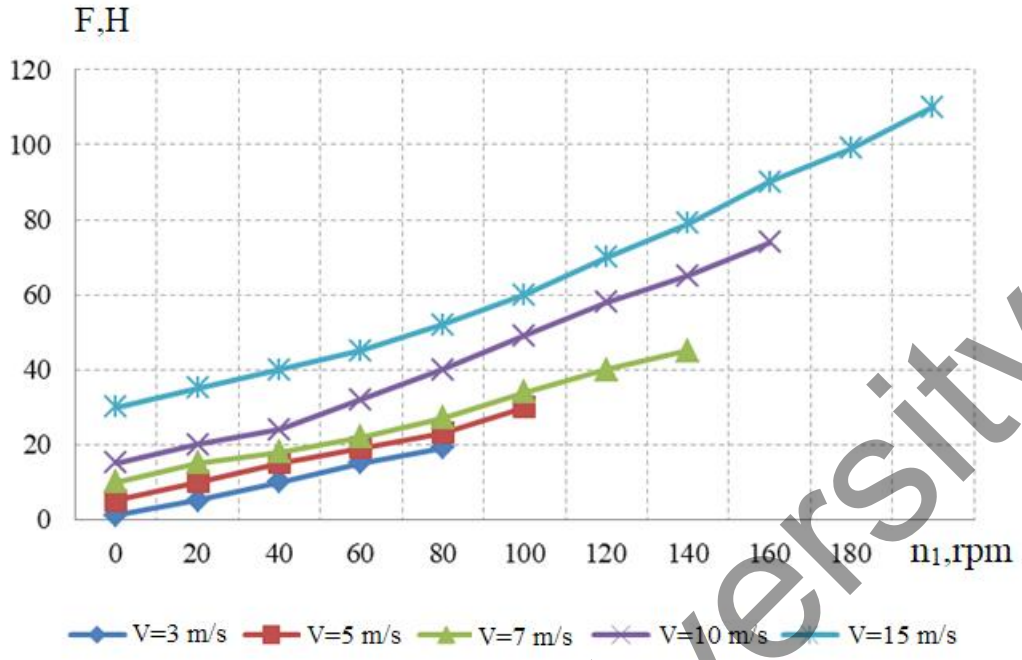

Fig. 4.14. Influence of the wind wheel rotation speed on the drag force n=500 rpm

n_1, rpm

As can be seen, the increase in the rotational speed of the wind wheel entails an increase in the drag force according to the quadratic law. Symbols denote the values of the resistance force obtained as a result of numerical modeling, solid lines – an indicator of approximation by the least squares method. The increase in the drag force (directed along the *z* axis) with the increase in the speed of rotation of the wind wheel is explained by the action of the Magnus force resulting from the rotation of the cylindrical blades around their own axes and the lateral flow of air around the cylinders resulting from the rotation of the wind wheel [60.61].

The scheme of the Magnus forces is shown in Figure 4.15.

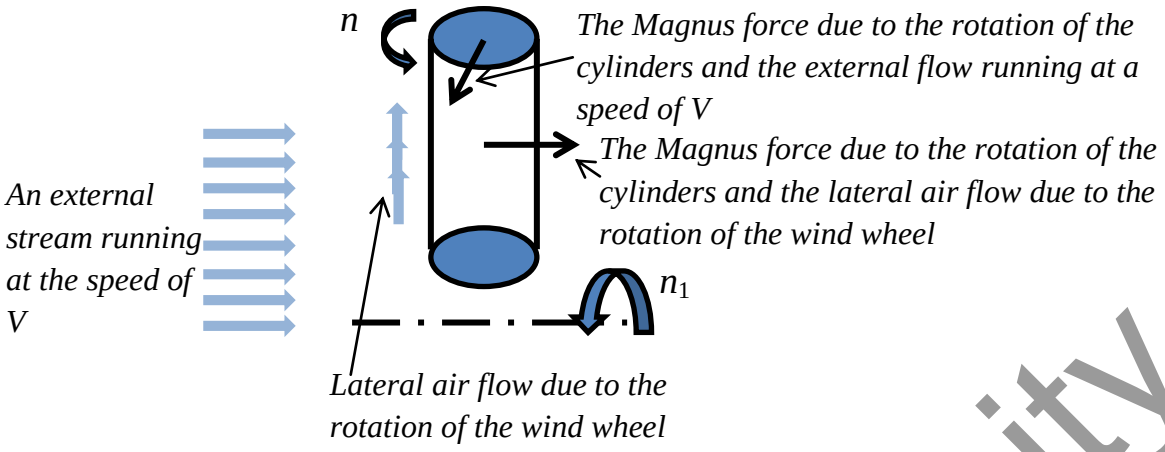

Fig. 4.15. The action of Magnus forces

Figures 4.16-4.20 show the influence of the rotation speed of the wind wheel on the moment of forces acting on the wind wheel for different speeds of the incoming flow and different speeds of rotation of the cylinders [60].

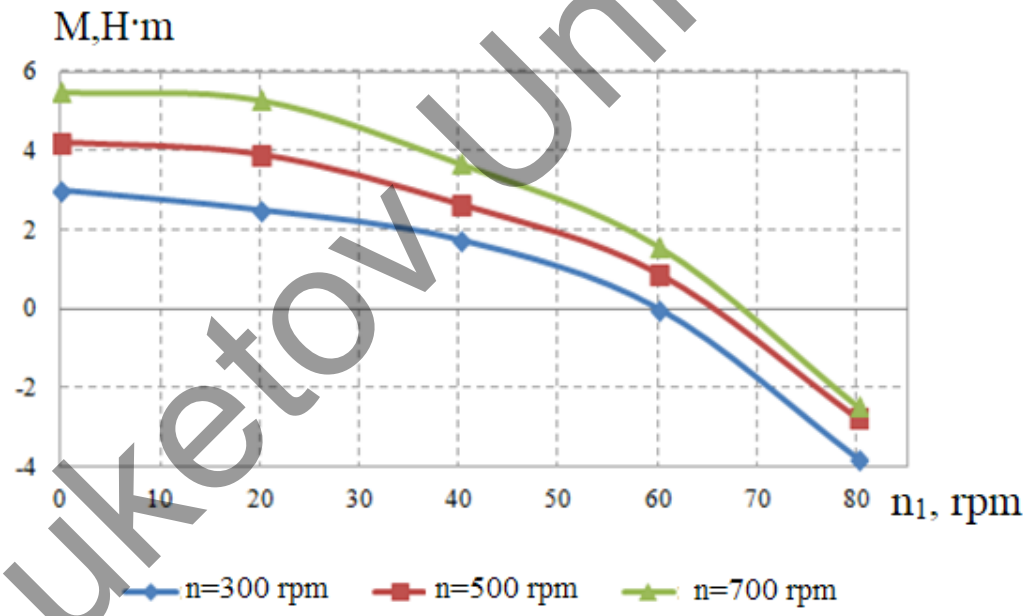

Fig. 4.16. Dependence of the rotation speed(free) from the wind speed (V=3 m/s)

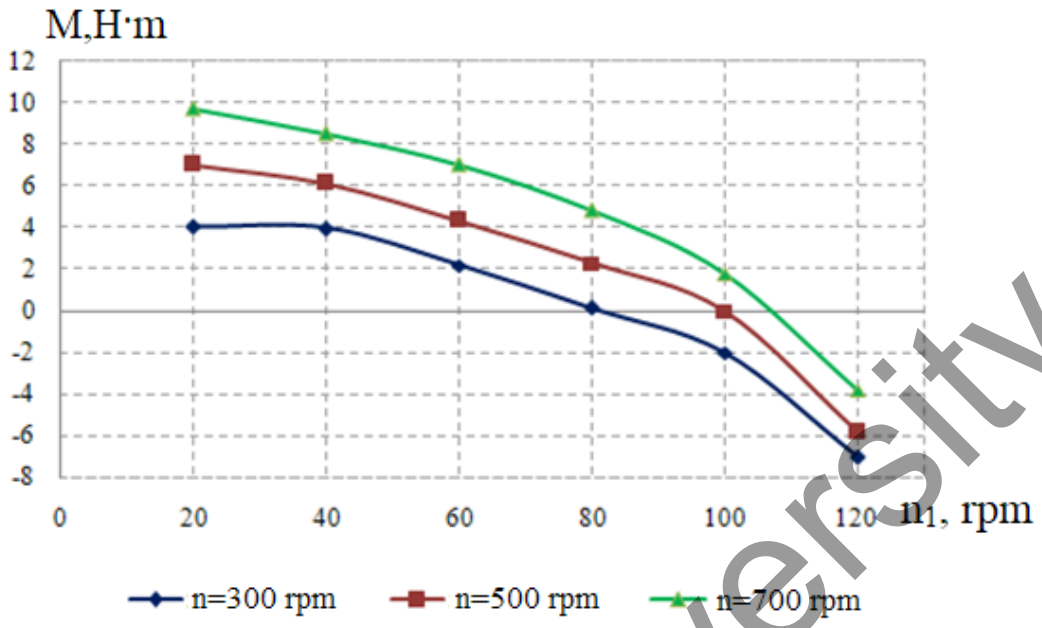

Fig.4.17. Dependence of the rotation speed(free) from the wind speed (V=5 m/s)

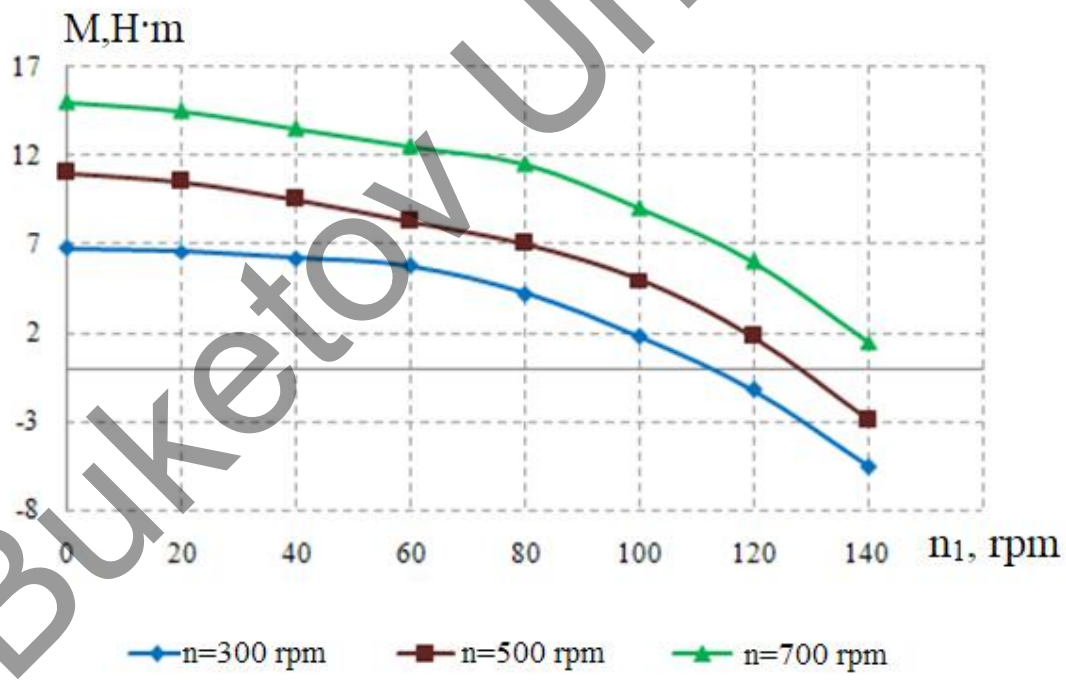

Fig. 4.18. Dependence of the rotation speed(free) from the wind speed (V=7 m/s)

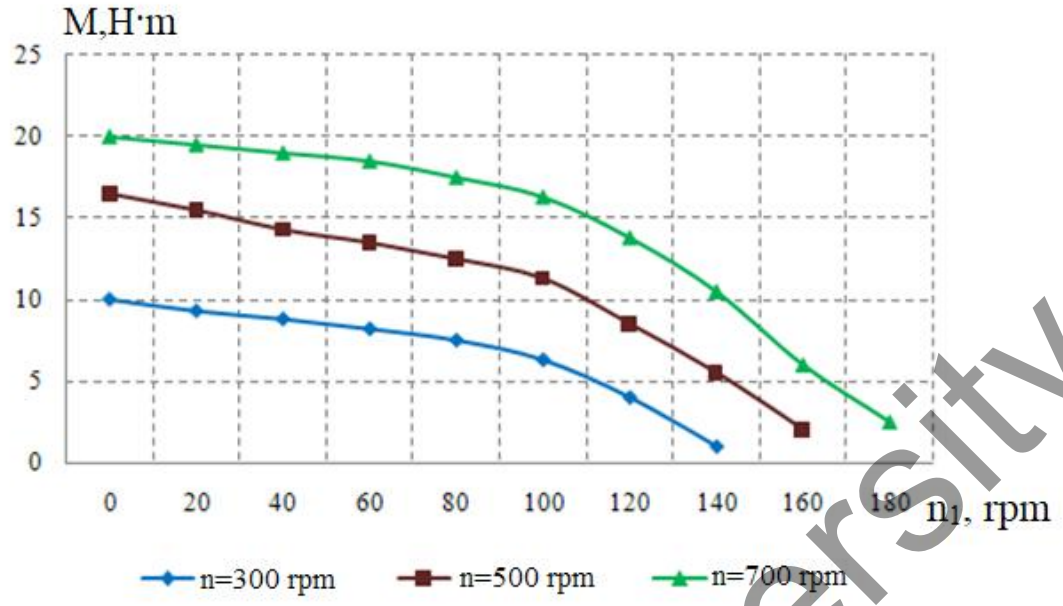

Fig. 4.19. Dependence of the rotation speed(free) from the wind speed (V=10 m/s)

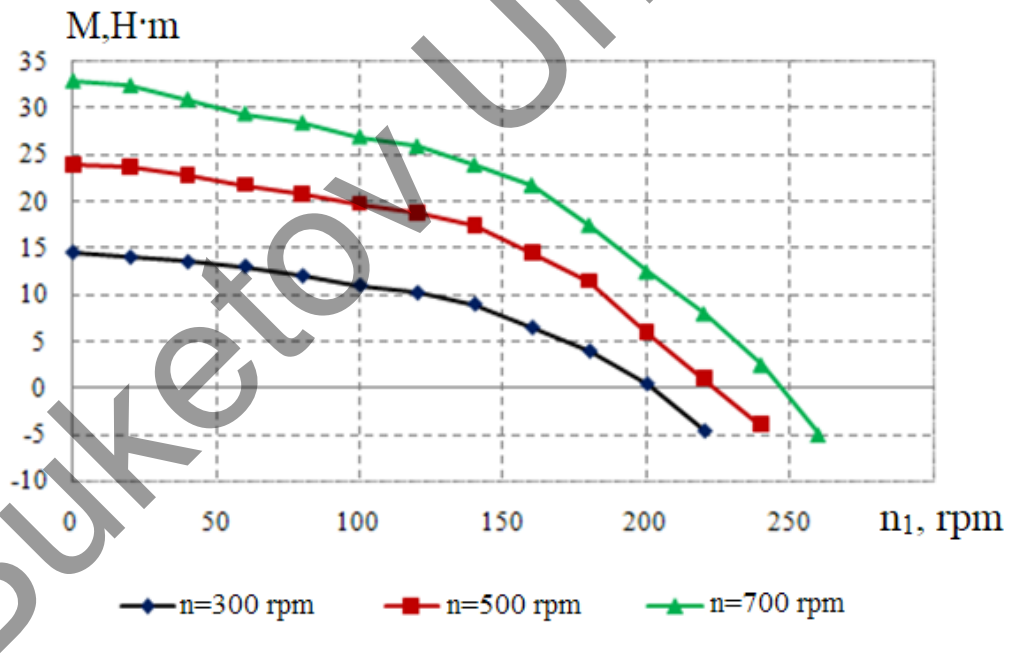

Fig. 4.20. Dependence of the rotation speed(free) from the wind speed (V=15 m/s)

The results of mathematical modeling are indicated by symbols. Solid lines are the result of processing by the least squares method [60-65].

An increase in the rotational speed of the wind wheel entails a decrease in the moment of forces that affect the wind wheel.

According to the above dependencies, it is possible to determine the speed of free rotation of the wind wheel, i.e. without taking into account the value of the moment of friction forces in the bearings and the moment of forces arising in the generator [62-64]. The speed of free rotation of the wind wheel is as a result of the intersection of solid lines with the abscissa axis.

Figure 4.21 shows the results of calculating the speed of free rotation of the wind wheel n_1 as a function of the speed of the incoming flow, obtained for different speeds of rotation of the cylinders.

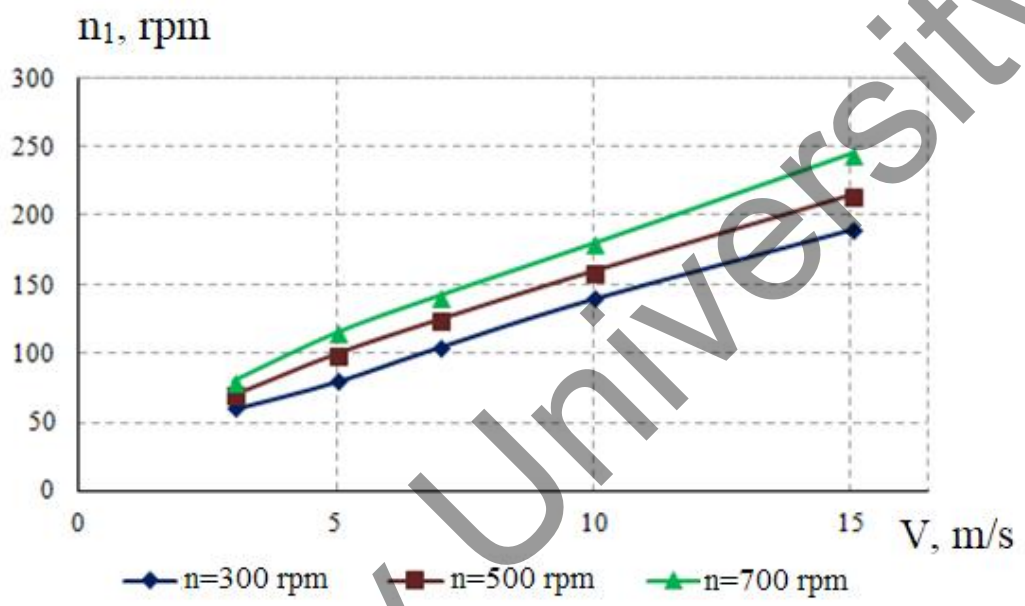

Fig. 4. 21. The speed of free rotation of the wind wheel depending on the speed of the incoming flow n_1, rpm

Hence it follows, the obtained results (Figure 4.21) are approximated with a sufficient degree of accuracy (R^2>0.9972) by dependencies of the form: $n_1(n,V) = A(n)V^{B(n)}$. In this formula, the speed of the incoming flow is given in m/s, and the rotation speeds of the cylinders n and n_1 in rpm [61]. It can be shown that the functions *A(n)* and *B(n)* have the following form $A(n) = 12.958n^{0.1224}$, $A(n) = 12.958n^{0.1224}$.

5. CALCULATION OF THE ELECTROPHYSICAL PARAMETERS OF A MAGNETOELECTRIC ELECTRIC GENERATOR ON PERMANENT MAGNETS

5.1 Electric generator of a wind power plant based on semiconductor electronics

Together with Tree-energy LLP, a new design of an electric generator using neodymium magnets was developed and designed.

Neodymium magnets are a permanent powerful rare earth magnet consisting of an alloy of neodymium, boron and iron. It is known for its attractive power and high resistance to demagnetization. It has a metallic appearance, is very popular and has found application in various fields of industry, medicine, in everyday life and electronics. Permanent magnets made of NdFeB (neodymium-iron-boron) alloy have a large magnetic induction and, accordingly, a large magnetic force. Over time, the loss of the magnetic properties of neodymium magnets (Figure 5.1) is 2 % for 5 years [80-89].

Fig.5.1-NdFeB permanent magnet

The electric generator is designed for a wind generator. We used small rectangular neodymium magnets, model 30×10, holding force 20 kg, weight 54 g. 24 magnets were purchased, from which individual parts of the wind generator rotor were made. The general design of our electric generator is shown in Figure 5.2.

In this development, we have moved away from the traditional approach [83-86], when a magnetic field is excited on the rotor based on currents flowing through a coil on a rotating rotor. The difference between our version and other previously known ones is that there is one disk with coil windings, it is located in the center of the system. Two disks with neodymium magnets are arranged symmetrically on both sides of the disk with coil windings. The diameter of the copper wire is 1.33 mm. According to calculations, this winding can generate power up to 800 W at a wind speed of up to 5 m/s. The disk with coil windings is movable and rigidly fixed, and two disks with magnets rotate.

In the center there is a disk on which 12 coils of copper wire are installed. On both sides of this disk there are two external disks, on which 24 permanent magnets are located.

Figures 5.2 and 5.3 show the general appearance of the electric generator and the appearance of the coil from the common coil circuit.

Fig.5.2. General view of the electric generator in the initial stage on permanent disk magnets

Fig.5.3. One coil from a common coil circuit

The coil is wound with a copper wire without a core, to avoid magnetic sticking between the coil and the magnets. In the absence of sticking, the generator shaft starts much earlier and generates electrical energy with a weak squat wind, and the generator, for example, from an asynchronous motor, most often has sticking, which creates difficulty for rotating the shaft, while not generating electrical energy, while the axial generator of our design rotates and charges the battery.

An experimental installation has been assembled on which the induced EMF can be directly experimentally measured. The principle is shown in Figure 5.4.

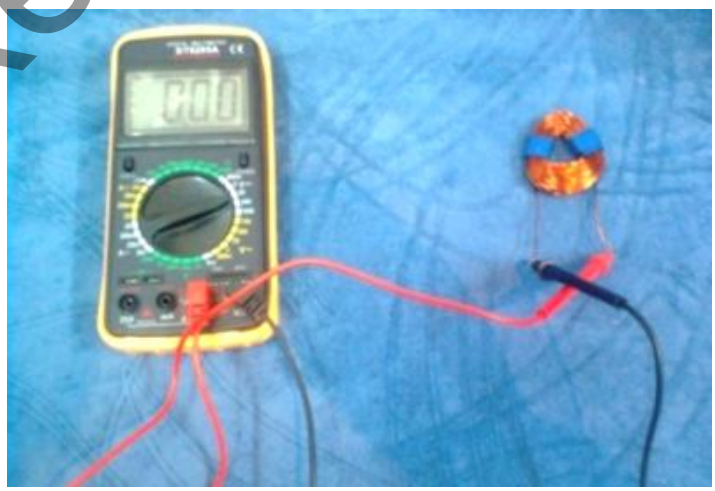

Fig.5.4.The scheme of the experiment to determine the average EMF

Figure 5.5 shows the general scheme of operation of the wind turbine.

The efficiency of axial generators due to the absence of a magnetic core (iron) in the stator is much lower, because of this, in order to achieve the same power, magnets need twice as large and their number is twice as large when compared with a generator on a stator made of electrical steel [80-89].

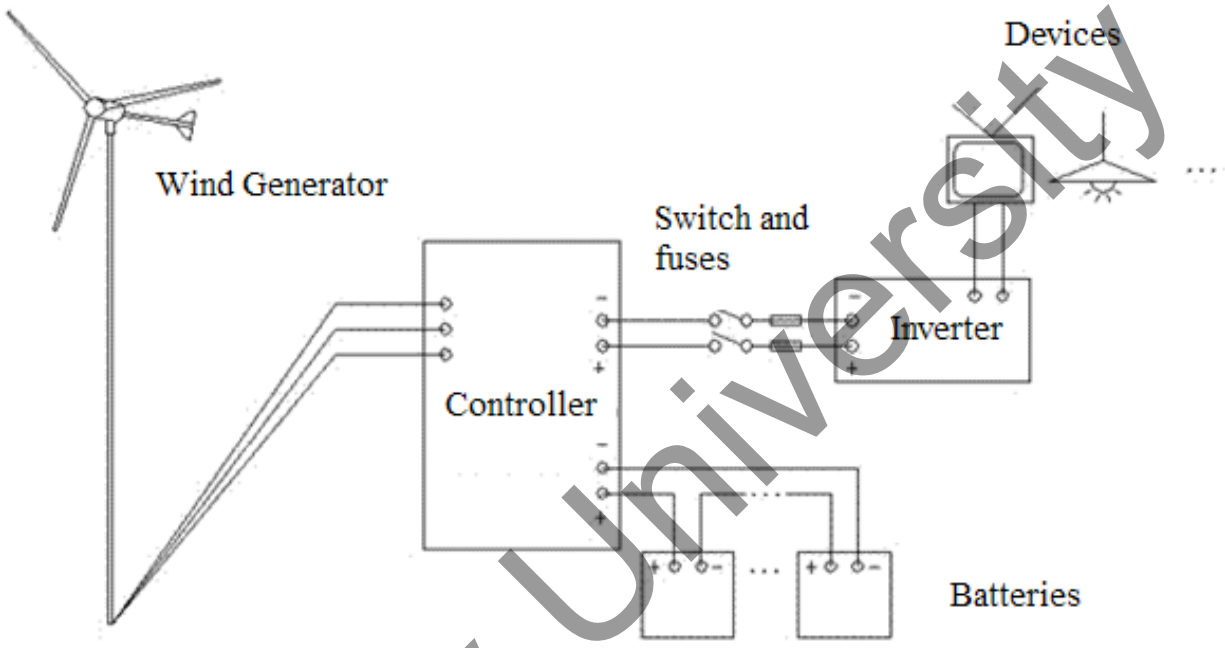

Fig.5.5.General scheme of operation of the wind generator set

The magnets on the disk are arranged with alternating poles. The more magnetic poles there are, the lower the speed at which the generator begins to give an acceptable charging current. But a very large number of magnets are often difficult to effectively place in the structure, since the dimensions of the coils become very small due to the limited size of the stators.

Figure 5.6 shows a general view of one disk with 12 magnets.

There are two phase connection schemes in 3-phase generators: "star" and "triangle". The triangle gives a lower voltage, but a greater current. The star is the opposite – a higher voltage and a lower current. In our case, we used a 3-phase generator "zvezda", where the ends of the phase windings are connected to one point U2, V2, W2, and the beginning of the windings U1, V1, W1 serve to connect the load.

Fig.5.6.General view of a disk with 12 magnets

Figure 5.7 shows the connection diagram of the stator coils.

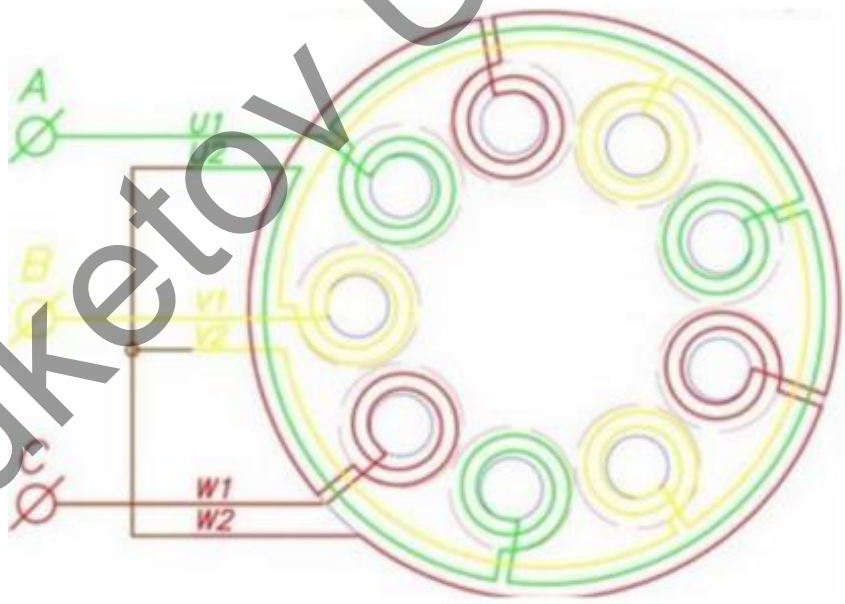

Fig. 5.7.Connection diagram of the stator coils (Star)

An experiment was conducted to study the effect of the values of the ring diameter of the coil winding wire on the level of the induced EMF. It turned out that the maximum EMF value is observed at values $d \sim (1{,}1\text{-}1{,}2)d_o$, where d_o is the diameter of

the magnetic disk. It is established that the EMF value decreases asymptotically with an increase in the diameter d of the coil.

The graphical dependence is shown in Figure 5.8.

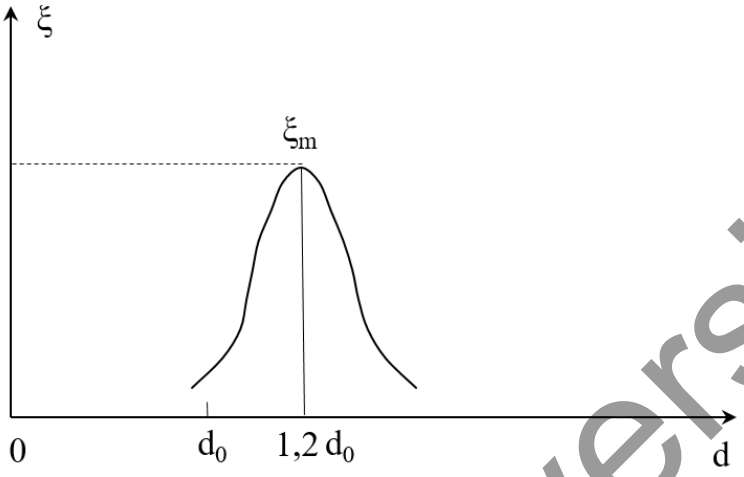

Fig.5.8.Change in the average level of induced EMF depending on the diameter of the winding of the ring coil

For one of the coils, with a weak movement of the magnet, the induced EMF was approximately 0.08 V. A calculation scheme has been developed according to which the magnetic field of induction near the end of a round magnetic disk can be calculated as a result of solving the inverse problem for the equation of the volumetric ponderomotor force acting on a ferromagnetic material (5.1,5.2).

$$f = \frac{1}{2}\frac{\mu_a - \mu_0}{\mu_a \mu_0}\,\mathrm{gradB}^2 \tag{5.1}$$

$$\mathrm{gradB}^2 = \frac{\partial B^2}{\partial x} + \frac{\partial B^2}{\partial y} + \frac{\partial B^2}{\partial z}, \tag{5.2}$$

where, $\mu_a = \mu_r \mu_0$ - absolute permeability of the steel sheet, $2\pi R$ - magnetic permeability of air, - the relative magnetic permeability of a ferromagnetic material, can have values of 200 (solid steel), 5000-band iron. The problem is solved numerically. IntelVisualFortran programs based on VisualStudio 2010 and Matlab 2013 were used to solve nonlinear iterative equations and partial differential equations. A special algorithm has been developed that preserves the convergence and stability of the grid calculation scheme for different values of steps for the grid region. The force of magnetic attraction can also be calculated from the equation for the force exerted on a circuit with a current in a magnetic field with a gradient (5.3).

$$F = p_m gradB, \tag{5.3}$$

where, $p_m = IS$ - the magnetic moment of some equivalent current circuit, which in the averaged version represents (replaces) microcurrents in a solid ferromagnetic material. Equation (5.3) is also solved numerically. For the convenience of calculations, equation (5.1) is converted to the form (5.4)

$$f = \frac{1}{2}\frac{\mu_r - 1}{\mu_r \mu_0} gradB^2 \tag{5.4}$$

According to the value of the magnetic field gradient, it is possible to approximately calculate the magnetic attraction force, as well as the induced EMF in a circuit with a coil. From the weight held by the magnet, we find the force $F = mg$. The thrust (holding force) is found as a result of integration $dF = fdV$.

One of the significant advantages of an electric generator without a ferromagnetic core is the absence of sticking, since the stator has no iron elements and is just copper coils filled in resin in the form of a disk, on both sides of which, at a minimum distance, disks with magnets rotate.

Figure 5.9 shows a stator with wound coils (12 pieces), which are installed in the matrix and prepared for filling with resin.

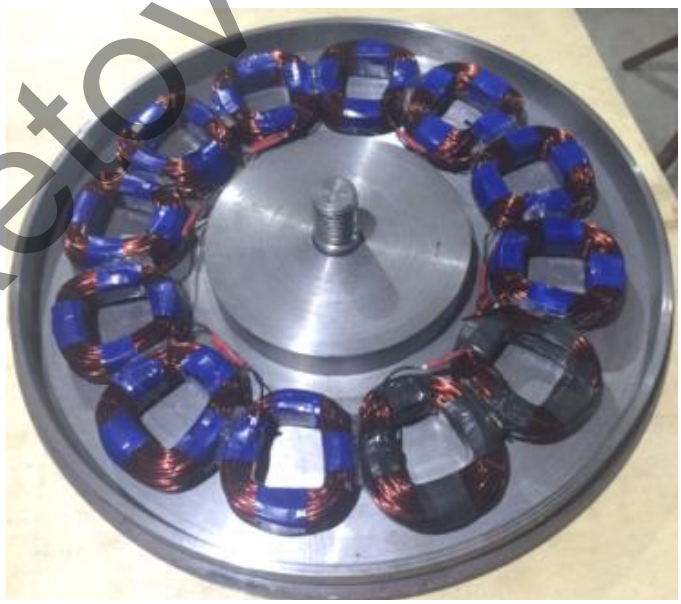

Fig. 5.9.Stator of an electric generator (12 coils)

The stator of this electric generator (Figure 5.9) consists of 12 coils of copper wire, with a diameter of 1.33 millimeters, for 100 turns each, thickness 18 mm, width 50 mm, length 70 mm connected according to the star scheme and the terminals of 3 phases with a zero wire. The zero wire is used to equalize the electrophysical values at all phases of the stator winding of an electric generator. The zero wire is necessary when switching on the star, since the load of the phases can be with differences. The profile of the zero wire in the considered design of the stator of the electric generator is equal to half of the cross-section of the wires of the stator phases. Since a copper wire with a cross-section of 1.33 mm is used in the phase wires, the zero wire in the stator of this electric generator has a cross-section equal to 1 mm.

The zero wire can also be used to ground the structure. According to calculations, this winding can generate power up to 1000 W, with a wind speed of up to 5-7 m/s.

To fix the coils on the stator, they are filled with epoxy resin (figure 5.10). For this purpose, a mold for filling is made so that the liquid resin does not spread, the matrix has an inner and outer sides equal in height to the thickness of the stator. At this stage, it is necessary to provide eyelets for fixing the stator.

It is important that you get a perfectly flat plane, so before filling the matrix with coils, you need to install it on a flat surface on the level. The coils must be carefully checked with a multimeter before filling and laid out on the matrix in a circle so that the rotor magnets are then located opposite the coils.

Fig.5.10. Stator filled with epoxy resin

Figure 5.11 shows the final version of a laboratory electric generator based on semiconductor electronics.

During the development, the following goals were set: 1-simplification of the design, 2-reduction of cost, 3-improvement of safety and reliability. According to calculations, when there is not a strong wind, the stator winding can generate a slight EMF, about 12-24 V. The discrepancy of this EMF with the level of 220 V was the main obstacle to the widespread introduction of a small-sized wind generator. With different winds, the amplitude and frequency of the generated EMF changes. In previously known models of wind turbines, the stabilization of variable parameters was carried out by mechanical or hydraulic units. This led to low efficiency and an increase in the weight and dimensions of wind turbines.

a) b)

Fig.5.11.Electric generator assembly: a) front view, b) side view

5.2 Results of electrophysical parameters of a magnetoelectric electric generator

A number of aerodynamic tests were carried out at the test site to determine the electrophysical parameters of a prototype wind power plant based on a wind generator with blades in the form of rotating cylinders (wind power plant).

The volt-ampere characteristics of a prototype wind power plant at a fixed value of the pulley diameter are studied (figure 5.12). Lamps with capacities of 5 and 21 watts were used as a load for removing the volt-ampere characteristics of the wind generator.

Fig.5.12.Load block system

The volt-ampere characteristics, when the wind increases and the generator speed increases, for an experimental wind power plant are shown in figures 5.13-5.14. The operating point of the generator connected to the load coincides with the point of maximum power. The connection of such loads can shift the operating point of the system to the area of minimum or even zero power. Therefore, an important component of the system is voltage converters that can coordinate the wind module with the load.

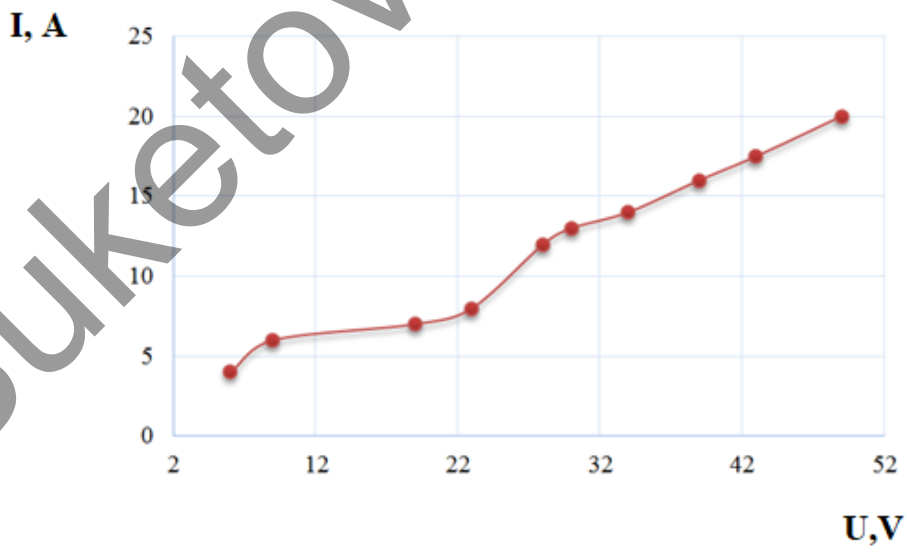

Fig.5.13.Volt-ampere characteristic of an experimental wind power plant

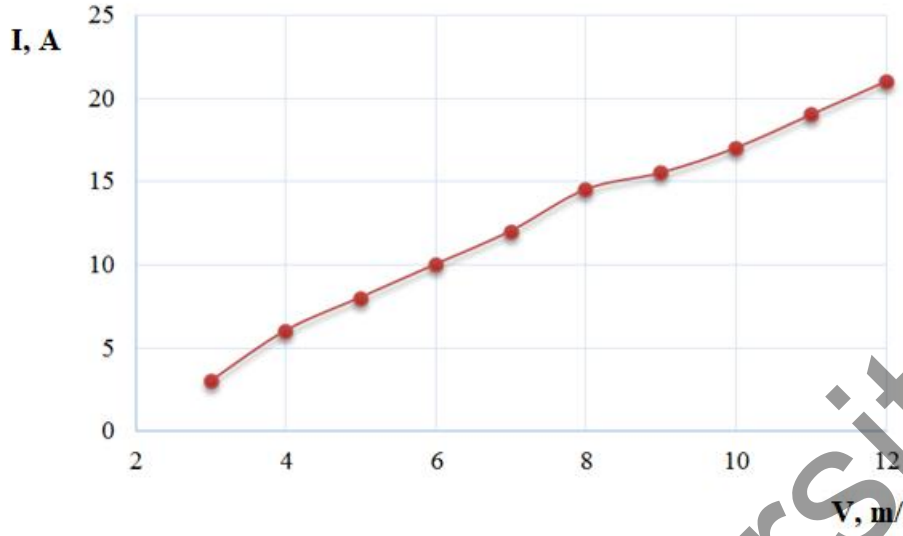

Fig.5.14. Change in the value of the current strength depending on the wind speed for a prototype wind power plant

Such electrophysical parameters of a wind power plant as voltage, current, power and speed of rotation depend on the value of the air flow velocity.

Figure 5.15 shows the dependence of the voltage on the wind speed. As the wind speed increases, the generated voltage and current increase.

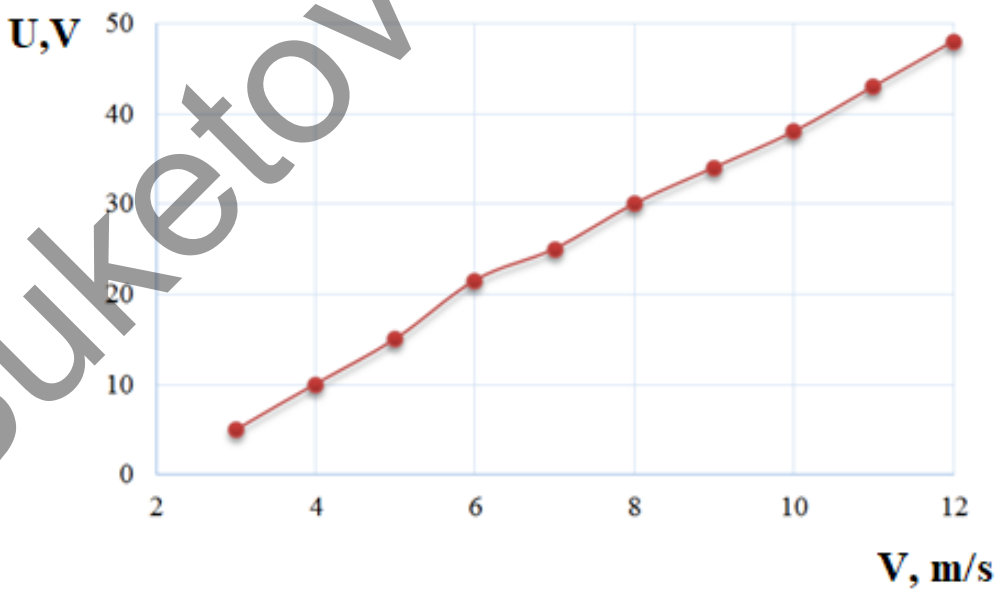

Fig.5.15.The dependence of the voltage on the wind speed

Figure 5.16 shows the dependence of the power of a prototype wind power plant, determined by the obtained experimental values of voltage and current on the wind speed. The conversion of alternating current to direct current was carried out using a semiconductor rectifier.

The DC power was calculated: W=U·I, where U is the voltage at the generator output, V; I is the current in the circuit, A. With the increase in wind speed, the generated power increases almost linearly, and at a speed of 7 m/s, the wind power plant gives us a nominal power of 330 watts. The maximum generating power at 12 m/s is 970 watts.

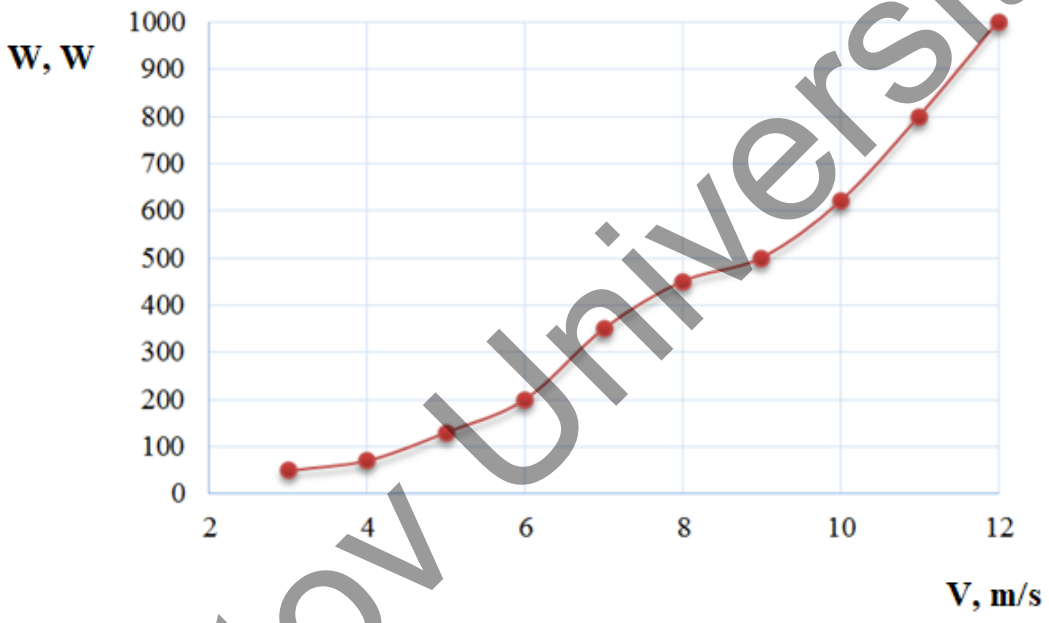

Fig.5.16. Change in power from wind speed for a prototype wind power plant

Figure 5.17 shows the dependence of the rotation frequency of the prototype wind power plant on the wind speed.

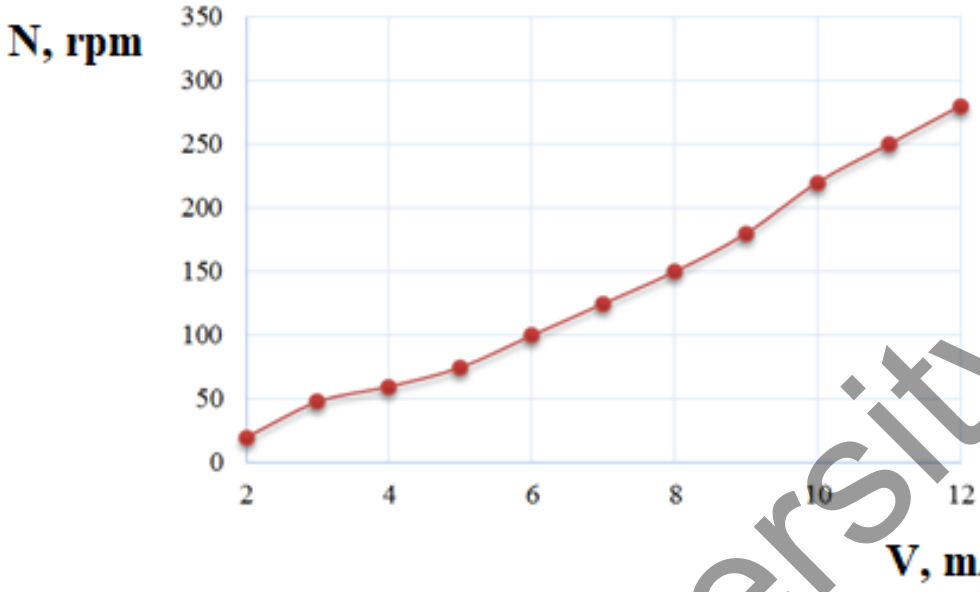

Fig.5.17. Changing the rotation frequency from the wind speed for a prototype wind power plant

Figure 5.17 shows that an increase in wind speed leads to an almost linear increase in the number of revolutions of the wind wheel per minute. This process is due to the fact that with an increase in the speed of the wind running into the wind wheel, the lifting force acting on the blades increases linearly.

Thus, the volt-ampere characteristics of a prototype wind generator with blades in the form of rotating cylinders, the dependence of the power of the wind power plant, voltage, current and shaft rotation frequency on wind speed are obtained. The number of revolutions of the wind wheel is 180 rpm, the minimum threshold of the operating wind speed is 2-4 m / s, the generated power of the wind turbine is -1 kW.

6. DEVELOPMENT OF AN EXPERIMENTAL WIND POWER PLANT WITH BLADES IN THE FORM OF ROTATING CYLINDERS OF CONSTANT CROSS-SECTION WITH A SMOOTH SURFACE

6.1 Assembly of an experimental wind power plant based on the Magnus effect

To study the process of converting the wind energy of the air flow into electrical energy in the laboratory, we have created a special prototype of a wind power plant with blades in the form of rotating cylinders of constant cross-section with a smooth surface, with the help of which the efficiency of using wind energy is estimated. The installation in question belongs to the class of wind turbines operating on the basis of the Magnus effect.

It is convenient to compare the characteristics and parameters of a wind turbine with the help of aerodynamic characteristics, which show how the wind energy utilization coefficient and torque change depending on the speed. The aerodynamic characteristics of a three-bladed and multi-bladed wind turbine presented in [90-104] allowed us to determine their main parameters, which are given in Table 6.1.

Table 6.1

Main parameters of multi-blade wind turbines

Indicator name/ number of blades	3 blades	12 blades	18 blades
Wind energy utilization factor	0.42	0.34	0.36
Relative moment of shear and rotation	0.03	0.28	0.48
Normal speed	4.0	2.5	1.5
Synchronous speed	8.0	6.0	2.6
Wind speed to start the rotational motion of the VD, m/s	5.0-7.0	2.5-3.0	3.0-4.0

Based on the experimental data obtained, it can be said that multi – blade wind turbines are characterized by a large shear and rotation moment and low speed, and a small-blade one is characterized by a relatively small shear moment and high speed.

The aerodynamic parameters of the flow have changed within the following limits:

- the first range – low wind speeds-2-5 m / s;
- the second range – average wind speeds-5-10 m / s;
- the third range – high wind speeds-over 10 m/s.

At the same time, the rotation speed changed from 500 to 1900 revolutions per minute. The directions of rotation could be co-directional and oppositely directed.

In order to activate the rotational movement of the cylinders, an electric current (voltage) is supplied to the engine through the brush-collector mechanism. The collector

is mounted on the shaft and insulated from it with an insulating material. After the collector, the current is directed to the electric motor, which rotates the cylindrical blades.

Electric motors drove cylindrical blades into rotation and regulated their rotation speed using semiconductor electronics.

Thus, based on the above, together with KB "TreeEnergy" LLP (Almaty), an experimental wind power plant with blades in the form of rotating cylinders of constant cross-section with a smooth surface was developed, which was subsequently created in the laboratory "Aerodynamic Measurements".

Figures 6.1 and 6.2 show a diagram of a prototype wind power plant with blades in the form of rotating smooth cylinders, as well as a blade designed in the laboratory "Aerodynamic Measurements".

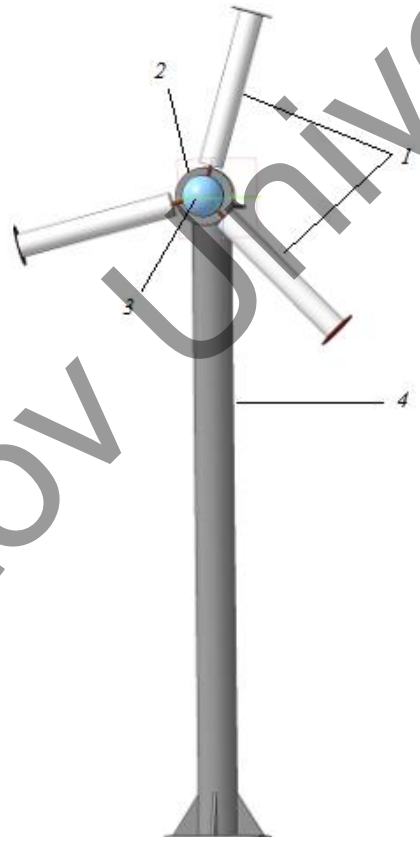

1-rotating cylinders; 2-generator; 3-radial disk with fairing; 4-mast

Fig.6.1.Diagram of a prototype wind power plant with blades in the form of rotating cylinders of constant cross-section with a smooth surface

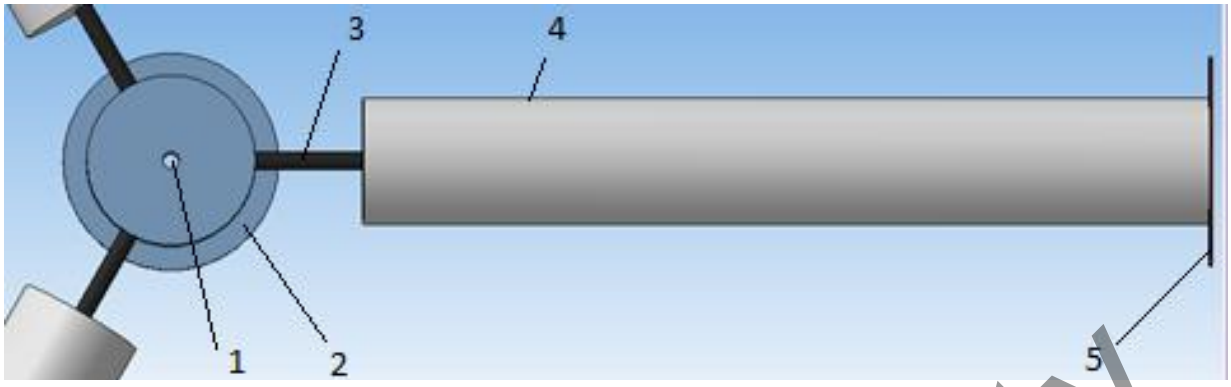

1 - the horizontal shaft of the wind turbine; 2 - the radial disk of the horizontal shaft for fixing the blade; 3 - the non-rotating root part of the wind turbine blade; 4 - the rotating cylindrical part of the blade; 5-the end disk

Fig.6.2.Diagram of the blade in the form of rotating cylinders of constant cross-section with a smooth surface

A wind power plant with blades in the id of rotating cylinders (Figure 6.1) contains a wind wheel with a horizontal axis of rotation, which consists of a radial disk 2 (Figure 6.2), a horizontal shaft 1, non-rotating root parts of the wind turbine blade 3 are attached to the radial disk 2; a rotating cylindrical part 4 and an end washer 5 mounted on it.

Figure 6.3 shows a sample of the blade of a rotating cylinder with a smooth surface.

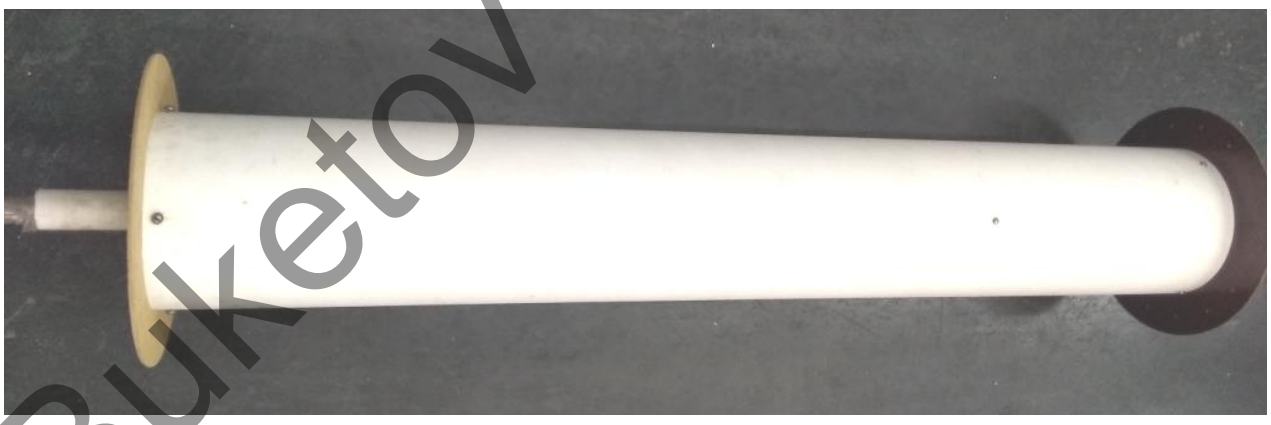

Fig.6.3.Blade of a rotating cylinder

When the cylinders rotate at the ends, the air flow is disrupted from the edge of the cylinder. In this case, the lifting force of the cylinder decreases during rotation. To eliminate the turbulence, end disks with a diameter of 24 cm were installed (Figure 6.2).

Figure 6.4 shows a developed and created prototype of a wind power plant for field tests with blades in the form of rotating cylinders, which can be rotated on a fixed support in the direction of the wind using the tail section.

The total diameter of the wind wheel is 2.4 m. The horizontal shaft is made of a steel rod with a diameter of 25 mm and is the rotational axis of the generator, which in turn is fixed to the upper zone of the mast. The radial disc is made of a steel sheet with a thickness of 10 mm. The diameter of the circular disk is 250 mm. The radial disk is mounted on the rotating root parts of the blades at an angle of 120 degrees relative to each other. The rotating cylindrical parts of the wind turbine blades are made of three cylinders of constant cross-section with a diameter of 150 mm. and a smooth surface. The length of the rotating cylinder is 1 m. End disks with a diameter of 240 mm are installed at the end of the cylinders.

Fig.6.4.A prototype of a wind power plant with blades in the form of rotating cylinders

The wind turbine works as follows (Figure 6.4): when an electric voltage is connected through a brush-collector unit to electric motors, they rotate the cylinders. The cylinders rotate synchronously in the direction and at the same speed. The wind generator is installed in the direction of the wind using a tail mechanism. When the air flows around the rotating cylinders, there is a lifting force that rotates the radial disk and the generator shaft. When the generator shaft rotates, electrical energy is generated.

The lifting force of the blades in the form of rotating cylinders, at low wind speeds, is greater in comparison with traditional blades.

The device promotes the use of a wind wheel in wind power plants that have the ability to operate at low air flow speeds, designed to supply electricity to consumers. The design allows you to ensure safety from breakdowns in case of sudden sharp gusts of wind. Several drawings of the development of a wind power plant are shown in figure 6.5.

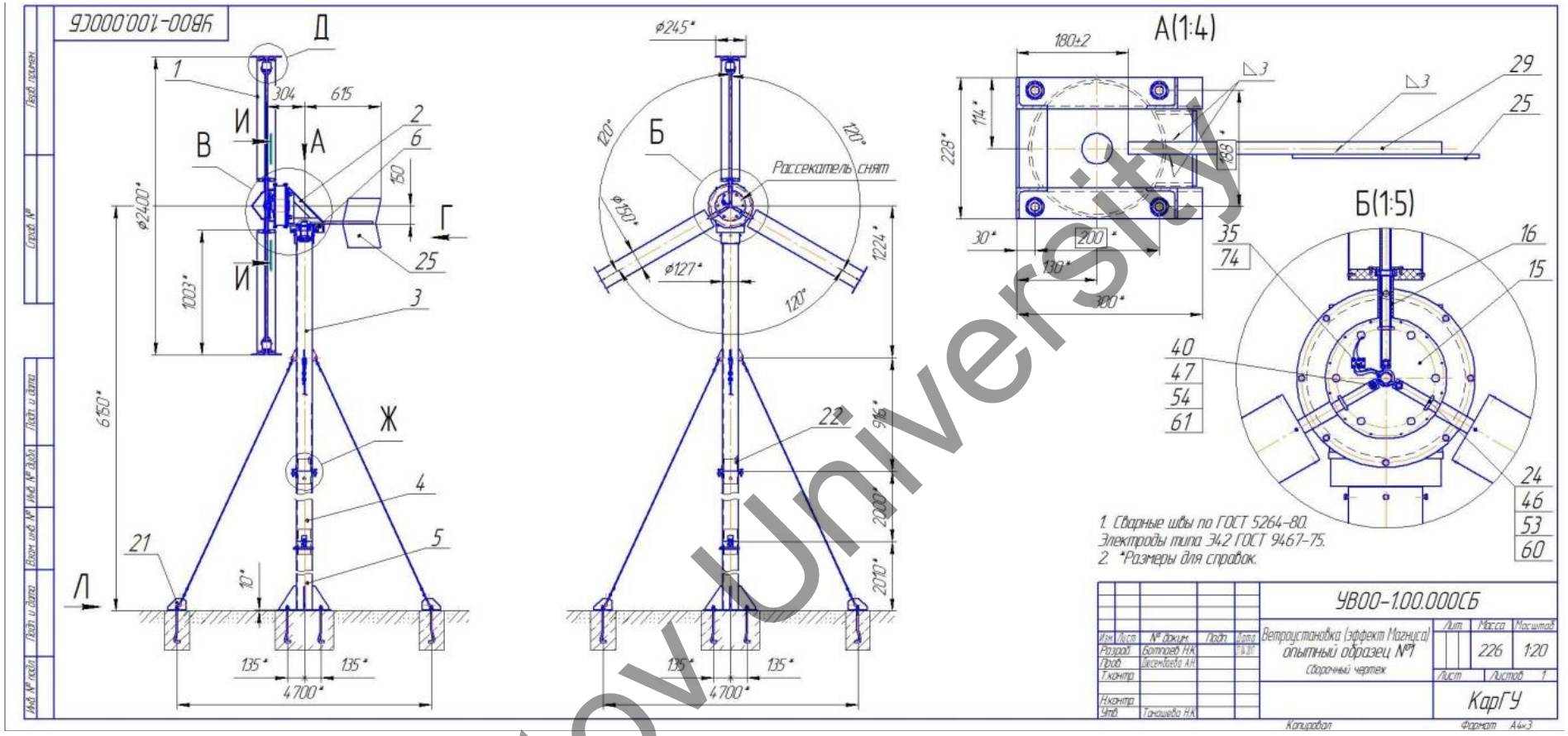

а)

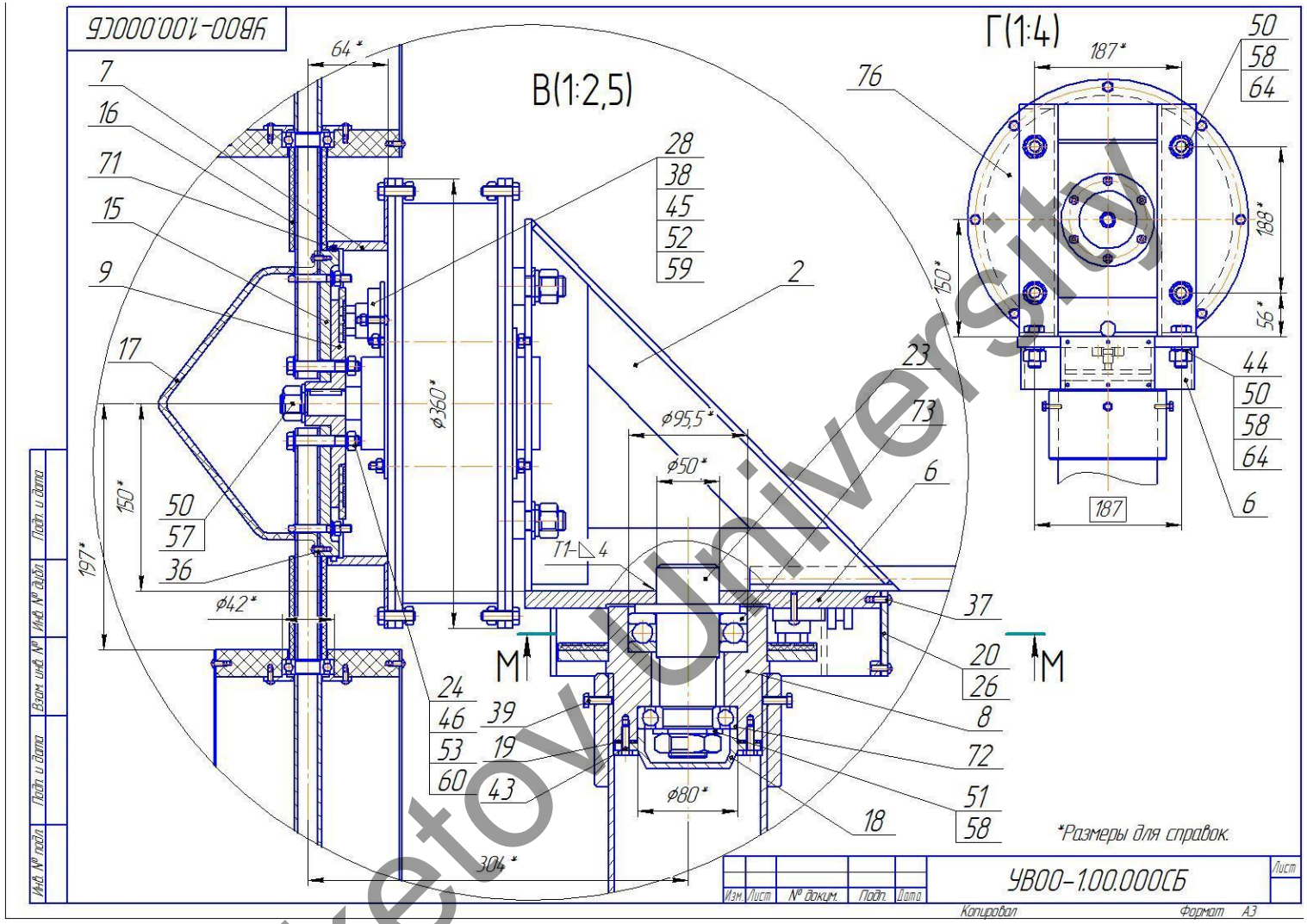

b)

Fig.6.5. Scheme of an experimental wind power plant a) general view b) the scheme of fixing the generator to the housing

Based on the developed wind power plant with blades in the form of rotating cylinders, a patent application was filed and received in June 2019: "Blade of a wind power plant in the form of rotating cylinders" Utility model Patent No. 4043 dated 07.06.2019.

6.2 Accounting for the influence of gyroscopic forces on the working part of the wind turbine

The rotating cylinder of a wind turbine is a fairly massive symmetrical body rotating around the axis of symmetry at a high speed, i.e. it is a source of gyroscopic forces [29-30].

When the cylinder does not rotate around the main axis of the wind turbine, while rotating around its own axis, the moment of momentum of the gyroscope coincides in the direction of its axis of rotation, which is one of the main axes of inertia of this gyroscope. In this case, no action of gyroscopic forces is observed.

For the gyroscopic effect to occur, it is necessary to act on the rotating cylinder by the moment of external forces, which occurs when the air flow affects the system of rotating cylinders, which, due to the Magnus effect, leads to the rotation of this system around the main axis of the wind turbine and the appearance of an increment of the gyroscope's angular momentum, which is the cause of the appearance of gyroscopic forces.

The forced rotation of the gyroscope axis leads, due to the gyroscopic effect, to the appearance of gyroscopic forces acting on the bases of the rotational axes of the cylinders, which contributes to the appearance of additional, sometimes significant, axis pressure on the bearings (Figure 6.6).

The working part of the wind turbine consists of an electric motor for rotating cylindrical rotors around its own axis; the axis of the working shaft; rotate around an axis perpendicular to both the own axis of the cylindrical rotors and around the axis of the working shaft. Thus, the rotor is a system with three intersecting axes of rotation. This makes it possible to use various combinations of aerodynamic forces and gyroscopic forces acting on the working system. The working part is affected by: 1) Magnus forces (with full compensation of gyroscopic forces); 2) gyroscopic precession forces (while minimizing Magnus forces); 3) a combination of Magnus forces and gyroscopic forces.

The magnitude of the gyroscopic forces acting on the supports of the axes of rotation of the cylinders depends on the mass of the rotating cylinder, on the angular velocity of its rotation and on the moment of external forces, depending on the speed of the air flow.

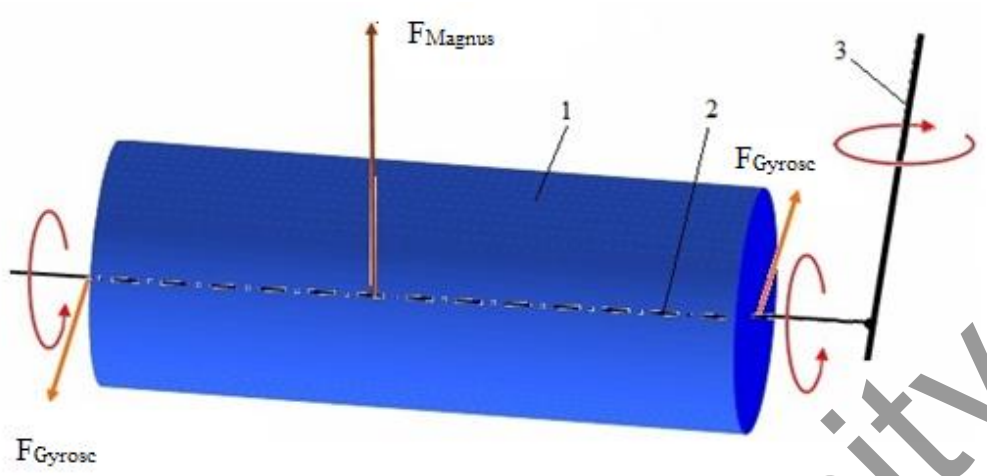

1-cylinder, 2 – cylinder axis, 3-main axis of the wind turbine

Fig.6.6. Diagram of a rotating cylinder of a wind turbine based on the Magnus effect, the appearance of gyroscopic forces

Thus, taking into account the above, in order to reduce the influence of gyroscopic forces when creating a prototype wind turbine, we propose:

1) reduce the mass of the rotating cylinders, as well as the angular velocity of rotation of the cylinders around its own axis;

2) to reduce the influence of the drive motor on the magnitude of the gyroscopic forces at a sufficiently high angular velocity of its rotation.

Figure 6.7 shows the proposed scheme of the rotating part of the wind turbine, which allows reducing the influence of gyroscopic forces.

It is also necessary: a) to use light polymer or composite materials for the manufacture of cylinders (3), which will reduce their weight; b) to rotate the cylinders in the low-speed range of about 500 900 rpm; c) to ensure the parallelism of the axes of the drive motor (1) and the main shaft of the wind generator (2), which will also reduce the influence of gyroscopic forces.

All these conditions in the design shown in Figure 6.7 are met and implemented on Figures 6.8 and 6.9 show photos of the prototype: Drive electric motors that are parallel to the axis of the main shaft of the prototype wind power plant; one of the installation options with blades in the form of rotating cylinders.

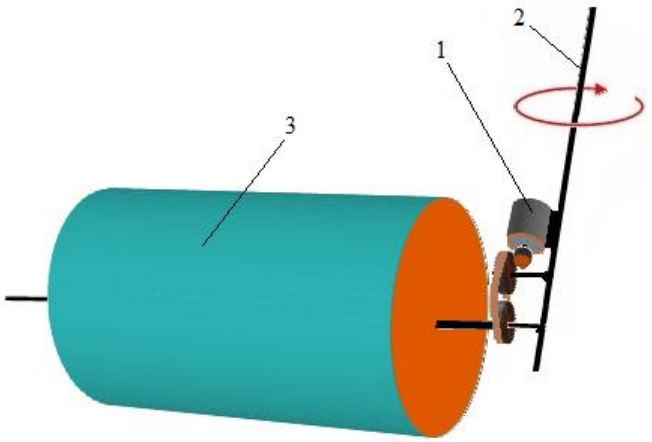

1 – the drive electric motor of the cylindrical rotor, 2 – the main axis of the wind turbine, 3-the cylindrical rotor

Fig.6.7. The layout of the drive motor of the rotor, which reduces the influence of gyroscopic forces

Conclusions:

1. The design of an experimental stand of a prototype wind power plant with blades in the form of rotating cylinders has been developed.

2. Analyzing the conducted studies aimed at studying the influence of gyroscopic forces on the working part of the wind turbine, we proposed: 1) to reduce the mass of the rotating part of the wind turbine using light polymer or composite materials; 2) to reduce the speed of rotation of the cylinders using low-speed generators; 3) to ensure the parallelism of the axes of the drive electric motor and the main shaft of the wind generator.

a)

b)

Fig.6.8. Electric drives a) a laboratory sample of the generator assembly,
b) a laboratory sample of engines for the generator

a)

b)

Fig.6.9. A prototype of a wind power plant with blades in the form of rotating cylinders a) front view, b) side view

7 ANALYSIS OF THEORY AND EXPERIMENT

7.1 Analysis of the results of the study of the wind utilization coefficient from the speed of a wind power plant with blades in the form of rotating cylinders

The speed of a wind wheel is defined as the ratio of the rotation speed of the end of the blade to the wind speed:

$$Z = \frac{2\pi R n_1}{60V} \quad (7.1)$$

where, R — radius of the wind wheel, m; n — number of revolutions; V — the speed of the incoming air flow, m/s.

Based on experimental studies, we will construct the Reynolds number based on the velocity of the incoming flow V and the diameter of the wind wheel D=2.372 m. We will take the viscosity of the air $1.795 \cdot 10^{-5}$ Pa·s, and the density 1.225 kg/m^3, $\mathrm{Re} = \frac{\rho D V}{\mu}$.

The linear dependence of the speed value of the wind wheel on Re, obtained for different speeds of rotation of the cylinders, is shown in Figure 7.1. As can be seen from the graph, the speed value decreases with an increase in the number of Re, but at the same time it increases with an increase in the speed of rotation of the cylinders.

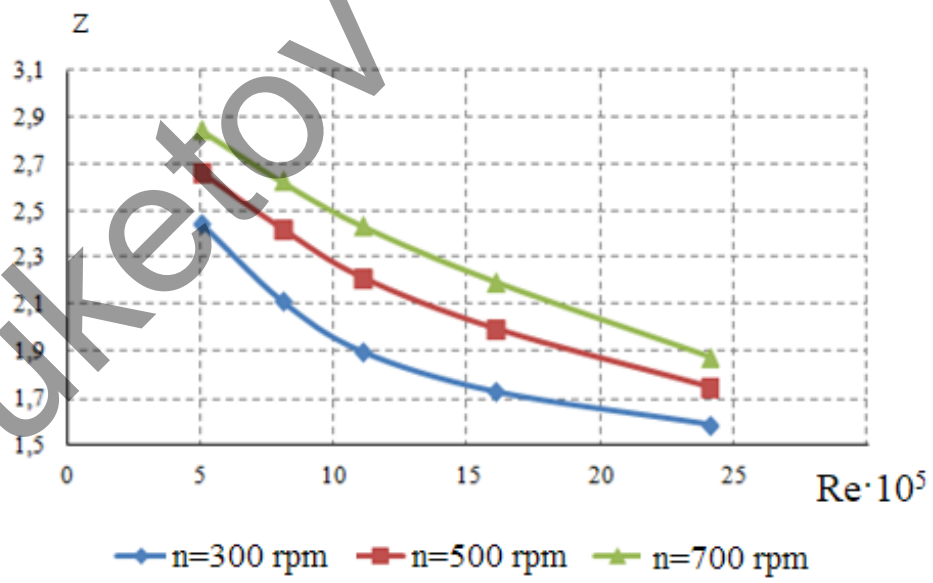

Fig.7.1. Change in the speed value depending on the Reynolds number for the wind wheel

The obtained data can be reduced to a single curve if we enter the dimensionless speed of rotation of the cylinder as the ratio of the speed of movement of the cylinder surface to the speed of the incoming flow $\alpha = \frac{2\pi rn}{60V}$.

The linear dependence of the speed of the wind wheel on the rotational speed of the cylinders is shown in Figure 7.2. The obtained dependence (points-rhombuses) is approximated with acceptable accuracy by the formula $Z = 2.5463\alpha^{0.2354}$. The speed rises with an increase in the dimensionless speed of rotation of the cylinders.

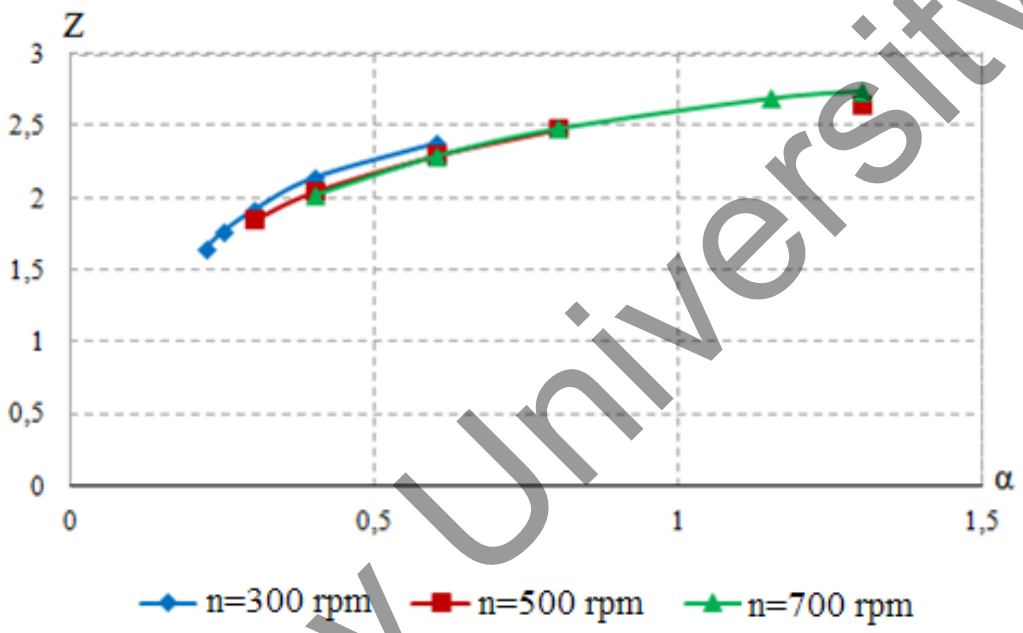

Fig.7.2. Change in the speed value depending on the dimensionless speed of rotation of the cylinders for the wind wheel

The obtained dependence (Figure 7.2) is approximated with acceptable accuracy by the formula $Z = 2.5463\alpha^{0.2354}$. With the increase in the dimensionless speed of rotation of the cylinders, the speed of the wind wheel monotonously increases.

We define the wind utilization factor as the ratio of the wind wheel rotation power minus the cylinder rotation power to the wind flow power per the surface area covered by the wind wheel:

$$\xi = \frac{N_{ww} - N_c}{N_{wf}}, \qquad (7.2)$$

where, $N_c = mM_c\omega_c$ – мощность вращения цилиндров.

m – number of cylinders; M_c – the moment of forces acting on the rotating cylinder; ω_c – the angular speed of rotation of the cylinder.

$N_{wf} = \frac{\rho V^3 S}{2}$ – wind flow power.

ρ – the density of air in the incoming flow; $S = \pi R^2$ – the area covered by the wind wheel; v – the speed of the incoming flow.

$N_{ww} = M_{ww}\omega_{ww}$ – wind wheel rotation power.

M_{ww} – the moment of forces acting on a movable wind wheel; ω_{ww} – the angular velocity of the free rotation of the wind wheel or $N_{ww} = M_{ww}\frac{2\pi n_1}{60}$.

The change in the wind energy utilization coefficient from the wind speed is shown in Figure 7.3.

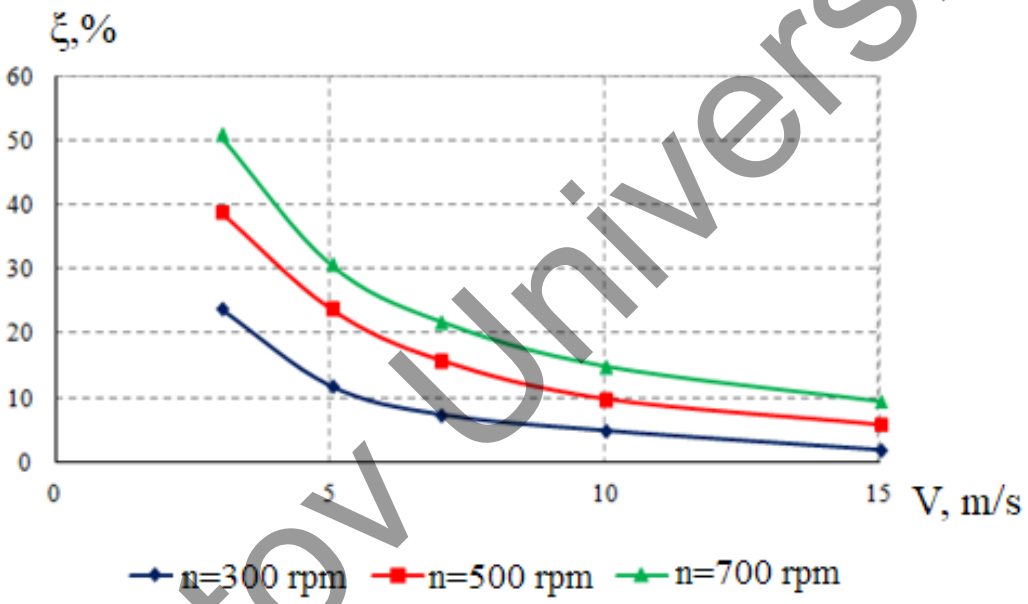

Fig.7.3.The dependence of the wind utilization coefficient on the speed of the incoming flow

As follows from Figure 7.3, to increase the efficiency of using wind, it is necessary to increase the speed of rotation of the cylinders, and the lower the speed of the incoming flow, the higher the efficiency of using wind.

All the data obtained, which are presented in Figure 7.3, can be combined into one dependence of the wind utilization coefficient on the speed of the wind wheel, Figure 7.4. As you can see, the efficiency of wind use can be represented by a power function of the speed of the wind wheel (7.3):

$$\xi = 0.3153 \cdot Z^{4.8325}. \qquad (7.3)$$

It follows from this dependence that the efficiency of wind use increases in proportion to the speed of the wind wheel to a degree close to 5.

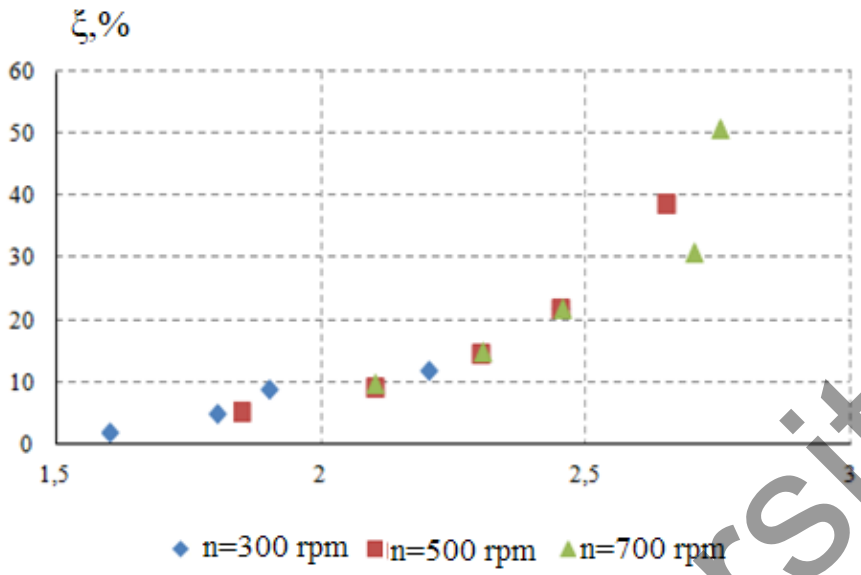

Fig.7.4.The dependence of the wind utilization coefficient on the speed of the wind wheel

7.2 Analysis of theoretical results on the pressure distribution in the vicinity of a wind power plant

Figures 7.5-7.14 show the distributions of static pressure ($p_{st} = p-p_{atm}$) in the field of the wind wheel (plane z=0), obtained for different speeds of the incoming flow (wind) and the speeds of rotation of the cylinders. Figures 7.5, 7.7, 7.9, 7.11, 7.13 correspond to a movable wind wheel, and Figures 7.6 7.8, 7.10, 7.12, 7.14 correspond to a freely rotating wind wheel .

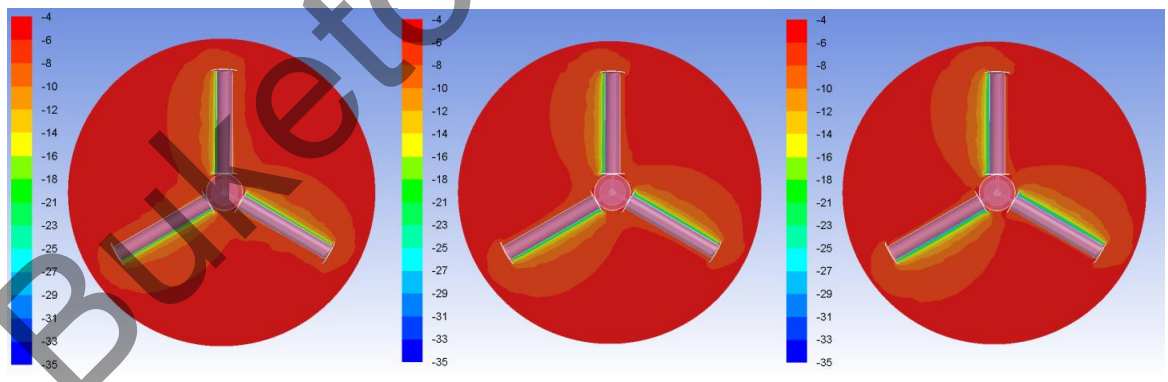

a) *b*) *c*)

a – *n*=300 rpm, *b*-*n*=500 rpm, *c*-*n*=700 rpm

Fig.7.5.Pressure distribution in the plane z=0 for a movable wind wheel V= 3 m/s

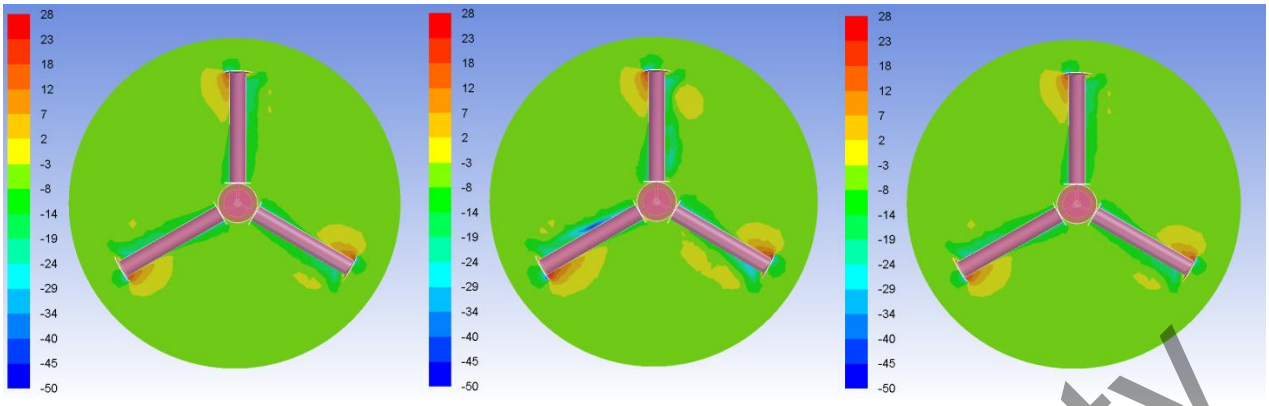

a) *b*) *c*)

a – *n*=300 rpm, *b*-*n*=500 rpm, *c*-*n*=700 rpm

Fig.7.6.Pressure distribution in the plane *z*=0 for a freely rotating wind wheel *V*= 3m/s

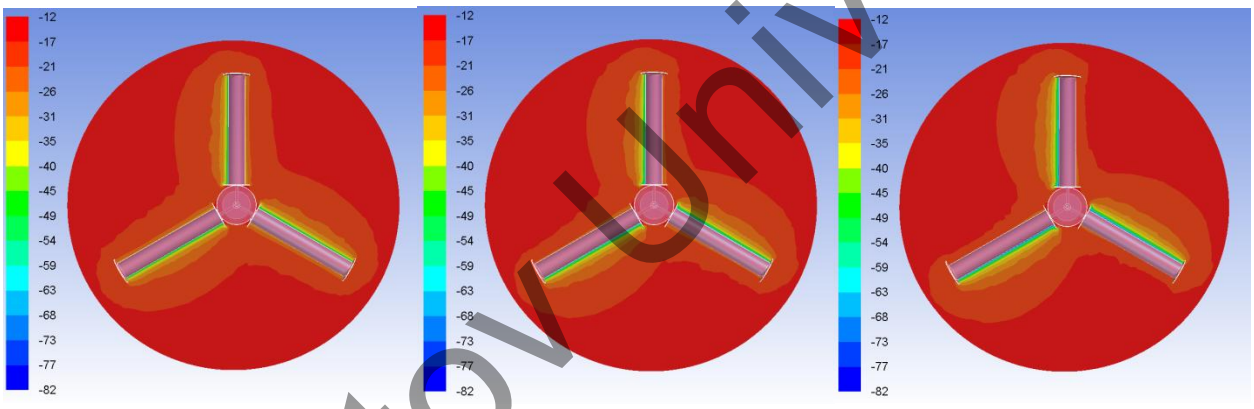

a) *b*) *c*)

a – *n*=300 rpm, *b*-*n*=500 rpm, *c*-*n*=700 rpm

Fig.7.7.Pressure distribution in the plane *z*=0 for a movable wind wheel *V*=5 m/s

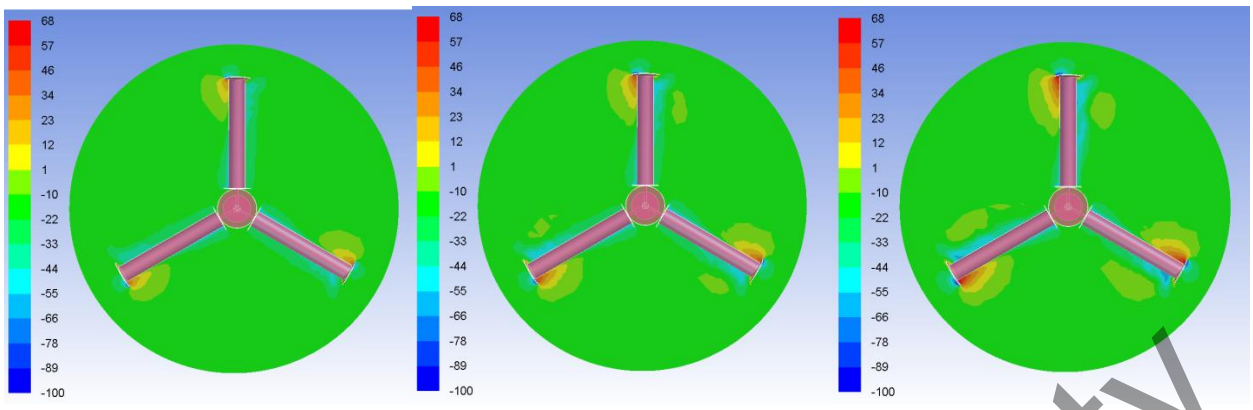

a) *b*) *c*)

a – *n*=300 rpm, *b*-*n*=500 rpm, *c*-*n*=700 rpm

Fig.7.8.Pressure distribution in the plane *z*=0 for a freely rotating wind wheel *V*=5 m/s

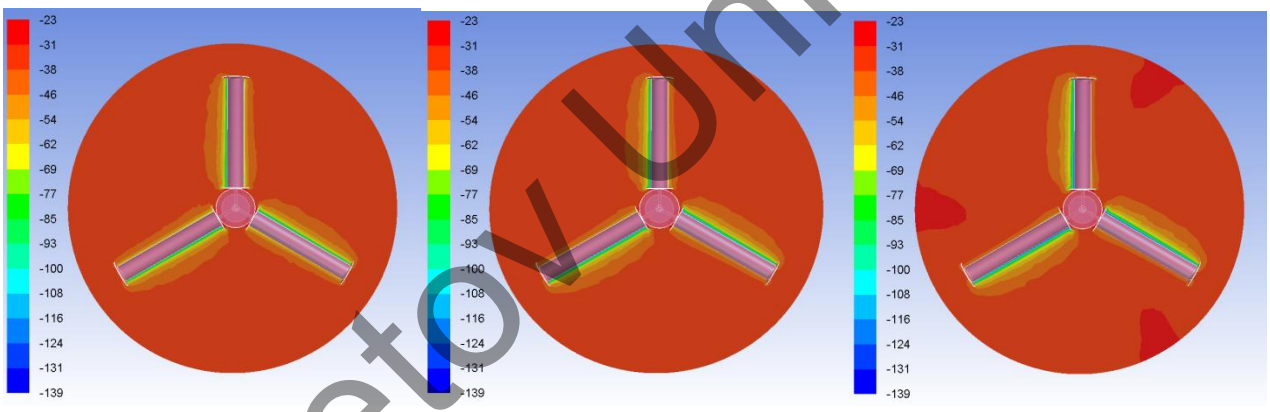

a) *b*) *c*)

a – *n*=300 rpm, *b*-*n*=500 rpm, *c*-*n*=700 rpm

Fig.7.9.Pressure distribution in the plane *z*=0 for a movable wind wheel *V*= 7 m/s

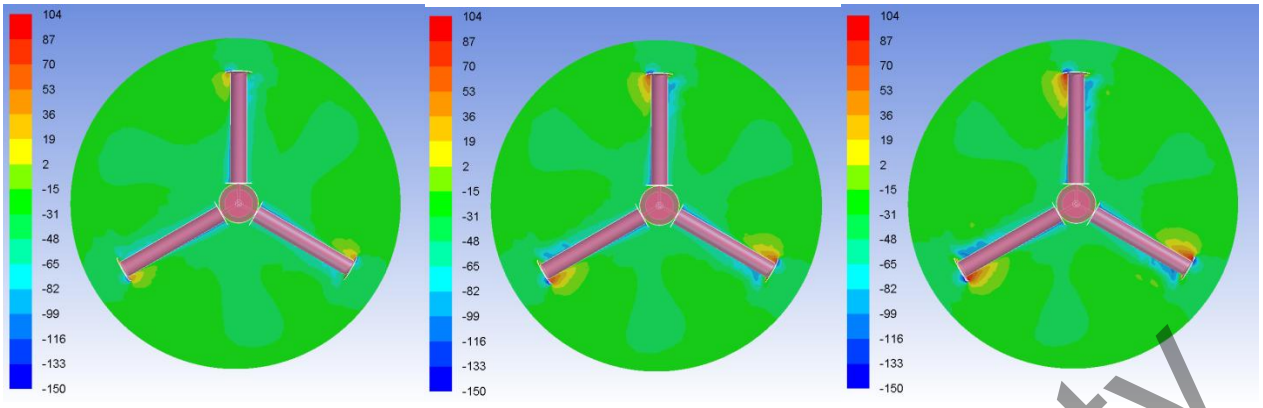

a) *b*) *c*)

a – *n*=300 rpm, *b*-*n*=500 rpm, *c*-*n*=700 rpm

Fig.7.10.Pressure distribution in the plane *z*=0 for a freely rotating wind wheel *V*= 7 m/s

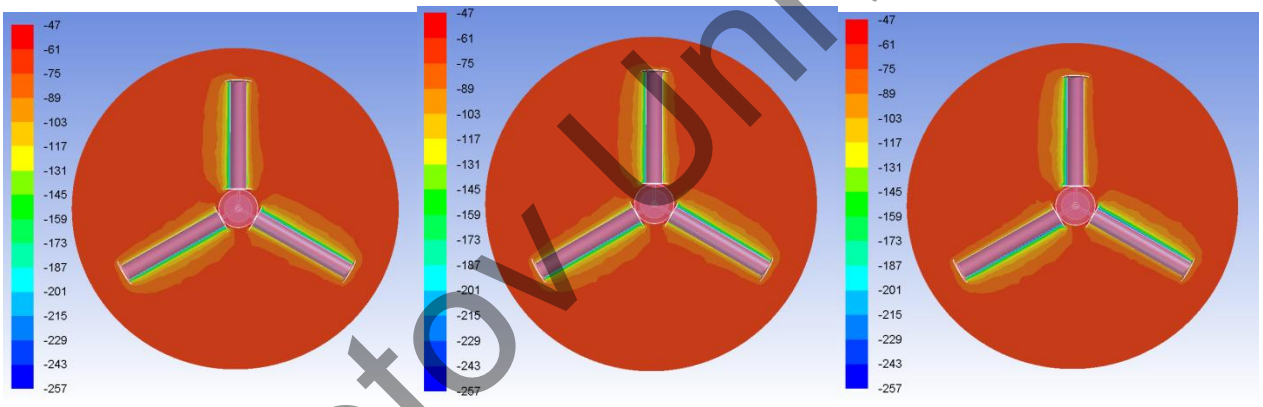

a) *b*) *c*)

a – *n*=300 rpm, *b*-*n*=500 rpm, *c*-*n*=700 rpm

Fig.7.11.Pressure distribution in the plane *z*=0 for a movable wind wheel *V*= 10 m/s

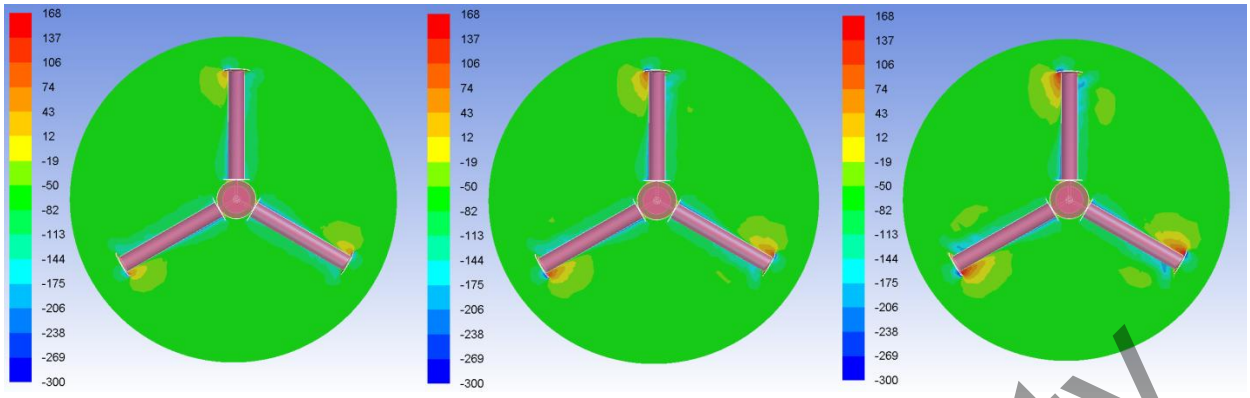

a) *b*) *c*)

a – *n*=300 rpm, *b*-*n*=500 rpm, *c*-*n*=700 rpm

Fig.7.12.Pressure distribution in the plane *z*=0 for a freely rotating wind wheel *V*= 10 m/s

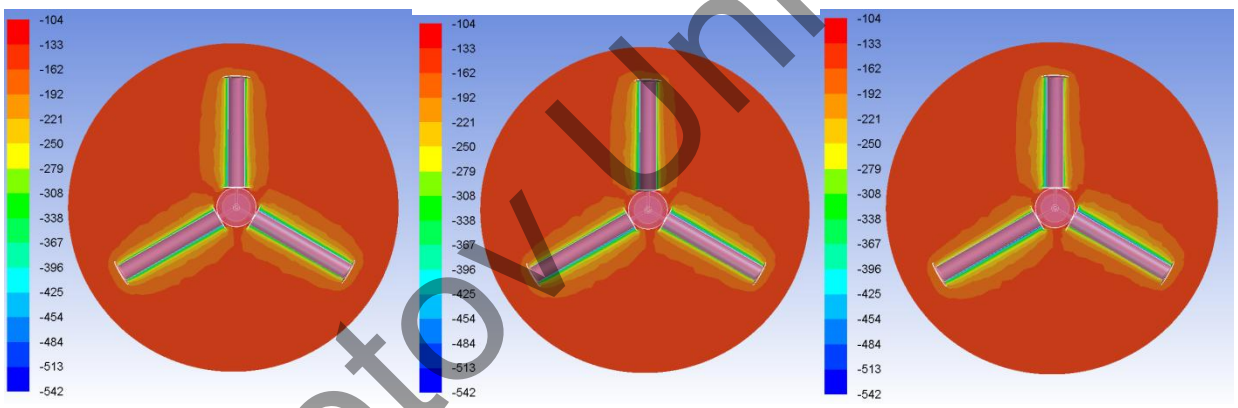

a) *b*) *c*)

a – *n*=300 rpm, *b*-*n*=500 rpm, *c*-*n*=700 rpm

Fig.7.13. Pressure distribution in the plane *z*=0 for a movable wind wheel *V*= 15 m/s

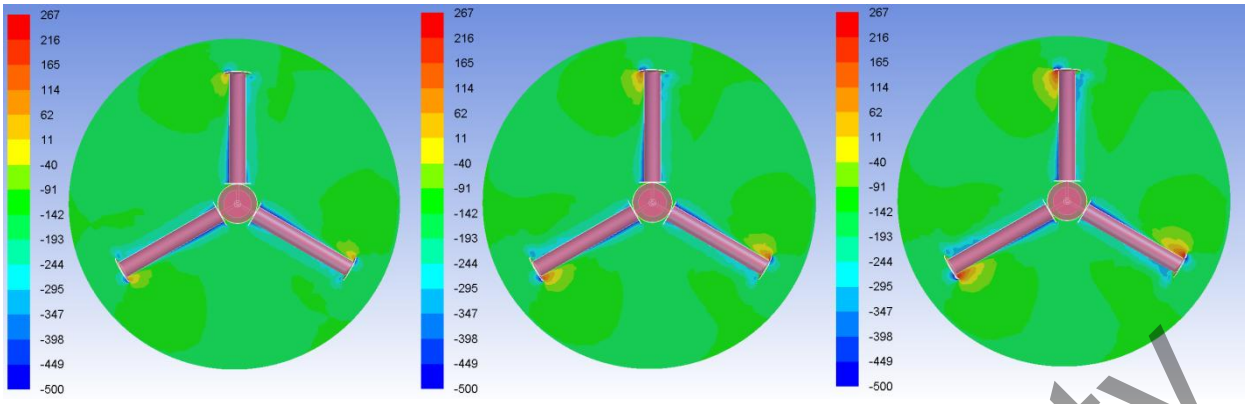

a) *b*) *c*)

a – *n*=300 rpm, *b*-*n*=500 rpm, *c*-*n*=700 rpm

Fig.7.14. Pressure distribution in the plane *z*=0 for a freely rotating wind wheel *V*= 15 m/s

The rotational movement of the cylinders in the conditions of an oncoming one leads to a speed difference, namely, on one side of the cylinder, the air speed will be higher than on the other side. According to Bernoulli's law, in the area where the flow velocity is higher, the pressure becomes lower. Therefore, on one side of the cylinders (in the figures shown, this left side), the pressure is lower than on the other, as a result of which there is a force (lifting) acting on each cylinder, which is directed at right angles to the axis of the cylinder and the direction of the wind. Since all the cylinders rotate in the same direction (counterclockwise) relative to their own axes, the lifting forces will create a moment of forces that causes the wind wheel to rotate counterclockwise relative to the z axis.

It follows from this that the pressure field in the field of the rotating wind wheel has an insignificant effect, the variation of the cylinder rotation speed in the range from 300 to 700 rpm has an insignificant effect. The explanation for this phenomenon is that the speed of movement of the cylinder surface at a rotation speed of 700 rpm is only about 5 m/s. At such a low speed of movement of the cylinder surface, a relative change in the pressure distribution should be expected for a wind speed of 3 m/s, Figure 7.6).

When the wind speed is 3 m/s, the static pressure in the field of the wind wheel changes from -35 Pa to -4 Pa. An increase in wind speed leads to an expansion of the range of pressure changes. So for a wind speed of 5 m/s, this range is from-82 Pa to -12 Pa, for 7 m/ s - from -139 Pa to -23 Pa, for 10 m/s - from -257 Pa to -47 Pa, for 15 m/s - from -542 Pa to -104 m/s.

The rotation of the wind wheel leads to the fact that the pressure range in the vicinity of the wind wheel changes, mainly due to a change in the upper limit. So for a flow velocity of 3 m / s, the extreme limit of static pressure becomes equal to 20 Pa, for 5 m/s it is 68 Pa, for 7 m/s it is 104 Pa, for 10 m/s it is 168 Pa, for 15 m/s it is 267 Pa.

Unlike a movable wind wheel, the pressure distribution along the cylinders ceases to be uniform. More pressure is observed on the periphery of the wind wheel from the windward side, while on the periphery from the leeward side the pressure is less. The explanation of this phenomenon is the high speed of movement of the sections of the cylinder surfaces on the periphery in the direction perpendicular to the z axis (25 m/s-30 m/s, Figure 7.14) and the low speed of rotation of the cylinder surfaces relative to their own axes (5 m/s). The higher the speed of rotation of the cylinders, and hence the speed of free rotation of the wind wheel, the higher the pressure drop at the periphery between the windward and leeward sides of the cylinders. In the field of zones of the surfaces of cylinders located closer to the axis of rotation, the picture is the opposite. The pressure from the windward side is less than from the leeward side, figure, since in this case the speed of the rotational movement of the cylinders around their own axes is greater than the speed of their movement in the plane of rotation of the wind wheel.

7.3 Comparative analysis of the theory and experiment of aerodynamic characteristics of a wind power plant

The data obtained by theoretical and experimental calculations were compared.

Figure 7.15 contains information about the values of the drag coefficient as a function of the Reynolds number, provided that the angular velocity is constant and equal to 1000 rpm.

It can be seen that the data of the numerical experiment are approximated by the power dependence $C_x = 160.81 \cdot \mathrm{Re}^{-0.471}$: The drag coefficient decreases with the growth of the Reynolds number

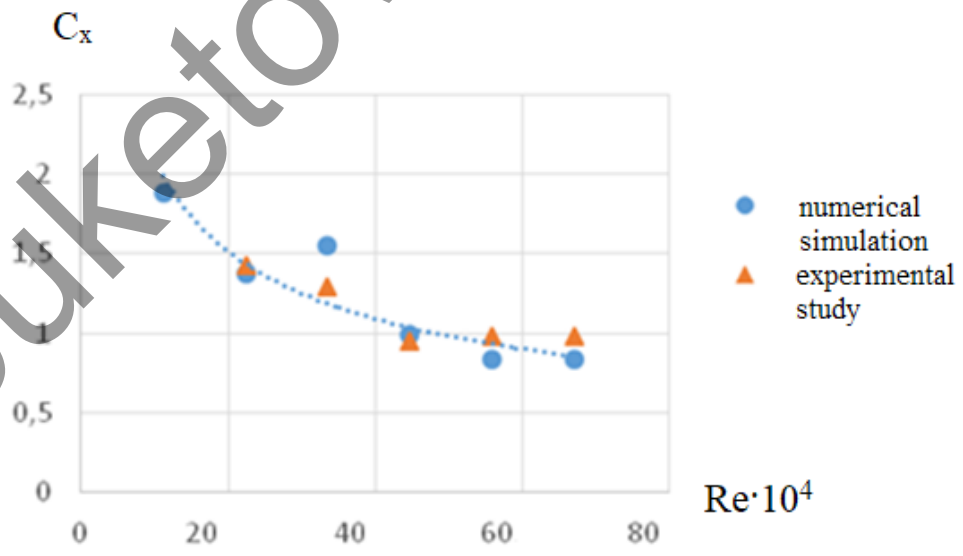

Fig.7.15. The change in the value of the drag coefficient as a function of the Reynolds number, provided that the angular velocity is equal to 1000 rpm

Figure 7.16 contains information about the values of the lift coefficient as a function of the Reynolds number, provided that the angular velocity is constant and equal to 1000 rpm. The power dependence can be approximated by the data $C_y = 3e + 0.6\,\mathrm{Re}^{-1.202}$ of a numerical study.

The lift coefficient decreases with the growth of the Reynolds number.

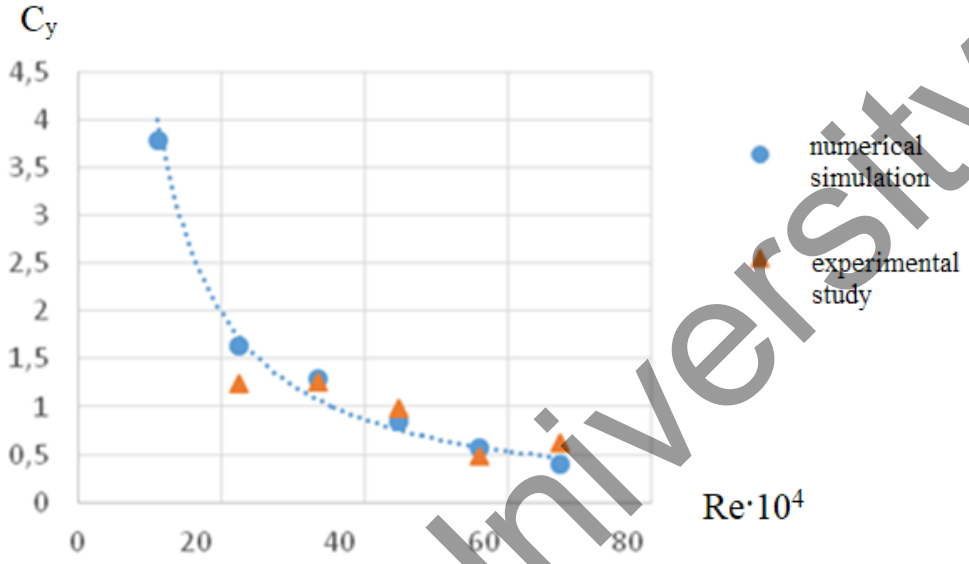

Fig.7.16. The dependence of the lift coefficient on the Reynolds number at an angular velocity equal to 1000 rpm

Thus, from the comparison of the results obtained in the simulation process using the ANSYS FLUENT program and the experimental data obtained during tests of a three-bladed wind turbine, we can see a satisfactory agreement between experimental and numerical calculations for aerodynamic characteristics. The maximum discrepancy between the numerical and experimental data does not exceed 1-2 %.

CONCLUSION

In this monograph, the basics of mathematical modeling of wind power plants based on the Magnus effect, with a different number of blades (2 and 3 blades), are considered and studied. These wind power plants have the main advantage – the generation of electric energy starting from 2-4 m/s of the incoming air flow.

It is shown that mathematical modeling of wind power installations is a set of fundamental and applied scientific directions for the study of processes and phenomena using mathematical methods, computational algorithms and information technologies implemented in software complexes, with the help of which a machine experiment is conducted and a decision is made based on the results of research.

As a means of mathematical modeling, the universal software system of finite element analysis ANSYS FLUENT is considered, which has proven itself as a powerful tool for solving problems ranging from deformable solid mechanics and structural mechanics to problems of aerogasodynamics.

The main results of theoretical calculations of aerodynamic characteristics are obtained. From the comparison of the results obtained during the simulation using the ANSYS FLUENT program and the experimental data obtained during the tests of the wind power plant, it is possible to see a minimal divergence between the data obtained by experiments and numerical studies on the aerodynamic parameters of the wind generator. The maximum discrepancy between the numerical and experimental data does not exceed 1-2 %.

An experimental sample of a low-speed electric generator with permanent magnets was also developed and studied.

It is established that the developed electric generator begins to produce EMF at significantly lower air flow speeds than its predecessors, and it has a reliable contactless excitation system and operates at 50-350 revolutions per minute.

On the windings of an experimental electric generator, EMF occurs at a noticeably lower number of revolutions of the generator shaft. This is achieved due to both a lower threshold of operation of the electric generator and its greater efficiency.

The volt-ampere characteristics of a prototype wind generator with blades in the form of rotating cylinders, the dependence of the power of the wind power plant, voltage, current and shaft rotation frequency on wind speed are obtained. The number of rotation of the wind wheel is 180 rpm, the speed at which its rotational movement is carried out is 2-4 m/s, the generated power of the wind turbine is -1 kW.

The results of the study of the wind utilization coefficient from the speed of a wind power plant with blades in the form of rotating cylinders are obtained.

It is established that with an increase in the rotation speed of the wind turbine cylinders and the lower the incoming speed, the higher the efficiency of wind use.

It is established that when the air flows around three rotating cylinders, a zone of high pressure appears at the point of contact of the pressure areas of each cylinder, and a

rarefaction zone appears behind the cylinders. On the basis of numerical modeling and the conducted experiment, universal dependences of aerodynamic characteristics on the velocity of the incoming flow at a constant angular velocity are obtained. The flow patterns of three rotating cylinders in the air flow are also given, which can explain the behavior of the aerodynamic characteristics.

A rotating cylinder can be used as an element of a wind turbine, which works much more efficiently than an element in the form of wing profiles at low flow rates up to 10 m/s.

The obtained theoretical and experimental data can be used in the development and creation of a wind turbine with cylindrical elements of variable cross-section, which works more efficiently, unlike other types of wind turbines with winged blades at low speeds of the incoming air flow.

For the first time, the obtained results of mathematical modeling of wind power plants, which are presented in this monograph, on the basis of which a prototype was developed and created, are an important step and the foundation for further research of wind turbines with other configurations and shapes of blades and wind wheels.

LIST OF SOURCES USED

1 Dukenbayev, K. D. Power engineering of Kazakhstan. Movement to the market. - Almaty: Gylym, 1998. - pp. 54-74, 88-98.

2 On support for the use of renewable energy sources: the law of the Republic of Kazakhstan of july 4, 2009, no. 165-iv3rk.

3 Decree of the president of the Republic of Kazakhstan. Strategy of territorial development of the Republic of Kazakhstan until 2015: approved on august 28, 2006, no. 167.

4 Breusov, V. P. Technologies of transformation of unconventional renewable energy sources. - st. Petersburg: Nestor, 2001. - 106 p.

5 https://www.akorda.kz/ru/addresses/addresses_of_president/poslanie-prezidenta-respubliki-kazahstan-nnazarbaeva-narodu-kazahstana-14-dekabrya-2012-g

6 Ushakov, V. Y. Modern and promising energy: technological, socio-economic and environmental aspects. - Tomsk: TPU publishing house, 2008. - 469 p.

7 Belyaev Y. M. Alternative energy strategy. - rostov n/a: publishing house of the south. - kavk. Of the scientific center of the higher school, 2003. - 206 p.

8 Contreras M.A. Renewable energy sources/ M.A. Contreras, s. Deb. - Cambridge: Cambridge university press, 2011.

9 Lukutin B. V. Renewable energy in decentralized electricity supply / B. V. Lukutin, O. A. Surzhikova, E. B. Shandarova. - Moscow: Energoatomizdat, 2008 –231 p.

10 I. V. Erofeev, E. N. Korzhov, A. I. Shashkin, A.V. Ivanov, M. V. Dobrosotskaya. Mathematical modeling of turbulent fluid flow in an annular confuser under the influence of a pressure drop // Bulletin of the VSU. Series: Physics. Mathematics. - 2011. - no. 1. - p. 138-146

11 Gorelov.N. D, Krivospitsky.P.V. Prospects for the development of wind power plants with an orthogonal rotor // Thermophysics and aeromechanics. - 2008. - Vol. 15. No. 1. - pp. 163-167.

12 Bobkov V. G., Bondarev A. E., Zhukov V. T., Manukovsky K. V., Novikova N. D., Feodoritova O. B. Numerical study of the dynamics of vertical-axial wind turbines / / Preprints of IPM named after M. V. Keldysh. -2019. - No. 119. -25 p.

13 Gurinov A. S., Gaponov V. L. Mathematical model of the dynamics of rotation of a wind turbine and rotation of a small wind power plant for farms by means of an automatic orientation system. // Bulletin of DSTU.-2011. - Volume 11. No. 10– pp. 1763-1770.

14 Obukhov S. G., Sarsikeev E. Zh. Mathematical model of a low-power wind turbine in the MATLAB Simulink environment / / International scientific journal "Alternative Energy and Ecology" -2012. – № 02 (106). – Pp. 42-48.

15 Martianov A. S. Research of control algorithms and development of a controller for a wind power plant with a vertical axis of rotation. dis. ... Candidate of Technical Sciences: 05.09.03 defended 08.04.16/ Martianov A. S.-Chelyabinsk, 2016 – - 174 p.

16 Mingaleeva R. D., Bessel V. V.. Methodology for estimating the total capacity of a wind farm // The territory of neftegaz. -2014. - p. 82-86
17 Sherich F., Fletcher T., Brown R. Modeling of aerodynamic characteristics and dynamics of the track of a wind turbine with a vertical axis // Wind energy. - 2010. - 14(2), - pp. 159-177.
18 Miroshnik V. Y., Podberezkin D. A., Kopeikin D. A., Sokolov P. S., Artamonova E. Y. Methods of aerodynamic design of wind turbines // International research journal. - 2016. –№ 12 (54) Part 3 . – S. 142-153.
19 Sayed M. Unsteady aerodynamic modeling of the blades of the wind turbine with a horizontal axis/ M. Sayed, A. A. El-Badawi // 10th world conference on wind energy/Cairo Soliman Abaza St.Mohandessin. - Cairo, 2011.
20 Yansuya P., Kumsuwan Yu. Designing MATLAB/Simulink simulation of a wind turbine with a fixed angle of inclination // The energy procedure of the simulator. - 2013. -34. - p. 362-370.
21 Tariq R., Hamdi A., Hussein M.A. Modeling and Simulation of Wind Turbine Generator Using Ma`tlab-Simulink // Journal of Al Rafidain University College. – 2017. – Issue No. 40. – P.282-300
22 Manyonge A.W., Manyala R., Onyango F. N., Shichika J. Mathematical Modelling of Wind Turbine in a Wind Energy Conversion System: Power Coefficient Analysis // Applied Mathematical Sciences. – 2012. – 6(91) . –P. 4527-4536.
23 Gul M., Tai N., Huang W., Nadeem Haroon M., Yu M. Evaluation of Wind Energy Potential Using an Optimum Approach based on Maximum Distance Metric. // Sustainability. –2020. – Vol.12.,Issue 5.–P.1999-2005.
24 Nikishin A. Yu., Kazakov V. P. Modern wind power installations based on asynchronous machines / / Journal Modern problems of science and education. -2012. - No. 6. - p. 122-129.
25 Tikhonov A. N. Improving the efficiency of combined autonomous power supply systems based on renewable energy sources: abstract of dis. ... candidate of Technical Sciences: 05.14.08.: - Moscow, 2013. - 27 p.
26 Shakenov K. B. Improvement of a closed-type wind power plant in a complex using solar energy: dissertations for the degree of Doctor of Philosophy (PhD): 6D071800:protected on 21.05.21/ Shakenov K. B.-Almaty, 2021 – 118c.
27 Qolipour M., Mostafaeipour A. , Rezaei M. A mathematical model for simultaneous optimization of renewable electricity price and construction of new wind power plants (case study: Kermanshah) // International Journal of Energy and Environmental Engineering. –2018. –9. –P.71–80.
28 Obukhov S. G., Plotnikov I. A., Sarsikeev E. Zh. Dynamic model of the longitudinal component of wind speed / / Journal Modern problems of science and education. – 2013. – № 5.
29 Pashchenko F. F., Torshin V. V. On the influence of the angle of inclination of the blade surface on the dynamic characteristics of wind turbines. // Problems of mechanical engineering and automation. -2012. - No. 3. - pp. 41-46.

30 Tandjaoui M. N., Benachaiba C., Abdelkhalek O., Dennai B., Mouloudi Y. The Impact of Wind Power Implantation in Transmission Systems // Energy Procedia. – 2013. –36 . –P. 260 – 267.
31 Wollz D.H., Oliveira da Silva S.A., Sampaio L. P. Real-time monitoring of an electronic wind turbine emulator based on the dynamic PMSG model using a graphical interface //Renewable Energy. – 2020.– 155.
32 Belsky A. A. Modeling of operating modes of a hybrid wind power complex / / Modern engineering and technologies. –2014. –№ 5.
33 Aitbayev M. M., Alexandrova R. A., Imanov A. N., Galiev A. Zh. Energy pools based on renewable energy sources / / Journal actual scientific research in the modern world . -2019. – № 9-1 (53) . –pp. 63-68.
34 http://old.unesco.kz/science/2012/kurs.pdf
35 Perminov E. M., Rustamov N. A. On the prospects of renewable energy // Energy: economics, technology, ecology. - 2016. - No. 11. - pp. 19-28.
36 Dosmukhanbetova R. S. Prospects for the development of energy in Kazakhstan // Collection of scientific articles based on the materials of participants of the International correspondence scientific and practical conference. Keynes Laboratory of Applied Economic Research. - Moscow, 2013, P. 9-12.
37 Bezrukikh P.P. Wind Energy. (Reference and methodological manual).- Moscow: Publishing house "Energia", 2010 – 320p.
38 Tanasheva N. K., Shrager E. R., Sakipova S. E., Dyusembayeva A. N., Nurgalieva Zh. G., Karsybekov R. Investigation of aerodynamic characteristics of a wind generator based on the Magnus effect // Bulletin of the Karaganda University .The series "Physics". – 2017. –№ 3(87) . –pp. 60-64.
39 Kusaiynov K., Tanasheva N.K., Turgunov M.M., Diusembaeva A., Kalikova A. The effect of porosity on the aerodynamic characteristics of a rotating cylinder // Eurasian Physical Technical Journal. — 2013. — Vol. 10. — № 2 (20). — P. 26–32.
40 Dulnev G. N. Theory of heat and mass transfer. - St. Petersburg: NIU ITMO, 2012 – 195 p
41 Mikheev M. A. Fundamentals of heat transfer / M. A. Mikheev, I. M. Mikheeva M.. - M: "Energy", 1975.
42 Landau L. D. Course of theoretical physics / L. D. Landau, E. M. Lifshits T. 6. Hydrodynamics. - M.: Nauka.- 1988.-736 p.
43 Sedov L. I. Mechanics of a continuous medium. Vol. 1, 2. Moscow: Nauka. -1978.
44 Shlichting G. The theory of the boundary layer. M.: Publishing house of foreign literature. -1956. -528 p.
45 Sebisi T. Convective heat transfer / T. Sebisi, P. Bradshaw. - M.: Mir. -1987 – 592 p.
46 Bennett K. O. Hydrodynamics, heat transfer and mass transfer/ K. O. Bennett, J. E. Myers. - M.: Nedra. -1966 – 725 p.
47 Van Dyke M. Album of liquid and gas flows. Moscow: Mir. - 1986. -182 p.
48 Frick P. G. Turbulence: approaches and models. Moscow-Izhevsk: Institute of Computer Research. -2003. -292 p.

49 Mazo A. B. Modeling of turbulent flows of an incompressible fluid. Training manual. Kazan: Publishing House of Kazan University. -2007. -109 s
50 ANSYS Fluent software. Available at: www.ansys.com/products/fluids/ansys-fluent
51 Computer modeling of 3D-models of aviation equipment and engineering calculations. Available at: www.ipm ce.ru/custom/vsop/themes/3dmodel/
52 Nallasamy M. Turbulence models and their applications to the prediction of internal flows: A review // Computers & Fluids.–1987. –Volume 15, Issue 2. –P. 151-194
53 Belov I. A. Modeling of turbulent flows: A textbook/ I. A. Belov, S. A. Isaev. - St. Petersburg: BSTU, 2001.
54 Belov I. A. Problems and methods of calculating separation flows of incompressible fluid / I. A. Belov, S. A. Isaev, V. A. Korobkov. - L.: Shipbuilding, 1989.
55 Belotserkovsky O. M. Numerical modeling in continuum mechanics. - M.: Fizmatlit, 1994.
56 Kusaiynov K., Tanasheva N. K., Minkov L. L., Nusupbekov B. R., Stepanova Yu. O., Rozhkova A.V. Mathematical modeling of the flow around a sailing triangular blade of a wind generator in the ANSYS FLUENT software package / / Journal of Technical Physics. -2016. - Vol. 86, No. 2. - pp. 143-145.
57 Isataev S. I., Zhangunov O. Transverse flow around a short cylinder with spherical ends by an air flow. Study of the transfer process. - Almaty, 1985. - pp. 17-21.
58 Tanasheva N. K., Shuyushbaeva N. N., Musenova E. K. Investigation of the aerodynamic characteristics of rotating cylinders from the angle of the air flow bevel / / Letters to the Journal of Technical Physics. - Saint Petersburg. -2018. - Vol. 44, No. 17 – - pp. 66-70
59 .Tanasheva N.K., Nusupbekov B.R., Dyusembaeva A.N, Kunakbaev T., Bazarbek M. Mathematical modeling of the cylinder rotation system in a turbulent air flow // ВестникВКГТУим. Д. Серикбаева (совместный выпуск СО РАН, Россия) Технические науки. –2018. – №3 (1) – Ч.3. – С. 45-50.
60 Tanasheva N.K., Bakhtybekova A.R., Sakipova S.E., Minkov L.L.,Shuyushbaeva N.N. Kasimov A.R. Numerical simulation of the flow around a wind wheel with rotating cylindrical blades // Eurasian Physical Technical Journal. – 2021. – Vol.18. – Issue 1(35). – P.51-56.
61 Sakipova S.E., Tanasheva N.K., Minkov L.L. Modeling aerodynamics of a wind turbine with cylindrical blades in a turbulent air flow // Eurasian Physical Technical Journal. –2020. –Vol.17, No.1(33) . –P.106-112.
62 Tanasheva N.K., Kusaiynov K., Turgunov M.M., Alibekova A.R. Analysis of aerodynamic characteristics of rotating porous cylinders // Technical Physics. Pleiades Publishing. –2015. –V.60, № 5– P. 656-659.
63 Tanasheva N.K., Kussaiynov K., Sakipova S.E. Experimental research of aerodynamics of the system of the revolved cylinders in a turbulent stream // Turbulence, Heat and Mass Transfer: 7th International Symposium (September 24-27) / Italy, 2012.– P.125-128.

64 Tanasheva N.K., Kusaiynov K., Turgunov M.M., Kalikova A., Dysembaeva A. The effect of porosity on the aerodynamic characteristics of a rotating cylinder // Eurasian Physical Technical Journal –2013. –Vol 0, No.2(20). – P. 26-32.
65 Tanasheva N. K., Kunakbayev T. O., Dyusembayeva A. N., Shuyushbaeva N. N., Damekova S. K. The influence of a rough surface on the aerodynamic characteristics of a two-bladed wind turbine with cylindrical blades // Journal of Technical Physics. - 2017. - Volume 87, Issue 11. - pp. 1628-1631.
66 Oleynikov A.M., Matveev Yu. V., Kanov L. N. Modeling of the mode of a low-power wind power plant // Electrical engineering and electromechanics. - 2010. - No. 2. - pp. 16-20.
67 Redchits D. A., Prikhodko A. A. Numerical solution of the problem of dynamics and aerodynamics of the rotor of wind turbines / / Space Science and Technology. – 2005. – T. 11, №1. – P. 27-35.
68 Eronin M. V., Kramerov D. V., V. M. Molochnikov, Danube O. V. Vortices of Pocket if the turbulence in the boundary layer on the body plaguebloom // Proceedings of the Fifth Russian national conference on heat transfer: 8 T. – M.: Publishing house MPEI, 2010. – T. 2. – P. 118-122.
69 Molochnikov V. M., Mikheev N. I., Kratirov D. V., Davletshin I. A. The vortex path of the pocket in the conditions of a pulsating flow // Mater. VI interd. school-seminar " Models and methods of aerodynamics. Evpatoria". - M.: ICNMO, 2006. - pp. 71-72.
70 Molochnikov V. M., Mikheev N. I., Davletshin I. A., Faskhutdinov R. E. Dynamics of the transfer of turbulent pulsations of hydrodynamic and thermal parameters in the wake of a transverse cylinder near the wall / / Izv. RAS Energetika. - 2007. - No. 6. - pp. 80-86.
71 Mushtak al-atabi. Aerodynamics of wing tip sails //Journal of Engineering Science and Technology. – 2006. – Vol. 1. – № 1. – C. 89-98
72 Clauss G., Heisen W. CFD Analysis On The Flying Shape of Modern Yacht Sails // 12th International Congress of the International Maritime Association of the Mediterranean.– Lisbon, 2005. – P. 26-30.
73 Baturin O. V. Calculation of flows of liquids and gases using the universal Fluent software package: a textbook. - Samara: Publishing house of the Samara State Aerospace. university, 2009 – 151 p.
74 Tanasheva N. K. Research on the occurrence of the lifting force of a rotating cylinder / N.K. Tanasheva, B.R. Nusupbekov, N.N. Shuyushbayeva, A.K. Dyusembayeva, G.A. Ranova, Zh.G. Nurgalieva // Ualikhanov readings-22: mat. international scientific and practical conference-Kokshetau, 2018. - Vol. 6. - pp. 149-152.
75 Kusaiynov K., Tanasheva N. K., Turgunov M. M., Kusaiynova A. K., Sadenova K. K. Modeling of the flow pattern of a rotating cylinder in an air flow // Bulletin of the Karaganda University. The series "Physics". – 2015. – № 1(77). – pp. 74-77.
76 Lanzafame R., Mauro S., Messina M. Wind turbine CFD modeling using a correlation-based transitional model // Renewable Energy. – 2013. – V.52. – P. 31-39.

77 Jansuya Ph., Kumsuwan Y. Design of MATLAB/Simulink Modeling of Fixed-pitch Angle Wind Turbine Simulator // Energy Procedia. – 2013. – V. 34. - P.362-370.
78 Sidorenko K. N., Ilinka A. Modeling of a wind installation with a device for collecting wind / / Electrotechnical and computer systems.-2011. - No. 4. - p. 102-110.
79 Voldek A. I., Popov V. V. Electric machines. Introduction to Electromechanics. DC machines and transformers: A textbook for universities. - St. Petersburg: "Peter", 2008. - 320 p.
80 Glazyrin, A. S. Sensorless control of an asynchronous electric drive with a synergetic regulator / A. S. Glazyrin / / Izvestiya Tomsk Polytechnic University. - 2012. - No. 4. - pp. 107-111.
81 Sklyar A.V. Evaluation of the rotor speed of auxiliary asynchronous motors by the method of signature analysis of the stator current / / Technological support of repair and improvement of dynamic qualities of railway rolling stock: materials of the III All-Russian Scientific and Technical Journal. conf. with internat. participation. At 3 h. h. 1 / Omsk State University of Railways. - Omsk, 2015 – - 377 p.
82 Balagurov V. A., Kizaris A. A., Lokhnin V. V. Prospects for the development of magnetoelectric generators using high-coercive permanent magnets/ / Electricity. - 1977. - No. 3. - pp. 54-58.
83 Balagurov V. A. Maximum power of synchronous generators with permanent magnets // Electrical engineering. -1983. - No. 5. - pp. 22-24.
84 Devederkin, I. V., Konoplev, E. V., Nikitenko, I. V. High-efficiency synchronous generator with permanent magnets for a wind power plant // Bulletin of the agro-industrial complex of Stavropol. -2013. –№ 4 (12) . –Pp. 80-84.
85 Bakenov K. A. An effective electromechanical converter for a wind power plant / / Bulletin of the Pavlodar State University. - 2009. - No. 3. - pp. 17-24.
86 Lukutin B. V., Shandarova E. B., Muravlev A. I. Energy-efficient controlled generators for wind power plants // Izvestiya vuzov. Ser. Elektromekhanika. - 2008. - No. 6. - pp. 63-66.
87 Shevchenko V. V. Kulish Ya. R. Analysis of the possibility of using different types of generators for wind power plants taking into account the power range// Bulletin of NTU "KhPI". – 2013. № 65 (1038).– Pp. 107-117.
88 Miller N. W., Clark K., Shao M. Frequency responsive wind plant controls: Impacts on grid performance // 2011 IEEE Power and Energy Society General Meeting. – 2011. – P. 1-8.
89 A. S. 21023. Wind turbine / A. B. Basimov, T. M. Munsyzbai, A. B. Bekbayev, N. R. Turapova, A. K. Atybekov; publ. 16.03.2009, Bul. No. 3 – 3 p.
90 A. S. 21023. Wind turbine "Alga" / N. A. Baubekov, A. A. Baubekov; publ. 15.06.2001, Bul. No. 3 – 4 p.
91 A. S. 11119. Wind turbine / A. P. Shushchkin; publ. 15.07.2004, Bul. No. 3 – 4 p.

92 A. S. 24624. Cylindrical confusor wind turbine / A. Iskendirov; publ. 15.09.2011, Bul. No. 3 –3 p.

93 A. S. 15999. Wind turbine / A. K. Nugerbekov; publ. 15.07.2005, Bul. No. 3 – - 4 p.

94 A. S. 3230. Wind turbine of the Savonus system / M. M. Mailibayev; publ. 15.03.1996, Bul. No. 3 – 3 p.

95 Bychkov N. M., Dovgal A. V., Kozlov V.V. Magnus wind turbines as an alternative to the blade ones // J. Phys.: Conf. Ser. –2007. – Vol. 75.

96 Bychkov N. M. Magnus wind turbine. 3. Calculated characteristics of the wind wheel // Thermophys. Aeromechanics . –2008. –15. –P.321–331.

97 Krasnov N.F. Aerodynamics. Part 2. Aerodynamical methodology. –Moscow: Higher school, 1980. – 416 p.

98 Bordogna G., Muggiasca S., Giappino S., Belloli M., Keuning J.A., Huijsmans R.H.M., van 't Veer A.P. Experiments on a Flettner rotor at critical and supercritical Reynolds numbers // Journal of Wind Engineering and Industrial Aerodynamics. – 2019. – Volume 188. –P.19-29.

99 Aoki K., Ito T., Flow characteristics around a rotating cylinder // Proc. Sch. Eng. Tokai Univ. –.2011. – 26. – P. 29–34.

100 Karabelas S.J., Koumroglou B.C., Argyropoulos C.D., Markatos N.C. High Reynolds number turbulent flow past a rotating cylinder // Applied Mathematical Modelling. –2012. –Volume 36, Issue 1, . –P.379-398.

101 Catalano P., Wang M., Iaccarino G., Moin P., Numerical Simulation of the Flow around a Circular Cylinder at High Reynolds Numbers // Int. J. Heat Fluid Flow. – 2003. –24. – P. 463–469.

102 Mittal S., Kumar, B. Flow past a Rotating Cylinder // J. Fluid Mech.. –2003. – 476. –P.303– 334.

103 Cai J.C., Pan J., E S. J. Jiao, W.-D., Wang, D.-Y. A preliminary study of the pressure and shear stress on a plane surface beneath a circular cylinder in turbulent flow fields // Journal of Naval Architecture and Marine Engineering. –2017. –14(1) .– P. 9-24.

TANASHEVA NAZGUL KADYRALIEVNA

MATHEMATICAL MODELING OF WIND POWER PLANTS BASED ON THE MAGNUS EFFECT

Monograph

Recommended for publication by the Academic Council
KarU named after E.A.Buketov

Recommended for publication by the Academic Council RSOE « Institute of Applied Mathematics» MDDIAI RK

Signed on 19.11.2021, the circulation is 500 copies.
Volume 6,21 printed sheets. Format 60x84 1/16.
«Altyn kitap» publishing house, Nur-Sultan, Saryarka district,
Karamendy bi Shakauly, 4
Tel. 8 702 548 5841